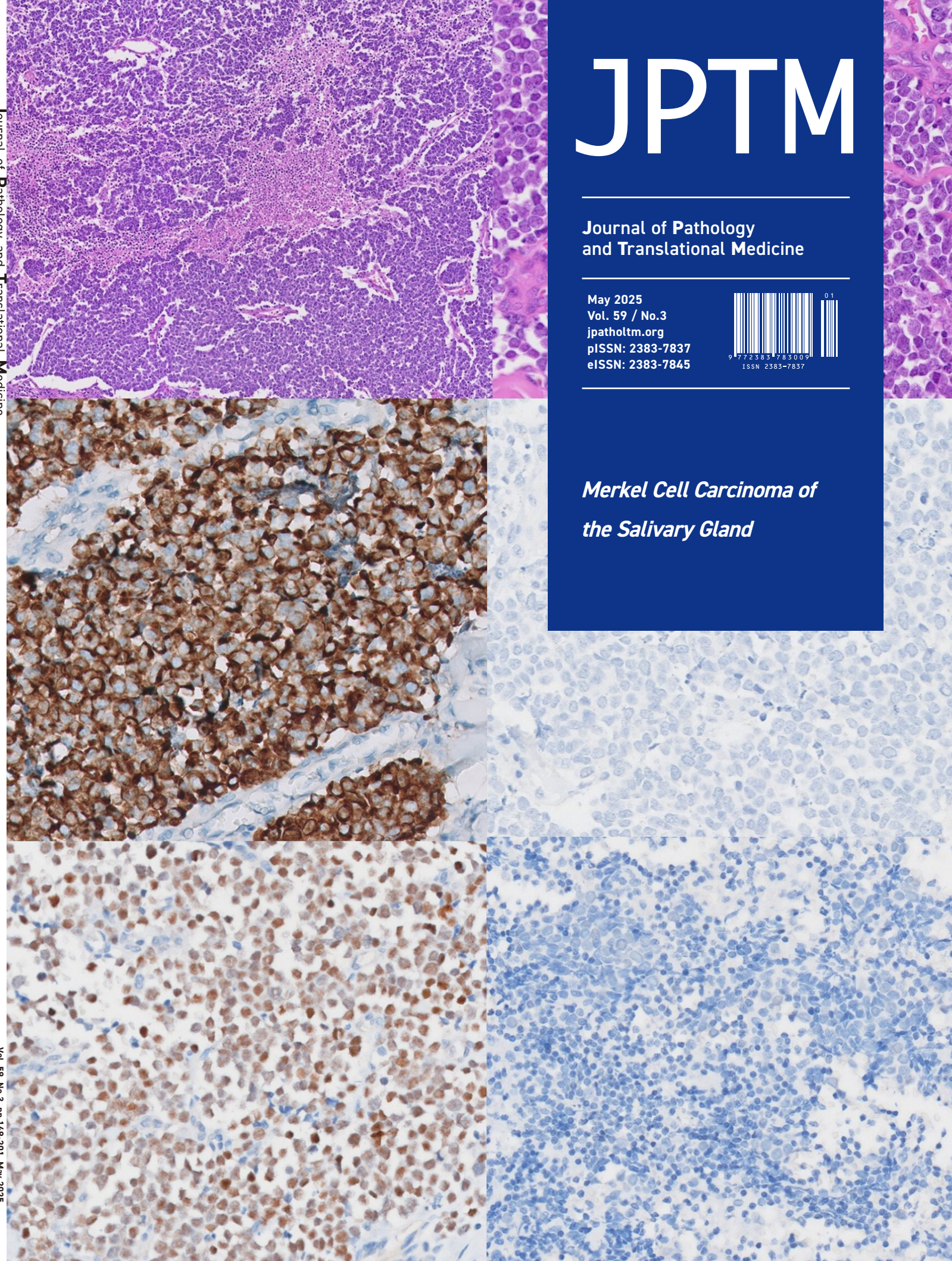




*Merkel Cell Carcinoma of
the Salivary Gland*



Aims & Scope

The Journal of Pathology and Translational Medicine is an open venue for the rapid publication of major achievements in various fields of pathology, cytopathology, and biomedical and translational research. The Journal aims to share new insights into the molecular and cellular mechanisms of human diseases and to report major advances in both experimental and clinical medicine, with a particular emphasis on translational research. The investigations of human cells and tissues using high-dimensional biology techniques such as genomics and proteomics will be given a high priority. Articles on stem cell biology are also welcome. The categories of manuscript include original articles, review and perspective articles, case studies, brief case reports, and letters to the editor.

Subscription Information

To subscribe to this journal, please contact the Korean Society of Pathologists/the Korean Society for Cytopathology. Full text PDF files are also available at the official website (<https://jpatholm.org>). *Journal of Pathology and Translational Medicine* is indexed by Emerging Sources Citation Index (ESCI), PubMed, PubMed Central, Scopus, KoreaMed, KoMCI, WPRIM, Directory of Open Access Journals (DOAJ), and CrossRef. Circulation number per issue is 50.

Contact the Korean Society of Pathologists/the Korean Society for Cytopathology

Publishers: Kang, Gyeong Hoon, MD; Choi, Yoon Jung, MD, PhD

Editors-in-Chief: Jung, Chan Kwon, MD; Park, So Yeon, MD

Published by the Korean Society of Pathologists/the Korean Society for Cytopathology

Editorial Office

Room 1209 Gwanghwamun Officia, 92 Saemunan-ro, Jongno-gu, Seoul 03186, Korea

Tel: +82-2-795-3094 Fax: +82-2-790-6635 E-mail: office@jpatholm.org

#1508 Renaissancetower, 14 Mallijae-ro, Mapo-gu, Seoul 04195, Korea

Tel: +82-2-593-6943 Fax: +82-2-593-6944 E-mail: office@jpatholm.org

Printed by M2PI

#805, 26 Sangwon 1-gil, Seongdong-gu, Seoul 04779, Korea

Tel: +82-2-6966-4930 Fax: +82-2-6966-4945 E-mail: support@m2-pi.com

Manuscript Editing by InfoLumi Co.

210-202, 421 Pangyo-ro, Bundang-gu, Seongnam 13522, Korea

Tel: +82-70-8839-8800 E-mail: infolumi.chang@gmail.com

Front cover image: Histopathologic features and expression of cytokeratin 20 and Merkel cell polyomavirus large T antigen in salivary gland Merkel cell carcinoma (p. 173, 175)

© 2025 The Korean Society of Pathologists/The Korean Society for Cytopathology

© Journal of Pathology and Translational Medicine is an Open Access journal under the terms of the Creative Commons Attribution Non-Commercial License (<https://creativecommons.org/licenses/by-nc/4.0>).

© This paper meets the requirements of KS X ISO 9706, ISO 9706-1994 and ANSI/NISO Z.39.48-1992 (Permanence of Paper).



VENTANA CLDN18 (43-14A) RxDx Assay

확장된 위암 진단 가능성, GC/GEJC 표적 치료의 기회를 더욱 높여보세요



GC/GEJC 환자의
FFPE 조직검체에서
CLDN18 단백질을 IHC로 검사합니다.



표적 치료제인 VYLOY™
(Zolbetuximab)의
적합성을 판단하는 데 사용됩니다.



자동화된 검사 장비(Benchmark 시리즈)로
CLDN18 단백질 발현을
신속하고 정확한 측정을 지원합니다.

Editorial Board

Editors-in-Chief

Jung, Chan Kwon, MD (*The Catholic University of Korea, Korea*) <https://orcid.org/0000-0001-6843-3708>
Park, So Yeon, MD (*Seoul National University, Korea*) <https://orcid.org/0000-0002-0299-7268>

Associate Editors

Bychkov, Andrey, MD (*Kameda Medical Center, Japan; Nagasaki University Hospital, Japan*) <https://orcid.org/0000-0002-4203-5696>
Kim, Haeryoung, MD (*Seoul National University, Korea*) <https://orcid.org/0000-0002-4205-9081>
Lee, Hee Eun, MD (*Mayo Clinic, USA*) <https://orcid.org/0000-0001-6335-7312>
Shin, Eunah, MD (*Yongin Severance Hospital, Yonsei University, Korea*) <https://orcid.org/0000-0001-5961-3563>

Editorial Board

Avila-Casado, Maria del Carmen, MD (*University of Toronto, Toronto General Hospital UHN, Canada*)
Bae, Jeong Mo, MD (*Seoul National University, Korea*)
Bae, Young Kyung, MD (*Yeungnam University, Korea*)
Bongiovanni, Massimo, MD (*Lausanne University Hospital, Switzerland*)
Bova, G. Steven, MD (*University of Tampere, Finland*)
Choi, Joon Hyuk (*Yeungnam University, Korea*)
Chong, Yo Sep, MD (*The Catholic University of Korea, Korea*)
Chung, Jin-Haeng, MD (*Seoul National University, Korea*)
Fadda, Guido, MD (*Catholic University of Rome-Foundation Agostino Gemelli University Hospital, Italy*)
Fukushima, Noriyoshi, MD (*Jichi Medical University, Japan*)
Go, Heounjeong (*University of Ulsan, Korea*)
Hong, Soon Won, MD (*Yonsei University, Korea*)
Jain, Deepali, MD (*All India Institute of Medical Sciences, India*)
Kakudo, Kennichi, MD (*Izumi City General Hospital, Japan*)
Kim, Jang-Hee, MD (*Ajou University, Korea*)
Kim, Jung Ho, MD (*Seoul National University, Korea*)
Kim, Se Hoon, MD (*Yonsei University, Korea*)
Komuta, Mina, MD (*Keio University, Tokyo, Japan*)
Lai, Chiung-Ru, MD (*Taipei Veterans General Hospital, Taiwan*)
Lee, C. Soon, MD (*University of Western Sydney, Australia*)
Lee, Hwajeong, MD (*Albany Medical College, USA*)
Lee, Sung Hak, MD (*The Catholic University of Korea, Korea*)
Liu, Zhiyan, MD (*Shanghai Jiao Tong University, China*)
Lkhagvadorj, Sayamaa, MD (*Mongolian National University of Medical Sciences, Mongolia*)
Lo, Regina, MD (*The University of Hong Kong, Hong Kong*)
Moran, Cesar, MD (*MD Anderson Cancer Center, U.S.A.*)
Paik, Jin Ho, MD (*Seoul National University, Korea*)
Park, Jeong Hwan (*Seoul National University, Korea*)
Sakhuja, Puja, MD (*Govind Ballabh Pant Hospital, India*)
Shahid, Pervez, MD (*Aga Khan University, Pakistan*)
Song, Joon Seon, MD (*University of Ulsan, Korea*)
Tan, Puay Hoon, MD (*National University of Singapore, Singapore*)
Than, Nandor Gabor, MD (*Semmelweis University, Hungary*)
Tse, Gary M., MD (*The Chinese University of Hong Kong, Hong Kong*)
Yatabe, Yasushi, MD (*Aichi Cancer Center, Japan*)
Zhu, Yun, MD (*Jiangsu Institution of Nuclear Medicine, China*)

Ethic Editor

Choi, In-Hong, MD (*Yonsei University, Korea*)
Huh, Sun, MD (*Hallym University, Korea*)

Statistics Editors

Kim, Dong Wook (*National Health Insurance Service Ilsan Hospital, Korea*)
Lee, Hye Sun (*Yonsei University, Korea*)

Manuscript Editor

Chang, Soo-Hee (*InfoLumi Co., Korea*)

Layout Editor

Jeong, Eun Mi (*M2PI, Korea*)

Website and JATS XML File Producers

Choi, Min Young (*M2PI, Korea*)

Administrative Assistants

Lee, Hye jin (*The Korean Society of Pathologists*)
Kim, Song Yeun (*The Korean Society for Cytopathology*)

Contents

Vol. 59, No.3, May 2025

ORIGINAL ARTICLES

- 149** Lessons learned from the first 2 years of experience with thyroid core needle biopsy at an Indonesian national referral hospital
Agnes Stephanie Harahap, Maria Francisca Ham, Retno Asti Werdhani, Erwin Danil Julian, Rafi Ilmansyah,
Chloe Indira Arfelita Mangunkusumso, Tri Juli Edi Tarigan
- 161** Thoracic aortic calcification as a predictor of coronary artery disease: a systematic review and meta-analysis
Hussein Nafakhi, Alaa Salah Jumaah, Akeel Abed Yasseen
- 171** Primary Merkel cell carcinoma of the salivary gland: a clinicopathologic study of four cases with a review of literature
Gyuheon Choi, Joon Seon Song, Hee Jin Lee, Gi Hwan Kim, Young Ho Jung, Yoon Se Lee, Kyung-Ja Cho
- 180** Diagnostic yield of fine needle aspiration with simultaneous core needle biopsy for thyroid nodules
Mohammad Ali Hasannia, Ramin Pourghorban, Hoda Asefi, Amir Aria, Elham Nazar, Hojat Ebrahimir, Alireza Mohamadian

CASE STUDIES

- 188** Histopathological characteristics of Epstein-Barr virus (EBV)-associated encephalitis and colitis in chronic active EBV infection
Betty A Kasimo, James J Yahaya, Sun Och Yoon, Se Hoon Kim, Minsun Jung
- 195** Cytological features of atypical adenomatous hyperplasia and adenocarcinoma in situ of the lung: a case report
Misa Takahashi, Seiya Homma, Chisato Setoguchi, Yoko Umezawa, Atsuhiko Sakamoto

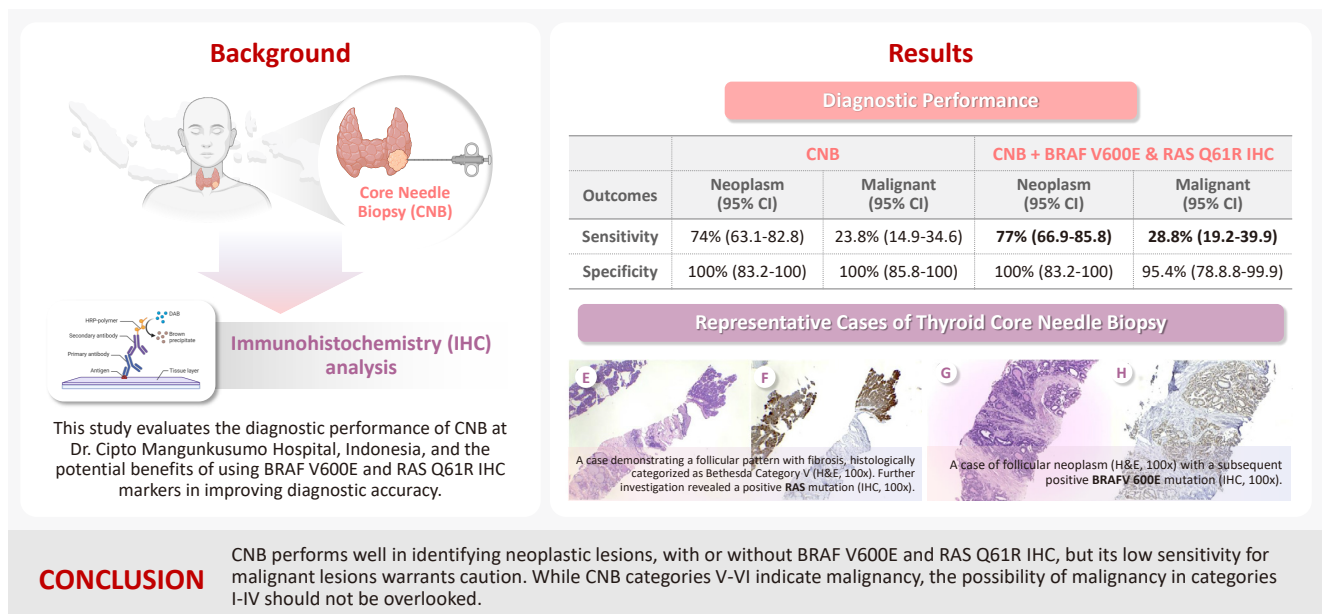
CORRESPONDENCE

- 201** Erratum: Diagnostic challenges in the assessment of thyroid neoplasms using nuclear features and vascular and capsular invasion: a multi-center interobserver agreement study
Agnes Stephanie Harahap, Mutiah Mutmainnah, Maria Francisca Ham, Dina Khoirunnisa, Abdillah Hasbi Assadyk, Husni Cangara,
Aswiyanti Asri, Diah Prabawati Retnani, Fairuz Quzwain, Hasrayati Agustina, Hermawan Istiadi, Indri Windarti, Krisna Murti, Muhammad Takbir,
Ni Made Mahastuti, Nila Kurniasari, Nungki Anggorowati, Pamela Abineno, Yulita Pundewi Setyorini, Kennichi Kakudo

Lessons learned from the first 2 years of experience with thyroid core needle biopsy at an Indonesian national referral hospital

Agnes Stephanie Harahap^{1,2}, Maria Francisca Ham^{1,2}, Retno Asti Werdhani³, Erwin Danil Julian⁴, Rafi Ilmansyah⁵, Chloe Indira Arfelita Mangunkusumso⁶, Tri Juli Edi Tarigan⁷

Graphical abstract



Lessons learned from the first 2 years of experience with thyroid core needle biopsy at an Indonesian national referral hospital

Agnes Stephanie Harahap^{1,2}, Maria Francisca Ham^{1,2}, Retno Asti Werdhani³, Erwin Danil Julian⁴, Rafi Ilmansyah⁵, Chloe Indira Arfelita Mangunkusumso⁶, Tri Juli Edi Tarigan⁷

¹Department of Anatomical Pathology, Faculty of Medicine Universitas Indonesia/Dr. Cipto Mangunkusumo Hospital, Jakarta, Indonesia

²Human Cancer Research Center-Indonesian Medical Education and Research Institute, Faculty of Medicine Universitas Indonesia, Jakarta, Indonesia

³Department of Community Medicine, Faculty of Medicine Universitas Indonesia, Jakarta, Indonesia

⁴Surgical Oncology Division, Department of Surgery, Faculty of Medicine Universitas Indonesia/Dr. Cipto Mangunkusumo Hospital, Jakarta, Indonesia

⁵Department of Medicine, Faculty of Medicine, Diponegoro University, Semarang, Indonesia

⁶Immunology and Infectious Disease Bachelor Science, College of Agricultural Science, Pennsylvania State University, University Park, PA, USA

⁷Division of Endocrinology, Metabolism, and Diabetes, Department of Internal Medicine, Dr. Cipto Mangunkusumo National General Hospital, Faculty of Medicine Universitas Indonesia, Jakarta, Indonesia

Background: Core needle biopsy (CNB) improves diagnostic accuracy by providing precise tissue sampling for histopathological evaluation, overcoming the limitation of inconclusive fine-needle aspiration results. This study evaluated the diagnostic performance of CNB in assessing thyroid nodules, with additional analysis of the benefits of BRAF V600E and RAS Q61R immunohistochemical (IHC) markers. **Methods:** This retrospective study enrolled patients with thyroid nodules who underwent CNB at Dr. Cipto Mangunkusumo Hospital, Jakarta, from July 2022 to July 2024. CNB diagnoses were classified using the Korean Thyroid Association Criteria. Diagnostic efficacy was evaluated for neoplastic and malignant lesions, both independently and with BRAF V600E and RAS Q61R IHC. The correlation between nodule size and postoperative diagnosis was also analyzed. **Results:** A total of 338 thyroid nodule samples was included, and 52.7% were classified as CNB category II. In the 104 samples with postoperative diagnoses, category IV was the most prevalent (39.4%). CNB demonstrated a sensitivity of 74% and a specificity of 100% for neoplastic lesions and 23.8% sensitivity and 100% specificity for malignant lesions. Combining CNB with BRAF V600E and RAS Q1R IHC increased the sensitivity to 77% for neoplastic lesions and 28.8% for malignant lesions. Larger nodules (>3 cm) were significantly associated with neoplastic ($p = .005$) and malignant lesions ($p = .004$). **Conclusions:** CNB performs well in identifying neoplastic lesions, with or without BRAF V600E and RAS Q61R IHC, but its low sensitivity for malignant lesions warrants caution. While CNB categories V–VI indicate malignancy, the possibility of malignancy in categories I–IV should not be overlooked.

Keywords: Thyroid cancer, papillary; Biopsy, large-core needle; BRAF V600E mutation; RAS Q61R mutation; Thyroid nodule

INTRODUCTION

Ultrasound (US)-guided fine-needle aspiration (FNA) is a reliable and precise technique for the evaluation of thyroid nodules [1]. A significant limitation of FNA is the occurrence of

nondiagnostic and indeterminate specimens classified by The Bethesda System for Reporting Thyroid Cytopathology, caused by insufficient cells or collection of bloody material [1]. Two previous studies indicated that the rates of malignancy for non-diagnostic and indeterminate FNA aspirates can reach as high

Received: November 30, 2024 **Revised:** February 13, 2025 **Accepted:** February 19, 2025

Corresponding Author: Tri Juli Edi Tarigan, MD, PhD

Division of Endocrinology, Metabolism, and Diabetes, Department of Internal Medicine, Dr. Cipto Mangunkusumo National General Hospital, Faculty of Medicine Universitas Indonesia, Jl. Salemba Raya No. 6, Jakarta 10430, Indonesia

Tel: +62-021-3160493, Fax: +62-021-3912477, E-mail: tri.judi@ui.ac.id

This is an Open Access article distributed under the terms of the Creative Commons Attribution Non-Commercial License (<https://creativecommons.org/licenses/by-nc/4.0/>) which permits unrestricted non-commercial use, distribution, and reproduction in any medium, provided the original work is properly cited.

© 2025 The Korean Society of Pathologists/The Korean Society for Cytopathology

as 10.9% and 60.0%, respectively [2,3]. For thyroid nodules that previously yielded nondiagnostic outcomes, the current guidelines suggest either repeating the FNA procedure or considering surgery if the nondiagnostic nodule presents an unclear cytological diagnosis [4].

Core needle biopsy (CNB) has emerged as a substitute for FNA that resolves several of the previously mentioned issues. CNB collects tissue samples with potential information on architectural histological structures and is useful for diagnosis of thyroid nodules [5]. Prior studies have illustrated that CNB significantly decreased the rates of nondiagnostic outcomes while simultaneously enhancing the accuracy of malignancy diagnoses in comparison with FNA cytology [6,7]. The American Association of Clinical Endocrinologists/American College of Endocrinology/Associazione Medici Endocrinologi (Italian Medical Endocrinologists Association) suggest the use of CNB in thyroid nodules with repeatedly nondiagnostic FNA, and the Korean Society of Thyroid Radiology extends the recommendations to nodules with indeterminate FNA or with troublesome cytological diagnosis [6,8,9].

Genetic modifications have been implicated in thyroid carcinoma, predominantly aberrant activation of the RAS-RAF-MEK-MAP signaling cascade [10]. Specific mutations in B-rapidly accelerated fibrosarcoma V600E (*BRAF* V600E) and rat sarcoma Q61R (*RAS* Q61R) are well-documented driver mutations in the pathogenesis of thyroid neoplasms [11]. A recent meta-analysis demonstrated that the integration of *BRAF* V600E assessment with FNA increased sensitivity by 6% while concurrently reducing the false-negative rate from 8% to 5.2% [12]. The incorporation of immunohistochemical (IHC) analysis of *BRAF* V600E and *RAS* Q61R expression status alongside CNB is posited to further amplify the diagnostic performance outcomes of the evaluation.

Despite the increase in CNB research, no studies from Indonesia have been documented on the diagnostic performance of thyroid CNB, including the utility of *BRAF* V600E and *RAS* Q61R IHC protein expression in identifying various thyroid nodules. CNB has been performed over the past 2 years at our institution. This study presents our initial experience with CNB, with a particular focus on its diagnostic performance and the utility of *BRAF* V600E and *RAS* Q61R IHC protein expression in the diagnosis of thyroid nodules.

MATERIALS AND METHODS

Selection of subjects

We gathered retrospective data from patients who underwent CNB for thyroid nodule at the Department of Anatomical Pathology, Dr. Cipto Mangunkusumo Hospital, Faculty of Medicine, Universitas Indonesia, between July 2022 and July 2024. In our institution, CNB is performed as a second-line diagnostic tool for thyroid nodule. Patients with thyroid nodules that warrant CNB are those with a clinically high suspicion for anaplastic carcinoma, medullary carcinoma, or thyroiditis; those with large thyroid nodules (>3 cm); those with nodules with sonographic characteristics of macrocalcification and hypervascularity; those that exhibit non-malignant FNA diagnosis while US findings show malignancy; and those with prior scanty, nondiagnostic, or inconclusive FNA aspirates.

CNB procedures were performed under US guidance and conducted by an endocrinologist, otorhinolaryngologist, or surgical oncologist with varying levels of experience in thyroid ultrasonography and interventional US. The CNB diagnosis is stratified into six categories based on the latest practice guidelines for thyroid CNB [13]: category I (nondiagnostic), category II (benign), category III (atypia of undetermined significance), category IV (follicular neoplasm), category V (suspicious for malignancy), and category VI (malignancy).

After excluding patients with inaccessible medical records, incomplete and/or disrupted hematoxylin and eosin-stained slides, or incomplete formalin-fixed paraffin-embedded (FFPE) tumor specimens, a total of 338 CNB samples was included in the study. Clinical data, including age, sex, location of thyroid nodule, CNB diagnostic category, and types of surgery performed, were obtained from medical records.

Of the 338 CNB samples, 104 were obtained from patients who underwent surgery with available postoperative diagnoses. The postoperative diagnosis was performed and re-reviewed by two board-certified endocrine pathologists (A.S.H. and M.F.H.) following the fifth edition of the World Health Organization classification of tumors [14]. The nodule size was determined as the largest diameter measured in the surgical specimen.

Immunohistochemistry examination of *BRAF* V600E and *RAS* Q61R

The expression of *BRAF* V600E and *RAS* Q61R proteins was assessed in 104 cases with postoperative diagnosis, irrespective of the CNB diagnostic category, using standard IHC proce-

dures. We performed immunostaining on 4- μ m-thick tissue sections from each FFPE tissue sample, which were the same as those used in the CNB diagnostic assessment [15,16]. The Optiview DAB IHC Detection Kit was used to perform immunostaining on a Starr Trek Universal HRP Detection (Biocare Medical, Concord, CA, USA) at the IHC Laboratory, Cipto Mangunkusumo Hospital, Jakarta. The manufacturers' instructions (CC1 pretreatment for 32 minutes at 100°C, pH 8.5, antibody dilution at 1:600 for anti-BRAF V600E [mutated V600E] antibody [VE1] [ab228461, Abcam, Cambridge, UK] and 1:100 for anti-RAS [mutated Q61R] antibody [SP174] [ab227658, Abcam], incubation at 37°C for 16 minutes, examination using the Optiview DAB IHC Detection Kit) were followed.

Statistical analysis

Data were processed using Statistical Program for Social Science (SPSS) ver. 29 (IBM Corp., Armonk, NY, USA). Data on patient sex, CNB category, histological subtype, and other categorical data are provided as frequencies and percentages. Data on age and tumor size are presented as median values based on the distribution abnormality of the numerical data. We conducted statistical analysis using the Pearson Chi-Square test to compare CNB category with postoperative diagnosis. CNB categories I–III were regarded as non-neoplastic, while CNB categories IV–VI were regarded as neoplastic. The CNB groups were statistically compared based on postoperative diagnosis of neoplasm, which include lesions such as papillary thyroid carcinoma (PTC), invasive encapsulated follicular variant papillary thyroid carcinoma (IEFVPTC), differentiated high-grade thyroid carcinoma (DHGTC), poorly differentiated thyroid carcinoma (PDTC), oncocytic carcinoma, and follicular adenoma (FA). We also analyzed CNB categories in identifying malignant lesions; CNB categories I–IV were regarded as non-malignant and CNB categories V–VI were regarded as malignant. The diagnostic performances of CNB in identifying both neoplasm and malignant lesions at postoperative diagnosis were evaluated using sensitivity, specificity, accuracy, positive predictive value (PPV), negative predictive value (NPV), positive likelihood-ratio (LR), and negative LR. Further analyses were conducted to assess the diagnostic performance of CNB based on the IHC expression of BRAF V600E and RAS Q61R protein. Samples exhibiting positive BRAF V600E and RAS Q61R proteins were reclassified into neoplasm and malignant categories irrespective of their previous CNB classifications. Secondary analysis using binary logistic regression was used to assess the correlation

between nodule size and postoperative diagnosis of both neoplasms and malignant lesions. A p-value less than .05 indicated statistical significance.

RESULTS

This study included 338 patients with thyroid nodules who underwent CNB. The demographic data of the patients are shown in Table 1. The mean age of the patients was 50.1 ± 16.1 years, and most were female (87.3%). CNB thyroid samples were predominantly collected from the right lobe of the thyroid gland (49.7%). The most common CNB category was II (52.7%), followed by IV, III, VI, I, and V, in this order (Fig. 1). The average core size was 0.65 ± 0.61 cm, and the average number of cores was 3.1 ± 2.1 .

Postoperative diagnoses were achieved for 104 of 338 CNB samples (30.8%). Most patients underwent total thyroidectomy (81.7%). This study identified thyroid lesions including PTC, IEFVPTC, DHGTC, PDTC, oncocytic carcinoma, FA, and multinodular goiter (MG). PTC was identified in 59.6% of the postoperative samples, including infiltrative follicular, oncocytic, classic, tall cell, solid, and columnar subtypes. Three cases were identified as DHGTC in postoperative diagnosis, including one tall cell subtype of PTC, one follicular subtype of PTC, and one oncocytic carcinoma. The most common concurrent disease found in thyroid nodules samples was MG (45.2%). Thyroid nodule size was measured in postoperative histological examination, and the mean nodule size was 3.62 ± 2.9 cm.

In the 104 cases with postoperative diagnosis, CNB diagnosis of category IV was the most prevalent (39.4%), followed by category II (32.7%) and category VI (16.3%). Table 2 provides a detailed distribution of thyroid carcinoma diagnosis across CNB categories. Most PTC cases were classified as CNB category IV (46.8%), followed by category VI (25.8%) and category II (17.7%). The infiltrative follicular subtype was the most common PTC subtype, with 48% of cases classified as CNB category IV. The oncocytic subtype of PTC cases was predominantly categorized as category IV (69.2%). We found eight cases of tall cell subtype of PTC; most were classified as category VI (87.5%). The only oncocytic carcinoma case was category IV. All three cases of DHGTC were CNB category IV. Most PDTC and IEFVPTC cases were category IV (50% and 40%, respectively). FA cases were classified as category IV (50%), II (25%), and III (25%), while all MG cases were category II.

Table 1. Demographic data

Characteristic	CNB (n = 338)
Age (yr)	50.1 ± 16.1
Sex	
Female	295 (87.3)
Male	43 (12.7)
Diagnostic category	
I	24 (7.1)
II	178 (52.7)
III	41 (12.1)
IV	51 (15.1)
V	13 (3.8)
VI	31 (9.2)
Location	
Right lobe	168 (49.7)
Left lobe	137 (40.5)
Isthmus	4 (1.2)
Unknown	29 (8.6)
Postoperative diagnosis	104
PTC	62 (59.6)
Infiltrative follicular	25 (24)
Oncocytic	13 (12.5)
Classic	10 (9.6)
Tall cell	8 (7.7)
Solid	4 (3.8)
Columnar	2 (1.9)
IEFVPTC	10 (9.6)
DHGTC	3 (2.9)
PDTC	4 (3.8)
Oncocytic carcinoma	1 (1.2)
FA	4 (3.8)
MG	20 (19.2)
Operation type	
Total thyroidectomy	85 (81.7)
Lobectomy	8 (7.7)
Isthmolebectomy	11 (10.6)
Concurrent	
MG	47 (45.2)
Absent	45 (43.3)
HT	8 (7.7)
GD	3 (2.9)
FA	1 (1)
Nodule size (cm)	
Mean ± SD	3.62 ± 2.9
>3.0	46 (44.2)
2.1–3.0	19 (18.3)
1.1–2.0	15 (14.4)
<1.0	22 (21.2)
Unknown	2 (1.9)

Values are expressed as mean ± SD or number (%).

CNB, core needle biopsy; PTC, papillary thyroid carcinoma; IEFVPTC, invasive encapsulated follicular variant papillary thyroid carcinoma; DHGTC, differentiated high-grade thyroid carcinoma; PDTC, poorly differentiated thyroid carcinoma; FA, follicular adenoma; MG, multinodular goiter; HT, Hashimoto thyroiditis; GD, Graves disease; SD, standard deviation.

Comparison of thyroid CNB categories with postoperative neoplastic diagnosis

Table 3 shows the significant association between CNB category and postoperative neoplastic diagnoses ($p < .001$). CNB categories IV–VI (follicular neoplasm, suspicious for malignancy, and malignant) were significantly associated with neoplastic lesions in postoperative diagnosis.

Comparison of thyroid CNB categories with postoperative malignancy diagnosis

Table 4 shows the relationship between the CNB category and postoperative malignancy diagnosis. CNB categories V–VI (suspicious for malignancy and malignant category) were more frequently associated with malignancy in postoperative diagnosis. This result highlights the limitations of CNB to rule out malignancy in CNB category I–IV and indicate the need for caution with such lesions, particularly in indeterminate or follicular neoplasm cases.

Diagnostic performance of CNB

We further compared the diagnostic performance of CNB in detecting both neoplastic and malignant lesions. Table 5 showed that CNB exhibited a higher sensitivity and overall accuracy in detecting neoplasms than malignant lesions (74% vs. 23.8% and 79% vs. 41.4%, respectively). When combined with BRAF V600E IHC, CNB showed superior sensitivity and overall accuracy in detecting neoplasms compared with malignant lesions (74% vs. 28.8% and 79% vs. 44.4%, respectively). When combined with RAS Q61R IHC, CNB showed better sensitivity and overall accuracy in detecting neoplasms than malignant lesions (77% vs. 23.8% and 82% vs. 41.4%, respectively). Other parameters such as specificity, PPV, and NPV showed no significant difference for detection of neoplasms and malignant lesions for CNB alone, CNB and BRAF V600E IHC, CNB and RAS Q61R, and CNB and BRAF V600E/RAS Q61R.

Association between nodule size and postoperative diagnosis

We further examined the association between thyroid nodule size and postoperative neoplastic diagnosis (Table 6). The analysis showed that nodules >3 cm in diameter were associated with neoplastic lesions in postoperative diagnosis ($p = .005$; odds ratio [OR], 8.19).

Table 7 displays the relationship between thyroid nodule size and postoperative malignant diagnosis. We found that thyroid

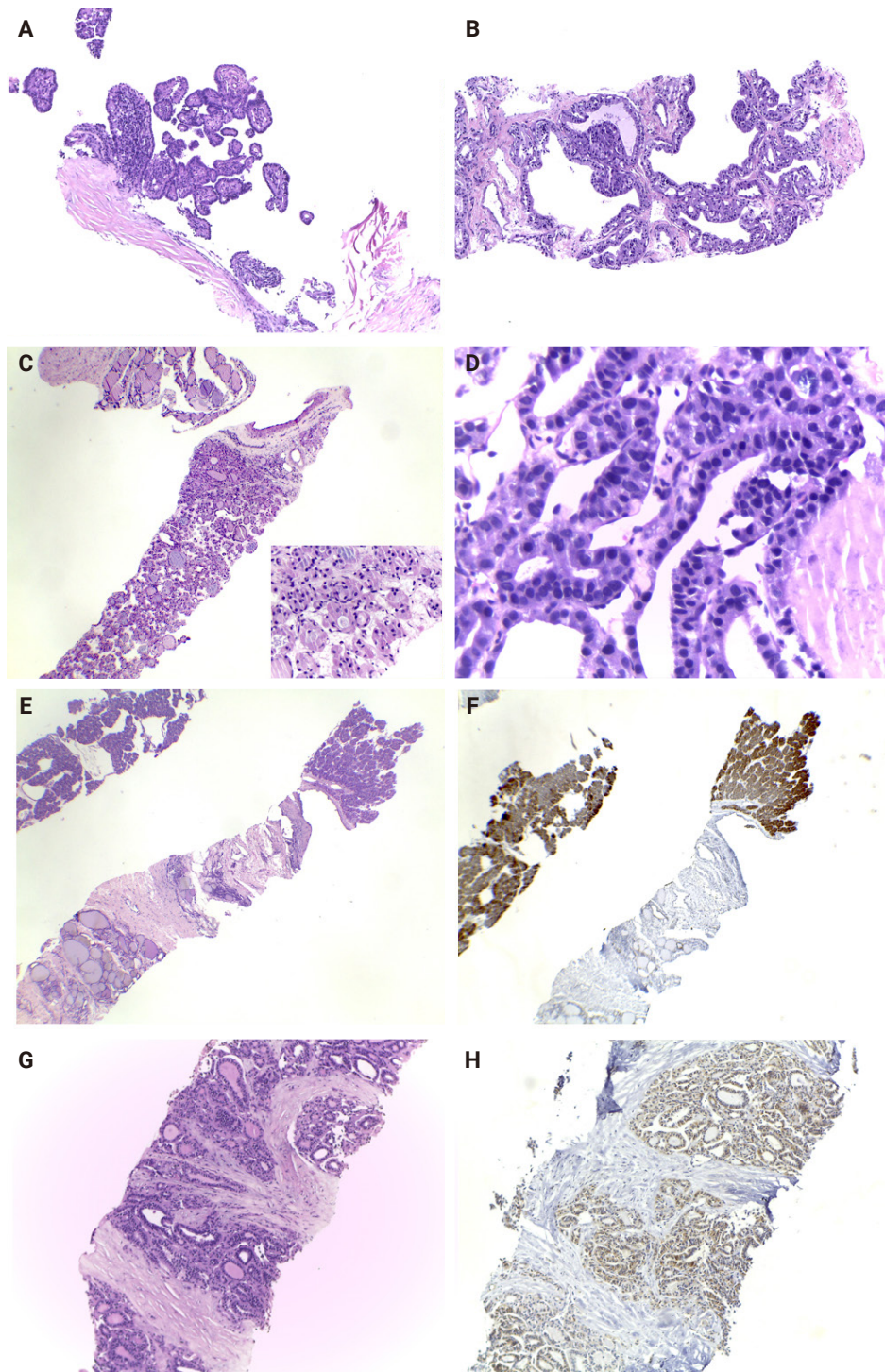


Fig. 1. Representative cases of thyroid core needle biopsy. (A) Papillary thyroid carcinoma with a papillary architecture, containing a fibrovascular core and lined by densely packed elongated atypical cells, classified as category VI. (B) A case of Graves' disease classified as category II, demonstrating hyperplastic follicles with hyperfunctioning cells and empty lumina. (C) A follicular neoplasm (category IV) exhibiting a microfollicular pattern and surrounded by a fibrous capsule. (D) Core needle biopsy showing tumor cells with enlarged atypical nuclei, condensed chromatin, and numerous bubble artifacts that should not be mistaken for true nuclear pseudoinclusions. (E, F) A case demonstrating a follicular pattern with fibrosis, histologically categorized as Bethesda category V. Further investigation revealed positivity for a *RAS* mutation (immunohistochemistry). (G, H) A case of follicular neoplasm with positive *BRAFV600E* mutation (immunohistochemistry).

Table 2. Postoperative diagnosis for each CNB category

Postoperative diagnosis	CNB category						Total
	I	II	III	IV	V	VI	
PTC	3 (4.8)	11 (17.7)	1 (1.6)	29 (46.8)	2 (3.2)	16 (25.8)	62 (59.6)
Classic	1 (10.0)	1 (10.0)	0	4 (40.0)	1 (10.0)	3 (30.0)	10 (9.6)
Tall cell	1 (12.5)	0	0	0	0	7 (87.5)	8 (7.7)
Solid	0	0	0	4 (100)	0	0	4 (3.8)
Oncocytic	0	2 (15.4)	0	9 (69.2)	1 (7.7)	1 (7.7)	13 (12.5)
Columnar	0	0	0	0	0	2 (100)	2 (1.9)
Infiltrative follicular	1 (4.0)	8 (32.0)	1 (4.0)	12 (48.0)	0	3 (12.0)	25 (24)
Oncocytic carcinoma	0	0	0	1 (100)	0	0	1 (1)
DHGTC	0	0	0	3 (100)	0	0	3 (2.9)
PDTC	0	1 (25.0)	1 (25.0)	2 (50.0)	0	0	4 (3.8)
IEFVPTC	3 (30.0)	2 (20.0)	0	4 (40.0)	0	1 (10)	10 (9.6)
FA	0	1 (25.0)	1 (25.0)	2 (50.0)	0	0	4 (3.8)
MG	0	20 (100)	0	0	0	0	20 (19.2)
Total	6 (5.8)	34 (32.7)	3 (2.9)	41 (39.4)	2 (1.9)	17 (16.3)	104

Values are presented as number (%).

CNB, core needle biopsy; PTC, papillary thyroid carcinoma; DHGTC, differentiated high-grade thyroid carcinomas; PDTC, poorly differentiated thyroid carcinoma; IEFVPTC, invasive encapsulated follicular variant papillary thyroid carcinoma; FA, follicular adenoma; MG, multinodular goiter.

Table 3. Thyroid CNB results and postoperative neoplastic diagnosis

CNB category	Postoperative diagnosis		p-value
	Neoplastic ^a (n = 84)	Non-neoplastic ^b (n = 20)	
Category I–III	22 (52.4)	20 (47.6)	<.001 ^{cd}
Category IV–VI	62 (100)	0	

Values are presented as number (%).

CNB, core needle biopsy; PTC, papillary thyroid carcinoma; IEFVPTC, invasive encapsulated follicular variant papillary thyroid carcinoma; DHGTC, differentiated high-grade thyroid carcinomas; PDTC, poorly differentiated thyroid carcinoma; FA, follicular adenoma; MG, multinodular goiter.

^aNeoplastic diagnoses included PTC, IEFVPTC, DHGTC, PDTC, oncocytic carcinoma, and FA; ^bNon-neoplastic: MG; ^cSignificant (p < 0.05); ^dPearson chi-square.

Table 4. Thyroid CNB result and postoperative malignancy diagnosis

CNB category	Postoperative diagnosis		p-value
	Malignant (n = 80)	Non-malignant (n = 24)	
Category I–IV	61 (71.8)	24 (28.2)	.004 ^{ab}
Category V–VI	19 (100)	0	

Values are presented as number (%).

CNB, core needle biopsy; PTC, papillary thyroid carcinoma; IEFVPTC, invasive encapsulated follicular variant papillary thyroid carcinoma; DHGTC, differentiated high-grade thyroid carcinomas; PDTC, poorly differentiated thyroid carcinoma; MG, multinodular goiter; FA, follicular adenoma.

^aSignificant (p < .05); ^bFisher exact test.

nodule >3 cm in diameter was significantly associated with malignant lesion (p = .004; OR, 5.83).

DISCUSSION

In the present study involving 338 thyroid nodule patients, the

most common CNB diagnosis was category II (52.7%), followed by category IV (15.1%). Category II indicates a benign lesion, which includes non-thyroid lesion or benign thyroid lesions, including Hashimoto thyroiditis or benign follicular nodules. Category IV refers to follicular thyroid neoplasms, including the conventional type, which may or may not exhibit nucle-

Table 5. Diagnostic performance of CNB, BRAF V600E IHC, and RAS Q61R IHC for diagnosis of neoplastic and malignant lesions

Outcomes	Neoplasm (95% CI, %)	Malignant (95% CI, %)
CNB		
Sensitivity	73.8 (63.1–82.8)	23.8 (14.9–34.6)
Specificity	100 (83.2–100)	100 (85.8–100)
PPV	100 (94.2–100)	100 (82.4–100)
NPV	47.6 (38.8–56.6)	28.2 (25.8–30.8)
Accuracy	78.9 (69.7–86.2)	41.4 (31.8–51.4)
LR +	NA ^a	NA ^a
LR –	0.3 (0.2–0.4)	0.8 (0.7–0.9)
CNB + BRAF V600E IHC		
Sensitivity	73.8 (63.1–82.8)	28.8 (19.2–39.9)
Specificity	100 (83.2–100)	95.4 (78.8–99.9)
PPV	100 (94.2–100)	95.8 (76.6–99.4)
NPV	47.6 (38.8–56.6)	28.8 (25.5–32.2)
Accuracy	78.9 (69.7–86.2)	44.2 (34.5–54.3)
LR +	NA ^a	6.9 (1.0–48.5)
LR –	0.3 (0.2–0.4)	0.7 (0.6–0.9)
CNB + RAS Q61R IHC		
Sensitivity	77.4 (66.9–85.8)	23.8 (14.9–34.6)
Specificity	100 (83.2–100)	100 (85.8–100)
PPV	100 (94.2–100)	100 (82.4–100)
NPV	51.3 (41.5–60.9)	28.2 (25.8–30.8)
Accuracy	81.7 (72.9–88.6)	41.4 (31.8–51.4)
LR +	NA ^a	NA ^a
LR –	0.2 (0.2–0.3)	0.8 (0.7–0.9)
CNB + BRAF V600E IHC + RAS Q61R IHC		
Sensitivity	77.4 (66.9–85.8)	28.8 (19.2–39.9)
Specificity	100 (83.2–100)	95.4 (78.8–99.9)
PPV	100 (94.2–100)	95.8 (76.6–99.4)
NPV	51.3 (41.5–60.9)	28.8 (25.5–32.2)
Accuracy	81.7 (72.9–88.6)	44.2 (34.5–54.3)
LR +	NA ^a	6.9 (1.0–48.5)
LR –	0.2 (0.2–0.3)	0.7 (0.6–0.9)

CNB, core needle biopsy; IHC, immunohistochemistry; CI, confidence interval; PPV, positive predictive value; NPV, negative predictive value; LR, likelihood-ratio; NA, not available.

^aCould not complete the computation because the denominators are 0.

ar features, and Hurthle cell neoplasm [5]. The management approach of thyroid nodule is multidisciplinary; however, the cytology findings of category II typically necessitate a watchful follow-up, often without the need for surgical intervention. This may explain why, among 338 CNB thyroid nodules, only 30.8% received postoperative diagnoses.

Most patients with postoperative diagnosis in this study underwent total thyroidectomy and were classified as CNB category IV. While other clinical considerations may suggest the need for surgical intervention, CNB category IV is not indicated for total thyroidectomy [5]. However, most category IV cases were identified as PTC in postoperative diagnosis, warranting further discussion. A previous study found that a significant proportion of category IV cases in CNB samples exhibited varying risk of malignancy (ROM), with those presenting nuclear atypia showing a higher ROM (40%–62%) [17]. Jung et al. [5] noted that, within category IV, there is a potential for noninvasive follicular thyroid neoplasm with papillary-like feature or an invasive follicular variant of PTC (NIFTP), particularly in those with some nuclear features typical of PTC. A study by Haq et al. [18] also highlighted the need to carefully evaluate the presence of nuclear features that suggest a diagnosis of PTC in category IV. From the substantial findings from previous studies and our cohort, the reclassification of category IV warrants consideration to improve diagnostic accuracy and clinical management.

This study identified several histological subtypes of PTC including classic, tall cell, solid, oncocytic, columnar, and infiltrative-follicular subtypes. Notably, the relative incidence of PTC subtypes in this study differs from a prior study conducted on all resection specimens diagnosed at our institution [11]. In contrast to findings in the study by Harahap et al. [11], the infiltrative follicular subtype was more prevalent than classic PTC in CNB samples with available postoperative diagnosis. This may result from a greater proportion of the classic subtype of PTC being detected early since the papillary architecture of the classic subtype is readily identifiable in FNA. While subtypes such as classic, infiltrative follicular, oncocytic, and solid are predominantly reported as category IV, the tall cell subtype of PTC is frequently presented as category VI (malignancy). The most common pitfall of diagnosing PTC in CNB material is false-negative identification of nuclear features, which is attributable to the smaller and darker chromatin in CNB aspirates compared with surgical specimens [5]. Nevertheless, previous research indicated that the majority of the tall cell subtype exhibits tall columnar cells in CNB specimens, with 41% of samples demonstrating 30% of tall columnar cells, indicative of a tall cell diagnosis [19].

In addition to PTC, we identified other malignant thyroid lesions, including IEFVPTC, DHGTC, PDTC, and oncocytic carcinoma, as well as benign thyroid lesions such as FA and non-neoplastic thyroid lesions like MG in the postoperative di-

Table 6. Association between nodule size and neoplastic postoperative histopathology

Nodule size (cm)	Postsurgery histopathology, n (%)		p-value	OR
	Non-neoplastic (n = 20)	Neoplastic (n = 84)		
>3.0	3 (6.5)	43 (93.5)	.005 ^{ab}	8.19
2.1–3.0	4 (21.1)	15 (78.9)	.287 ^a	2.14
1.1–2.0	4 (26.7)	11 (73.3)	.538 ^a	1.57
<1.0	8 (36.4)	14 (63.6)	Reference	-
Unknown	1 (50)	1 (50)	NA	-

OR, odd ratio; NA, not available.

^aBinary logistic regression; ^bp < 0.05.

Table 7. Association between nodule size and malignant postoperative histopathology

Nodule size (cm)	Postsurgery histopathology, n (%)		p-value	OR
	Non-malignant (n = 24)	Malignant (n = 80)		
>3.0	6 (12.5)	42 (87.5)	.004 ^{ab}	5.83
2.1–3.0	3 (17.6)	14 (82.4)	.077 ^a	3.89
1.1–2.0	4 (26.7)	11 (73.3)	.252 ^a	2.29
<1.0	10 (45.5)	12 (54.5)	Reference	-
Unknown	1 (50)	1 (50)	NA	-

OR, odd ratio; NA, not available.

^aBinary logistic regression; ^bp < 0.05.

agnosis. IEFVPTC is an encapsulated follicular subtype of PTC with invasion and was commonly reported as category IV and category I in the present study. We identified one IEFVPTC case that was reported as category VI. The obscure manifestation of nuclear atypia, along with the lack of tumor invasion, complicates the identification of IEFVPTC in biopsy materials. Despite the predominance of cases in category IV in this study, no NIFTP cases were identified in postoperative diagnoses. The phenomenon can be explained by the rare occurrence of NIFTP in our institutional setting, along with the limited number of thyroid nodule cases included in this study.

DHGTC and PDTC are both rare and underrecognized neoplasms, accounting for less than 3% of all thyroid malignancies [20,21]. Three cases were diagnosed as DHGTC in the present study: the PTC tall cell subtype, the PTC follicular subtype, and oncocytic carcinoma. All DHGTC cases in this study were reported as CNB category IV. In one case of the DHGTC tall cell subtype, the tall cell component was estimated to constitute roughly 30% of the area, while most of the structure was largely follicular. In line with our present finding, oncocytic carcinoma is a rare type of thyroid neoplasm originating from oncocytic cells of the thyroid gland and is commonly reported as category IV in biopsy [22]. Distinguishing oncocytic carcinoma from adenoma, however, requires evidence of capsular and vascular

invasion, which is challenging to assess in biopsy aspirates.

The second most common CNB diagnosis in patients with postoperative diagnosis was category II. Notably, MG constituted 58.8% (20 of 34) of diagnoses in category II (benign lesion). A prior study indicated that category II exhibits the lowest ROM among CNB categories, with values between 2%–6%, as determined by final diagnosis through clinical and/or surgical follow-up [13]. This finding emphasizes the necessity for a careful reevaluation of surgical treatment options for category II, except in cases requiring urgent airway management.

In comparison with US-FNA, CNB has lower rates of inconclusive results [23-26]. Approximately, 20%–30% of FNA are nondiagnostic and require repeated FNA or are treated with unnecessary lobectomy [27-29]. With the use of the relatively bigger gauge needle, CNB is considered more effective at obtaining larger tissue samples than the FNA procedure and allows cytological and architectural evaluation of tumor samples. The present study supports previous findings in which we found a low proportion of inconclusive CNB results. Category I (nondiagnostic) and category III (atypia of undetermined significance) represent only 7.1% and 12.1% of all CNB specimens in the study, respectively. However, compared with category II, categories I and III typically display higher ROM, ranging from 18%–50% and 32%–45%, respectively [13]. A significant

proportion of category III cases is differentially diagnosed as category IV or V because of the obscure presence of nuclear or oncocyctic atypia, a small amount of tumor cells, and the conflicting presence of tumor capsule [13,30]. Similarly, in the present study, all CNB category I cases were diagnosed postoperatively as either PTC or IEFVPTC, whereas CNB category III may be diagnosed postoperatively as FA, PTC, or aggressive PDTC. Therefore, meticulous attention with ongoing monitoring and repeat biopsy procedure is recommended.

In the present study, we found a significant association of CNB category with neoplastic and malignant lesions. CNB achieved a sensitivity of 74% and specificity of 100% in detecting neoplastic lesions. In contrast, CNB yielded a sensitivity of 23.8% and specificity of 100% for detecting malignant lesions. Previous studies reported that the CNB sensitivity for detecting malignancy in thyroid nodules was greater than 90%, with a specificity ranging from 90%–100% [2,3,31,32]. A recent meta-analysis revealed a wider range of CNB sensitivity, ranging from 44.7–85%, with a specificity of 100% [29]. CNB diagnostic performance varies in prior publications, with consistently high specificity but lower sensitivity. While a CNB diagnosis of category V and VI represents true thyroid malignancy in surgical diagnosis, categories I–IV could not exclude the possibility of thyroid malignancy. This is particularly significant as the exclusion of critical features such as vascular and capsular invasion may limit the accuracy of malignancy diagnosis in these categories. The same rationale applies to CNB performance in identifying neoplastic lesions.

This study demonstrated a lower sensitivity and higher specificity for neoplastic lesions, indicating that CNB categories IV–V are specific for neoplastic lesions, and the presence of neoplastic lesions remains possible in CNB categories I–III. This phenomenon may be explained by the non-representative and low-cellularity samples obtained from CNB procedures compared with surgical specimens.

CNB allows IHC examination that aids in diagnosis and predicting tumor behavior [29]. Recent studies reported on the use of molecular testing to identify thyroid nodules in CNB specimens, particularly when initial CNB results are indeterminate [33–35]. In the study by Jung [13], in CNB samples where histologic morphologies indicate a differential diagnosis of categories III and IV, a positive result of RAS Q61R IHC simplifies the decision favoring categorization into category IV. BRAF V600E IHC is useful when CNB samples display nuclear atypia yet lack sufficient histologic features for definitive malignancy features.

These cases may be assigned to category III or category V based on the extent of nuclear atypia and the quantity of atypical cells involved. A positive result of BRAF V600E IHC in indeterminate CNB results typically points toward a definitive diagnosis of PTC [13]. IHC is economical, feasible, and sensitive for detecting *BRAF* V600E and *RAS* Q61R mutations in thyroid nodules [36]. A previous study revealed a sensitivity of 100% and specificity of 42.86% of IHC for detecting *BRAF* V600E mutation [37]. Thus, IHC would be beneficial as a preliminary screening method to detect *BRAF* V600E and *RAS* Q61R mutations [37]. Moreover, Crescenzi et al. [38] found that IHC performed on CNB samples of thyroid nodules perfectly matched the genetic analysis of *BRAF* V600E status.

To the best of our knowledge, this is the first study that incorporated IHC of BRAF V600E and RAS Q61R in addition to CNB. In evaluating the performances for detecting neoplastic lesion by incorporating BRAF V600E IHC, RAS Q61R IHC, or both with CNB, the sensitivity was 74%, 77%, and 77%, respectively. The specificity was 100% for all analyses, while the overall accuracy was 82%. For detection of malignant lesions, incorporating BRAF V600E IHC increased the sensitivity to 28.8% and overall accuracy to 44.2%, while RAS Q61R IHC did not enhance the diagnostic performance of CNB. In our cohort, categories II, IV, and VI remained unchanged with respect to BRAF V600E and RAS Q61R IHC results, while three samples previously classified as category III based on CNB examination alone were reclassified into category IV and one sample initially classified as class V was reclassified as class VI based on BRAF V600E IHC results. The sensitivity increase was not significant compared with that of CNB examination alone, indicating that IHC staining is not clinically meaningful in differentiating neoplasms in thyroid lesions.

In our cohort, the thyroid nodule size was larger than 3 cm, which showed a significant association with neoplastic and malignant postoperative diagnosis and higher odds ratio of being neoplastic and malignant at postoperative diagnosis. Hong et al. [20] stated that malignancy risks increased as the nodule size increased in low- and intermediate-suspicion nodules determined by US results. The malignancy rate of large nodules (≥ 3 cm) was higher than that of small nodules (< 3 cm) in intermediate-suspicion nodules (40.3% vs. 22.6%; $p = .001$) and low-suspicion nodules (11.3% vs. 7.0%; $p = .035$) [20]. In agreement, Hahn et al. [21] reported that thyroid nodules larger than 2 cm are an important factor in the superiority of CNB to FNA in the detection of low-to-intermediate lesions from US. Large

nodules are often heterogeneous and contain areas of both benign and malignant tissues, more complex architecture, and higher proportions of cystic areas; samples obtained by FNA were inadequate for interpretation, leading to higher false-negative results [39].

While the performance of CNB in detecting thyroid neoplastic lesions is satisfactory, its detection of malignant thyroid lesions has not yet reached optimal levels at our institution, particularly compared with prior studies. We attribute this primarily to the limited number of cases involved, limited duration of CNB implementation, and operator skillsets and expertise. Ahn et al. [40] stated that the diagnostic results of CNB may differ by pathologist, operator, and institution.

This study has several limitations. First, it was a retrospective study performed in a tertiary hospital in Indonesia. Thus, there might be concerns of patient selection bias, and the results may not reflect the entire general population. This study did not evaluate operator variability and ultrasonographic features in the performance of CNB. The number of samples with post-operative diagnosis in our study was not large compared with previous studies that included hundreds to thousands of participants. This is because CNB has been applied in our institution only for the previous 2 years, and there have been few cases. However, these limitations can be overcome with prospective, randomized-controlled trials and multicenter studies.

The present study demonstrated a lower rate of inconclusive results and a higher category IV CNB diagnostic rate in the diagnosis of thyroid nodules for CNB compared to FNA. The diagnostic performance of CNB in detecting malignancy was relatively poor, while its performance for detection of neoplastic lesions was stronger.

Ethics Statement

This study was approved by the Faculty of Medicine at Universitas Indonesia's Institutional Review Board and performed following the 2013 revision of the Declaration of Helsinki (IRB No: KET-1316/UN2.F1/ETIK/PPM.00.02/2023). Informed consent was waived by the board (No-602/UN2.F1/ETIK/PPM.00.02/2024).

Availability of Data and Material

All data analyzed during this study are included in this published article.

Code Availability

Not applicable.

ORCID

Agnes Stephanie Harahap <https://orcid.org/0000-0001-8920-7873>

Maria Francisca Ham <https://orcid.org/0000-0002-7915-5536>

Retno Asti Werdhani <https://orcid.org/0000-0002-3280-4295>

Erwin Danil Julian <https://orcid.org/0000-0003-4149-4281>

Rafi Ilmansyah <https://orcid.org/0000-0002-1074-4252>

Chloe Indira Arfelita Mangunkusumso <https://orcid.org/0009-0001-8757-7982>

Tri Juli Edi Tarigan <https://orcid.org/0000-0001-6086-700X>

Author Contributions

Conceptualization: ASH, MFH, TJET, RAW, EDJ. Data curation: ASH, MFH, TJET, EDJ, RI, CIAM. Formal analysis: ASH, TJET, RAW, EDJ, RI, CIAM. Funding acquisition: ASH, MFH, TJET, RAW, EDJ. Investigation: ASH, MFH, TJET, EDJ. Methodology: ASH, TJET, RAW, EDJ. Project administration: RI, CIAM. Resources: ASH, MFH, TJET, RAW, EDJ. Supervision: MFH, EDJ. Validation: ASH, MFH, TJET, RAW, EDJ. Visualization: ASH. Writing – original draft: ASH, RI. Writing – review & editing: ASH, MFH, TJET, RAW, EDJ, RI, CIAM. Approval of final manuscript: all authors.

Conflicts of Interest

The authors declare that they have no potential conflicts of interest.

Funding Statement

This research was funded by Dr. Cipto Mangunkusumo Hospital Operational and Innovation Research Grant 2024.

REFERENCES

1. Suh CH, Baek JH, Lee JH, et al. The role of core-needle biopsy in the diagnosis of thyroid malignancy in 4580 patients with 4746 thyroid nodules: a systematic review and meta-analysis. *Endocrine* 2016; 54: 315-28.
2. Chung SR, Baek JH, Choi YJ, et al. The role of core needle biopsy for the evaluation of thyroid nodules with suspicious ultrasound features. *Korean J Radiol* 2019; 20: 158-65.
3. Cortazar-Garcia R, Martin-Escalante MD, Robles-Cabeza L, Martinez-Santos C. Usefulness of ultrasound-guided core biopsy

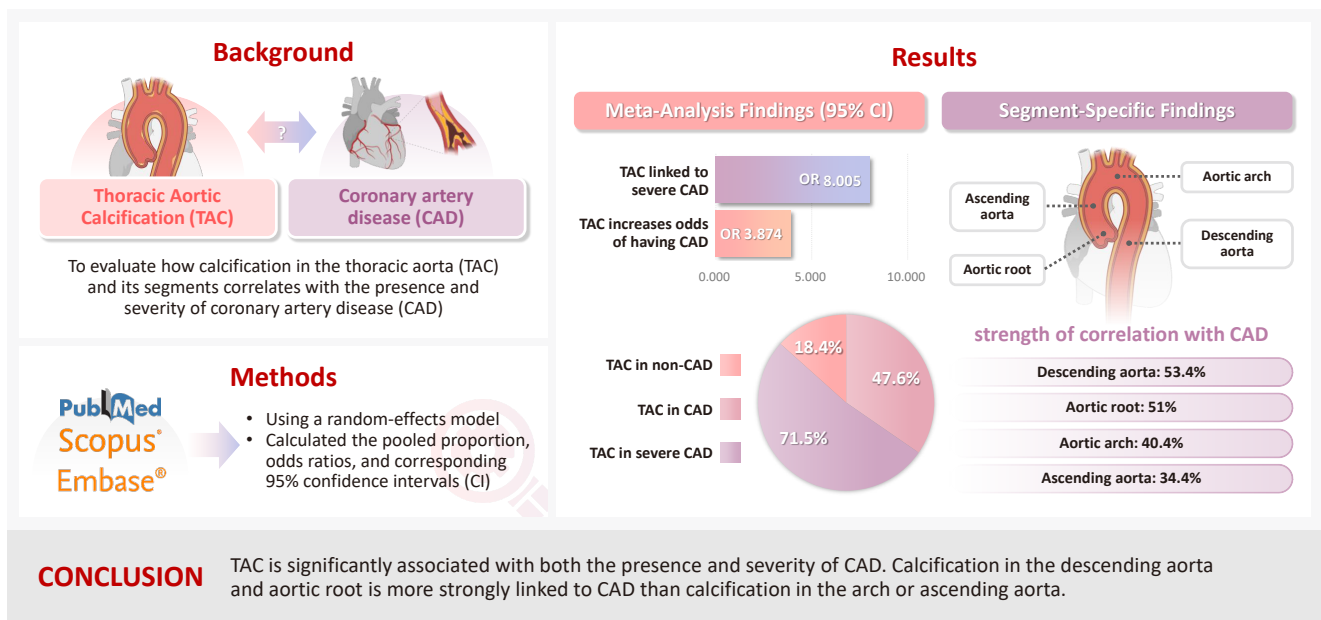
- in thyroid nodules with inconclusive fine-needle aspiration biopsy findings. *Radiologia (Engl Ed)* 2022; 64: 195-205.
4. AlSaedi AH, Almalki DS, ElKady RM. Approach to thyroid nodules: diagnosis and treatment. *Cureus* 2024; 16: e52232.
 5. Jung CK, Baek JH, Na DG, Oh YL, Yi KH, Kang HC. 2019 Practice guidelines for thyroid core needle biopsy: a report of the Clinical Practice Guidelines Development Committee of the Korean Thyroid Association. *J Pathol Transl Med* 2020; 54: 64-86.
 6. Na DG, Baek JH, Jung SL, et al. Core needle biopsy of the thyroid: 2016 consensus statement and recommendations from Korean Society of Thyroid Radiology. *Korean J Radiol* 2017; 18: 217-37.
 7. Yeon JS, Baek JH, Lim HK, et al. Thyroid nodules with initially nondiagnostic cytologic results: the role of core-needle biopsy. *Radiology* 2013; 268: 274-80.
 8. Jung CK, Baek JH. Recent advances in core needle biopsy for thyroid nodules. *Endocrinol Metab (Seoul)* 2017; 32: 407-12.
 9. Gharib H, Papini E, Garber JR, et al. American Association of Clinical Endocrinologists, American College of Endocrinology, and Associazione Medici Endocrinologi medical guidelines for clinical practice for the diagnosis and management of thyroid nodules: 2016 update. *Endocr Pract* 2016; 22: 622-39.
 10. Chen D, Qi W, Zhang P, et al. Investigation of BRAF V600E detection approaches in papillary thyroid carcinoma. *Pathol Res Pract* 2018; 214: 303-7.
 11. Harahap AS, Subekti I, Panigoro SS, et al. Profile of *BRAF*V600E, *BRAF*K601E, *NRAS*, *HRAS*, and *KRAS* mutational status, and clinicopathological characteristics of papillary thyroid carcinoma in Indonesian national referral hospital. *Appl Clin Genet* 2023; 16: 99-110.
 12. Su X, Jiang X, Xu X, et al. Diagnostic value of *BRAF* (V600E)-mutation analysis in fine-needle aspiration of thyroid nodules: a meta-analysis. *Onco Targets Ther* 2016; 9: 2495-509.
 13. Jung CK. Reevaluating diagnostic categories and associated malignancy risks in thyroid core needle biopsy. *J Pathol Transl Med* 2023; 57: 208-16.
 14. Jung CK, Bychkov A, Kakudo K. Update from the 2022 World Health Organization classification of thyroid tumors: a standardized diagnostic approach. *Endocrinol Metab (Seoul)* 2022; 37: 703-18.
 15. Capper D, Preusser M, Habel A, et al. Assessment of *BRAF* V600E mutation status by immunohistochemistry with a mutation-specific monoclonal antibody. *Acta Neuropathol* 2011; 122: 11-9.
 16. Crescenzi A, Fulciniti F, Bongiovanni M, Giovanella L, Trimboli P. Detecting *N-RAS* Q61R mutated thyroid neoplasias by immunohistochemistry. *Endocr Pathol* 2017; 28: 71-4.
 17. Na HY, Woo JW, Moon JH, et al. Preoperative diagnostic categories of noninvasive follicular thyroid neoplasm with papillary-like nuclear features in thyroid core needle biopsy and its impact on risk of malignancy. *Endocr Pathol* 2019; 30: 329-39.
 18. Haq F, Bychkov A, Jung CK. A matched-pair analysis of nuclear morphologic features between core needle biopsy and surgical specimen in thyroid tumors using a deep learning model. *Endocr Pathol* 2022; 33: 472-83.
 19. Ahn J, Jin M, Kim WG, et al. Limitations of fine-needle aspiration and core needle biopsies in the diagnosis of tall cell variant of papillary thyroid carcinoma. *Clin Endocrinol (Oxf)* 2023; 98: 110-6.
 20. Hong MJ, Na DG, Baek JH, Sung JY, Kim JH. Impact of nodule size on malignancy risk differs according to the ultrasonography pattern of thyroid nodules. *Korean J Radiol* 2018; 19: 534-41.
 21. Hahn SY, Shin JH, Oh YL, Park KW, Lim Y. Comparison between fine needle aspiration and core needle biopsy for the diagnosis of thyroid nodules: effective indications according to US findings. *Sci Rep* 2020; 10: 4969.
 22. Kiran T, Guler B. The histopathologic checkpoints for thyroid core needle biopsy compared with resection sections. *Pol J Pathol* 2022; 73: 310-9.
 23. Choi YJ, Baek JH, Suh CH, et al. Core-needle biopsy versus repeat fine-needle aspiration for thyroid nodules initially read as atypia/follicular lesion of undetermined significance. *Head Neck* 2017; 39: 361-9.
 24. Chen Z, Wang JJ, Guo DM, Zhai YX, Dai ZZ, Su HH. Combined fine-needle aspiration with core needle biopsy for assessing thyroid nodules: a more valuable diagnostic method? *Ultrasonography* 2023; 42: 314-22.
 25. Jung SM, Koo HR, Jang KS, et al. Comparison of core-needle biopsy and repeat fine-needle aspiration for thyroid nodules with inconclusive initial cytology. *Eur Arch Otorhinolaryngol* 2021; 278: 3019-25.
 26. Su X, Yue C, Yang W, Ma B. A comparative analysis of core needle biopsy and repeat fine needle aspiration in patients with inconclusive initial cytology of thyroid nodules. *Front Endocrinol (Lausanne)* 2024; 15: 1309005.
 27. Paja M, Del Cura JL, Zabala R, Korta I, Ugalde A, Lopez JL. Core-needle biopsy in thyroid nodules: performance, accuracy, and complications. *Eur Radiol* 2019; 29: 4889-96.
 28. Jeong SY, Baek JH, Chung SR, et al. Diagnostic performance of core needle biopsy for characterizing thyroidectomy bed lesions. *Korean J Radiol* 2022; 23: 1019-27.

29. Suh CH, Baek JH, Park C, Choi YJ, Lee JH. The role of core needle biopsy for thyroid nodules with initially indeterminate results on previous fine-needle aspiration: a systematic review and meta-analysis. *AJNR Am J Neuroradiol* 2017; 38: 1421-6.
30. Harahap AS, Jung CK. Educational exchange in thyroid core needle biopsy diagnosis: enhancing pathological interpretation through guideline integration and peer learning. *J Pathol Transl Med* 2024; 58: 205-13.
31. Kim K, Bae JS, Kim JS, Jung SL, Jung CK. Diagnostic performance of thyroid core needle biopsy using the revised reporting system: comparison with fine needle aspiration cytology. *Endocrinol Metab (Seoul)* 2022; 37: 159-69.
32. Suh CH, Baek JH, Choi YJ, et al. Efficacy and safety of core-needle biopsy in initially detected thyroid nodules via propensity score analysis. *Sci Rep* 2017; 7: 8242.
33. Jang EK, Kim WG, Kim EY, et al. Usefulness of *NRAS* codon 61 mutation analysis and core needle biopsy for the diagnosis of thyroid nodules previously diagnosed as atypia of undetermined significance. *Endocrine* 2016; 52: 305-12.
34. Kim TH, Jeong DJ, Hahn SY, et al. Triage of patients with AUS/FLUS on thyroid cytopathology: effectiveness of the multimodal diagnostic techniques. *Cancer Med* 2016; 5: 769-77.
35. Trimboli P, Guidobaldi L, Amendola S, et al. Galectin-3 and HBME-1 improve the accuracy of core biopsy in indeterminate thyroid nodules. *Endocrine* 2016; 52: 39-45.
36. Riju J, Thomas N, Paul TV, et al. Role of genetic testing in the management of indeterminate thyroid nodules in the Indian setting. *Indian J Endocrinol Metab* 2024; 28: 3-10.
37. Zhang Y, Liu L, Liu Y, Cao N, Wang L, Xing C. Clinical significance of immunohistochemistry to detect *BRAF* V600E mutant protein in thyroid tissues. *Medicine (Baltimore)* 2021; 100: e25566.
38. Crescenzi A, Guidobaldi L, Nasrollah N, et al. Immunohistochemistry for *BRAF*(V600E) antibody VE1 performed in core needle biopsy samples identifies mutated papillary thyroid cancers. *Horm Metab Res* 2014; 46: 370-4.
39. Kang S, Kim E, Lee S, et al. Do large thyroid nodules (≥ 4 cm) without suspicious cytology need surgery?. *Front Endocrinol (Lausanne)* 2023; 14: 1252503.
40. Ahn HS, Youn I, Na DG, Kim SJ, Lee MY. Diagnostic performance of core needle biopsy as a first-line diagnostic tool for thyroid nodules according to ultrasound patterns: Comparison with fine needle aspiration using propensity score matching analysis. *Clin Endocrinol (Oxf)* 2021; 94: 494-503.

Thoracic aortic calcification as a predictor of coronary artery disease: a systematic review and meta-analysis

Hussein Nafakhi¹, Alaa Salah Jumaah², Akeel Abed Yasseen²

Graphical abstract



Thoracic aortic calcification as a predictor of coronary artery disease: a systematic review and meta-analysis

Hussein Nafakhi¹, Alaa Salah Jumaah², Akeel Abed Yasseen²

¹Department of Internal Medicine, Faculty of Medicine, University of Kufa, Kufa, Iraq

²Department of Pathology and Forensic Medicine, Faculty of Medicine, University of Kufa, Kufa, Iraq

Background: The relationship between coronary atherosclerosis (progression, outcome) and calcification in the thoracic aorta (TAC), particularly across its various segments, is complex and often shows conflicting associations in the literature. To address this debated and complex relationship, we aimed to evaluate how TAC and its segments correlate with the presence and severity of coronary artery disease (CAD). **Methods:** We reviewed all articles published between January 1990 and September 2024 that examined the link between TAC and CAD and were indexed in PubMed, Scopus, or EMBASE. Using a random-effects model, we calculated pooled proportions, odds ratios, and corresponding 95% confidence intervals (CIs) to evaluate the association between TAC and CAD, with consideration of severity. **Results:** The study included 17 studies with 8,187 participants, 2,775 of whom had CAD (1,059 with severe CAD), and 5,412 of whom did not. The pooled odds ratio of TAC in patients with CAD compared to that in those without was 3.874 (95% CI, 2.789 to 5.381). For severe CAD versus mild CAD, the odds ratio was 8.005 (95% CI, 2.611 to 24.542). Calcification of the aortic root (pooled proportion, 51%; 95% CI, 0.282 to 0.733) or descending aorta (pooled proportion, 53.4%; 95% CI, 0.341 to 0.718) had the strongest association with CAD compared to calcification of the arch or ascending aorta. **Conclusions:** TAC is significantly associated with both the presence and severity of CAD. Calcification in the descending aorta and aortic root is more strongly linked to CAD than calcification in the arch or ascending aorta.

Keywords: Coronary artery disease; Aortic calcification; Thoracic aorta; Meta-analysis

INTRODUCTION

The aorta, the body's largest elastic artery, is located in close proximity to the coronary arteries and heart. Due to its large surface area, it is particularly susceptible to the harmful effects of cardiovascular risk factors, leading to atherosclerotic plaques [1,2].

Coronary artery calcification (CAC) and thoracic aortic calcification (TAC) share common risk factors, such as diabetes, aging, hypertension, and smoking, despite differences in their embryology and calcification patterns [3,4].

TAC can be detected using the same imaging protocols employed for CAC, and it can be identified easily through chest radiography and computed tomography (CT) imaging, which

are often used for non-cardiac screenings or cardiovascular risk assessments [5,6]. Several clinical studies have explored the associations between TAC, its individual segments, and coronary artery disease (CAD), demonstrating that TAC helps to predict CAD and cardiovascular risk by indicating increased arterial stiffening without requiring additional radiation or cost [2,3,7,8].

While CAC is widely recognized as a reliable predictor of CAD and coronary adverse events across several guidelines, neither the primary prevention guidelines of the European Society of Cardiology nor those of the American College of Cardiology/American Heart Association incorporate aortic calcification in their stepwise approach to preventing major adverse cardiac events in patients with atherosclerotic cardiovascular

Received: November 5, 2024 **Revised:** January 7, 2025 **Accepted:** March 4, 2025

Corresponding Author: Akeel Abed Yasseen, PhD

Department of Pathology and Forensic Medicine, Faculty of Medicine, University of Kufa, Kufa, P.O. Box 21, Iraq

Tel: +964-7811131586, E-mail: akeelyasseen@uokufa.edu.iq

This is an Open Access article distributed under the terms of the Creative Commons Attribution Non-Commercial License (<https://creativecommons.org/licenses/by-nc/4.0/>) which permits unrestricted non-commercial use, distribution, and reproduction in any medium, provided the original work is properly cited.

© 2025 The Korean Society of Pathologists/The Korean Society for Cytopathology

disease [2].

Large population-based studies such as the Multi-Ethnic Study of Atherosclerosis (MESA) and the Heinz Nixdorf Recall (HNR) study have reported an age- and sex-related distribution of TAC that is like that of CAC. However, the prevalence rates of CAC and TAC vary between studies. For example, in MESA, the TAC prevalence was 28%, while CAC was present in about 50% of patients, with TAC showing independent predictive value for CAD in women but not in men [9-11]. In contrast, the HNR study found a TAC prevalence of 63.1% and a CAC prevalence of 67.9% [10-12].

In the literature, the relationship between coronary atherosclerosis and TAC, including its various segments, remains complex, with contradictory findings reported in studies using the MESA database [2,13,14].

The present study seeks to address this gap by estimating a more accurate prevalence of TAC in patients with CAD and evaluating its severity using various imaging modalities. Additionally, we conducted a subgroup analysis to assess the relationship between calcification in different segments of the thoracic aorta—the aortic root, arch, ascending aorta, and descending aorta—and the presence of CAD.

MATERIALS AND METHODS

Study protocol

This meta-analysis followed the guidelines of the Preferred Reporting Items for Systematic Reviews and Meta-Analyses statement [15]. The protocol for the study was not registered in any database.

Search strategy

We conducted a comprehensive electronic search of the PubMed Central, Scopus, and EMBASE literature databases from January 1990 to September 2024. No language restrictions were applied during the search, although all included articles were published in English. We used a combination of the following search terms: “thoracic aorta calcification,” “aortic calcification,” “aortic root calcification,” “arch of aorta calcification,” “ascending aorta calcification,” “descending aorta calcification,” “coronary atherosclerosis,” “coronary artery calcification,” and “coronary artery disease.” In addition, the reference lists of relevant studies were manually searched to identify other pertinent publications.

CAD and TAC definitions

CAD is defined as stenosis of any severity in at least one coronary arterial segment. However, the definition of CAD severity varies across studies. For example, one study used conventional angiography to categorize CAD as mild (0%–50% stenosis), severe (51%–99% stenosis), or advanced (100% luminal stenosis) [14]. Another study defined severe CAD based on coronary angiography results that led to stent placement or bypass surgery [16]. Some studies classified patients by Syntax score, with a low score defined as ≤ 22 points and a high score defined as > 22 points [17]. In our study, severe CAD was considered present when coronary stenosis was $\geq 50\%$, a high Syntax score was recorded, or stent placement or bypass surgery was required. Patients with stenosis severity $< 50\%$ or a low Syntax score were classified as having mild CAD. TAC was defined as the sum of calcium scores in the ascending and descending aortas or the presence of calcification in any aortic segment, as detected by CT imaging, chest radiography, or echocardiography.

Inclusion criteria

This investigation encompassed all studies involving CAD patients as the experimental group and non-CAD patients as the control group, with documented sample sizes for both groups. Additionally, quantitative TAC measurements obtained via CT, echocardiography, or plain chest radiography were included, provided they were classified under the same category. Finally, studies comparing TAC prevalence between CAD and non-CAD groups, along with those with full-text versions available in English, were included.

Exclusion criteria

Literature reviews, case reports, letters to the editor, editorials, or studies without original data were excluded. Similarly, animal studies and studies lacking sufficient information on sample sizes, CAD versus non-CAD groups, or those presenting TAC solely as a continuous or median variable instead of a binary variable were excluded. Finally, duplicate publications identified through reference checking or bibliographic databases and non-English articles were removed from consideration.

Statistical analysis

We used a random-effects model to estimate pooled proportions, odds ratios (ORs), and corresponding 95% confidence intervals (CIs) for the association between TAC and CAD, as well as the severity of CAD. This model accounts for potential vari-

ability across studies, considering differences in study design, population, and methodology. The analysis was performed using the Comprehensive Meta-Analysis software (Biostat, Inc; Englewood, NJ, USA) [18].

Heterogeneity assessment

To assess variability in effect sizes across studies, we used a multi-pronged approach. Formal heterogeneity testing included Cochran's Q statistic, I-squared (I^2) to quantify the percentage of variability due to heterogeneity, and Tau-squared (τ^2) to estimate between-study variance. I^2 values were interpreted using established guidelines [19,20]: 0%–25% suggested low or no heterogeneity, 25%–50% moderate, 50%–75% substantial, and 75%–100% considerable heterogeneity. Observed heterogeneity, reflected in I^2 values, was partly attributed to differences in methodological approaches used for assessing the thoracic aorta.

In this study, both the I^2 test and τ^2 test were used to explore heterogeneity. The τ^2 test quantifies the amount of heterogeneity by estimating the between-study variance, which represents the variability in true effect sizes across studies. As a general rule, a larger τ^2 value indicates greater heterogeneity; $\tau^2 = 0$ indicates no significant heterogeneity, while $\tau^2 > 0$ indicates significant heterogeneity.

Publication bias assessment

We evaluated publication bias using funnel plots and Egger's regression test. Publication bias occurs when studies with statistically significant results are more likely to be published than those with non-significant findings. Egger's regression test was employed to assess publication bias. $p < .05$ suggests asymmetry in the funnel plot, indicating a potential risk of bias. Conversely, $p > .05$ suggests no strong evidence of bias.

Study quality assessment

The Quality Assessment Tool for Diagnostic Accuracy Studies-2 (QUADAS-2) was used to evaluate the risk of bias in the included studies. This tool assesses four domains related to study design (patient selection, index test, reference standard, and flow and timing) and three domains concerning applicability (patient selection, index test, and reference standard). Signaling questions in each domain helped assess potential bias, with responses categorized as "yes," "no," or "unclear." Based on the QUADAS-2 scoring system, the overall risk of bias was judged as "low," "high," or "unclear." If a study scored "low" in all domains related to bias or applicability, it was regarded as

displaying "low risk for both." Conversely, if the study scored "high" or "unclear" in one or more domains, it was judged as having a "risk of bias" or "applicability concern" [21].

RESULTS

Study characteristics and quality assessment

A total of 647 potentially relevant studies was identified through the electronic literature search. Following a rigorous screening process, 563 studies were excluded based on pre-defined criteria. The remaining 84 full-text articles underwent eligibility assessment, and 17 studies were included in the final meta-analysis (Fig. 1) [5,6,8,14,16,17,22-32].

The risk of bias and applicability concerns of the included studies were assessed using the QUADAS-2 tool, with most studies demonstrating low risk (Supplementary Fig. S1). The study characteristics are summarized in Table 1. The included studies involved 8,187 individuals, 2,775 of whom were assigned to the CAD group and 5,412 of whom were assigned to the non-CAD group. Within the CAD group, 1,576 patients had mild CAD, while 1,059 had severe CAD. Separately, a total of 1,366 patients was identified as having TAC. The pooled proportion of TAC was 0.476 (95% CI, 0.365 to 0.590) (Table 2). The study publication dates spanned from 1996 to 2022, with all articles published in English. Methods for detecting TAC included CT ($n = 12$), chest radiography ($n = 3$), and echocardiography ($n = 2$).

Frequency and subgroup analysis

The overall proportion of TAC in CAD patients was 47.6% (pooled proportion, 0.476; 95% CI, 0.365 to 0.590). Due to significant heterogeneity ($I^2 = 96.36\%$, $p < .001$, $\tau^2 = 0.866$), a random-effects model was used. Publication bias was evaluated using funnel plots and Egger's regression test (Table 2, Fig. 2).

The problem of heterogeneity was solved by adopting a random-effects model throughout the analysis. On other hand, subgroup analysis was performed with regard to the TAC detection method and study location.

Subgroup analyses explored potential sources of heterogeneity, including study location (Asia, the United States, or Europe), as shown in Supplementary Fig. S2, and the TAC detection method (CT, echocardiography, or chest radiography), as depicted in Supplementary Fig. S3.

Sensitivity analysis

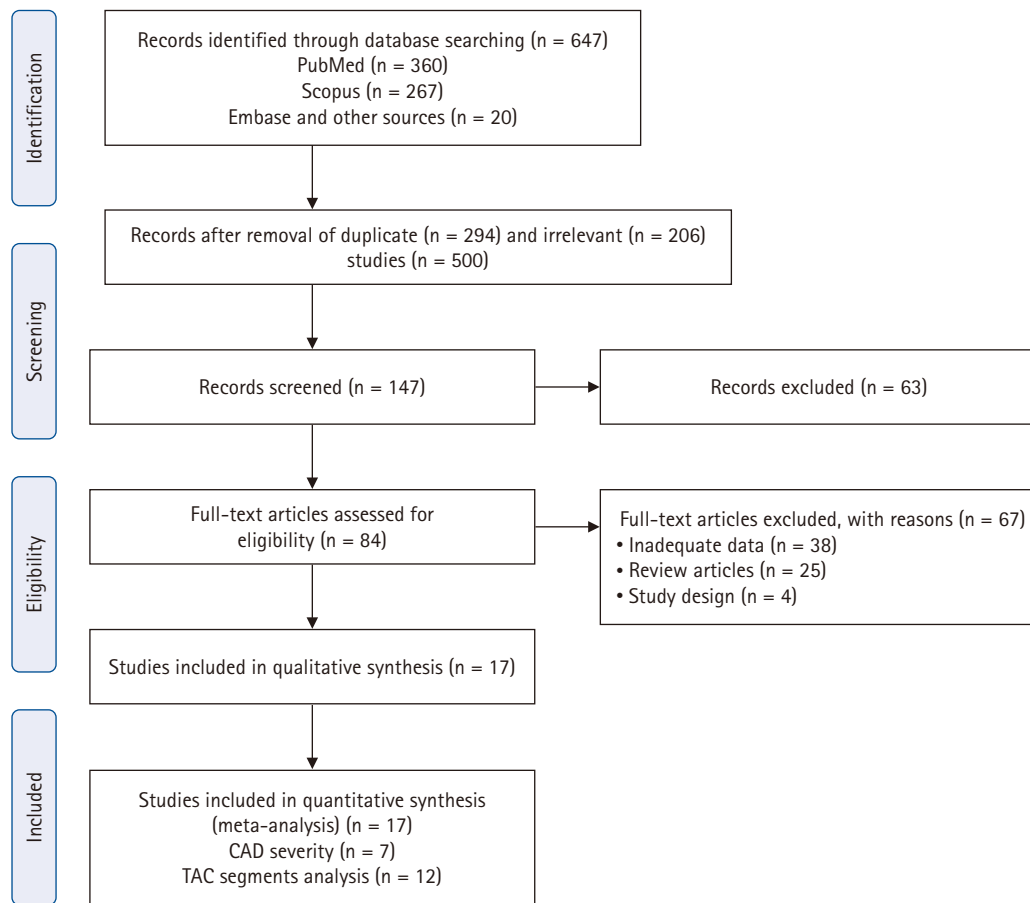


Fig. 1. Study flowchart. CAD, coronary artery disease; TAC, thoracic aortic calcification.

To ensure the reliability of our findings, we performed sensitivity analyses by omitting individual studies from the meta-analysis and recalculating the pooled proportion. This approach helped assess the impact of each study on the overall results. The findings, presented in [Supplementary Table S1](#), indicate that our results were stable. Omitting individual studies did not significantly alter the pooled estimates, demonstrating that the findings are robust and not overly dependent on any single study.

Clinical and demographic data characteristics

We extracted clinical and demographic data from the eligible studies included in the meta-analysis, focusing on the pooled proportions and ORs for various variables. The pooled mean age of participants was 61.3 years (standard error, 1.292).

TAC

The pooled proportion of TAC in patients with CAD was 47.6%

(95% CI, 0.365 to 0.590), whereas, in non-CAD patients, it was 18.4% (95% CI, 0.113 to 0.287) as shown in [Table 2](#), [Fig. 2](#), and [Supplementary Fig. S4](#). In mild CAD, the proportion of TAC was 25.1% (95% CI, 0.086 to 0.544), while in severe CAD was 71.5% (95% CI, 0.287 to 0.940) as shown in [Table 2](#) and [Supplementary Figs. S5 and S6](#).

The proportion of TAC by site in CAD patients was as follows. In the aortic arch, it was 40.4% (95% CI, 0.184 to 0.670); in the aortic root, it was 51% (95% CI, 0.282 to 0.733); in the ascending aorta, it was 34.4% (95% CI, 0.117 to 0.673); and, in the descending aorta, it was 53.4% (95% CI, 0.341 to 0.718), as shown in [Fig. 3](#) and [Supplementary Table S2](#). These results suggest a significant association ($p < .001$) between TAC and CAD. Moreover, TAC may indicate a greater likelihood of severe CAD, with calcification in the descending aorta and aortic root showing stronger associations with CAD compared to that in the ascending aorta and aortic arch.

Table 1. Study characteristics

Study	Study sample size (CAD)	TAC in CAD	TAC in CAD proportion	Study country	Method used for detection of TAC	Thoracic aorta site
Parthenakis et al. (1996) [31]	28	10	0.357	Greece	Echocardiography	TAC
Li et al. (2002) [16]	570	329	0.577	USA	Chest radiography	Arch
Yamamoto et al. (2003) [14]	56	21	0.375	USA	CT	TAC, ascending, descending
Takasu et al. (2003) [27]	37	15	0.405	USA	CT	Descending
Watanabe et al. (2003) [24]	141	55	0.390	Japan	CT	Descending
Atak et al. (2004) [23]	61	28	0.459	Turkey	Chest radiography	TAC
Goland et al. (2008) [22]	60	41	0.683	USA	Echocardiography	ARC
Takeda et al. (2009) [26]	47	33	0.702	Japan	CT	Descending
Kim et al. (2011) [5]	120	77	0.642	Soth Korea	CT	TAC
Yuce et al. (2015) [25]	92	50	0.543	Turkey	CT	Descending
Nafakhi et al. (2015) [28]	54	17	0.315	Iraq	CT	ARC
Hu et al. (2015) [29]	101	50	0.495	Germany	CT	ARC
Tesche et al. (2017) [30]	105	57	0.543	USA	CT	ARC
Kim et al. (2017) [6]	74	9	0.122	USA	CT	TAC
Ma et al. (2019) [17]	597	84	0.141	China	Chest radiography	Arch
van 't Klooster et al. (2020) [8]	474	335	0.707	Netherland	CT	TAC
Otsuka et al. (2022) [32]	158	119	0.753	Japan	CT	TAC

CAD, coronary artery disease; TAC, thoracic aortic calcification; CT, computed tomography; ARC, aortic root calcification.

Table 2. The associations of TAC with CAD and its severity

Variable	Pooled proportion (95% CI, %)	No. of studies	p-value	Heterogeneity testing			Publication bias (Egger's regression test)		Model
				I ²	p-value	τ ²	Intercept (95% CI)	p-value	
TAC in CAD	0.476 (0.365 to 0.590)	17	.684	96.36	<.001	0.866	-1.680 (-7.960 to 4.580)	.570	Random effect
TAC in non-CAD	0.184 (0.113 to 0.287)	17	<.001	96.818	<.001	1.365	1.692 (-2.807 to 6.193)	.217	Random effect
TAC in mild CAD	0.251 (0.086 to 0.544)	7	.091	98.127	<.001	2.826	-4.372 (-22.151 to 13.405)	.277	Random effect
TAC in severe CAD	0.715 (0.287 to 0.940)	7	.325	98.439	<.001	5.907	8.888 (-2.444 to 20.221)	.049	Random effect

TAC, thoracic aortic calcification; CAD, coronary artery disease; CI, confidence interval.

TAC in relation to CAD severity

The ORs for TAC compared between CAD and non-CAD patients, as well as those compared between severe and mild CAD, are provided in Table 3 and Supplementary Figs. S7 and S8.

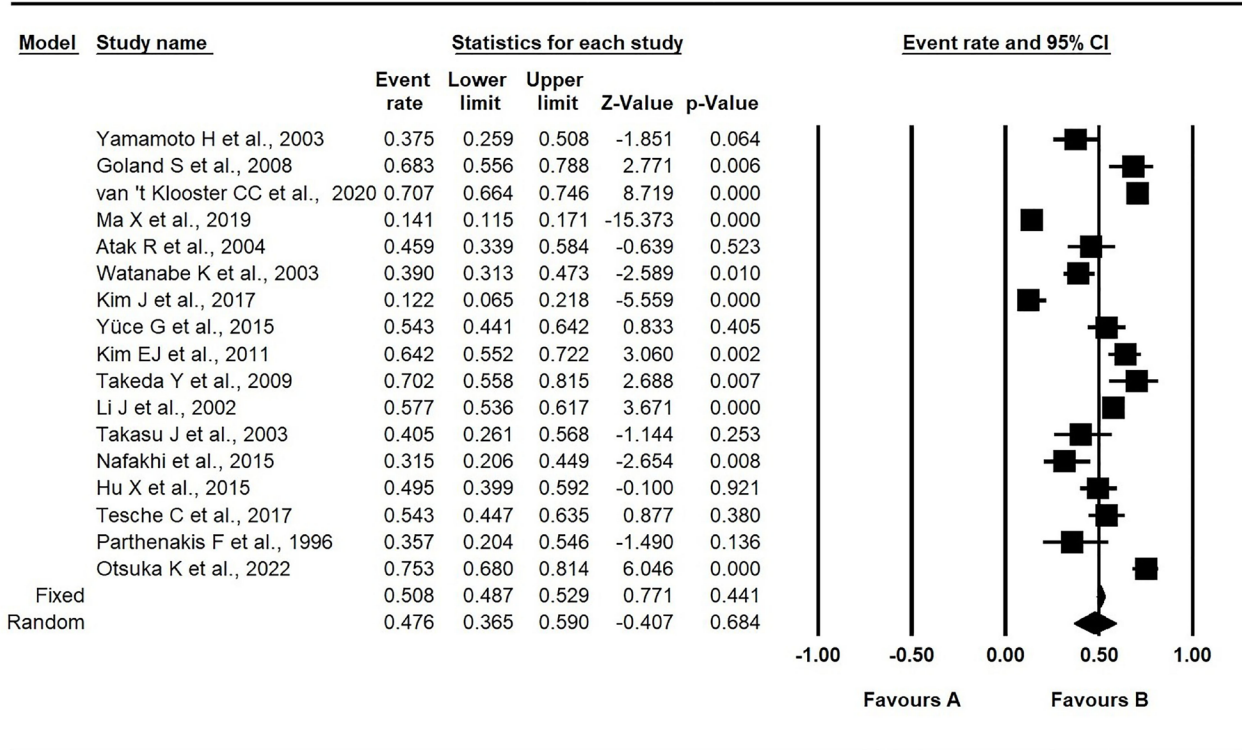
The pooled OR for TAC in CAD versus non-CAD cases was 3.874 (95% CI, 2.789 to 5.381) as depicted in Table 2 and Supplementary Fig. S7. On other hand, the pooled OR for TAC in severe CAD versus mild CAD was 8.005 (95% CI, 2.611 to 24.542), as noted in Table 2 and Supplementary Fig. S8.

These findings suggest that the presence of TAC increases the risk of CAD by four times and the risk of severe CAD by eight times.

DISCUSSION

This meta-analysis and systematic review found three key results: (1) TAC was significantly linked to CAD, despite variations between the studies analyzed. These differences were addressed using a random-effects model to calculate pooled proportions and ORs; (2) TAC was strongly associated with severe CAD; and (3) calcification in the descending segment and aortic root of the thoracic aorta showed a stronger correlation with CAD than that in the aortic arch or ascending segment. However, significant heterogeneity was observed between the included studies. This variation is most likely attributable to

Meta-analysis: All Cases



Meta Analysis

Fig. 2. Forest plot showing pooled proportions of thoracic aorta calcification in patients with coronary artery disease [5,6,8,14,16,17,22-32]. CI, confidence interval.

several factors, including geographical differences in patient populations. Diverse ethnicities and environmental exposures can influence both the prevalence and severity of TAC in CAD. The second factor is detection methods, where techniques with lower sensitivity or specificity may fail to detect the disease or produce false positives, contributing to heterogeneity. The third factor is the inclusion criteria employed by individual studies, as stricter criteria might result in a lower prevalence compared to broader inclusion criteria.

Atherosclerosis is a gradual systemic disease that starts in childhood, first affecting the aorta. Over time, it evolves from fatty streaks to more severe lesions, causing changes in blood flow in adulthood [14]. Some studies suggest that changes in the aorta, especially in the aortic root and abdominal aorta, occur before coronary atherosclerosis or cardiovascular disorders, even in patients who have no CAC or normal myocardial perfusion scans [33,34].

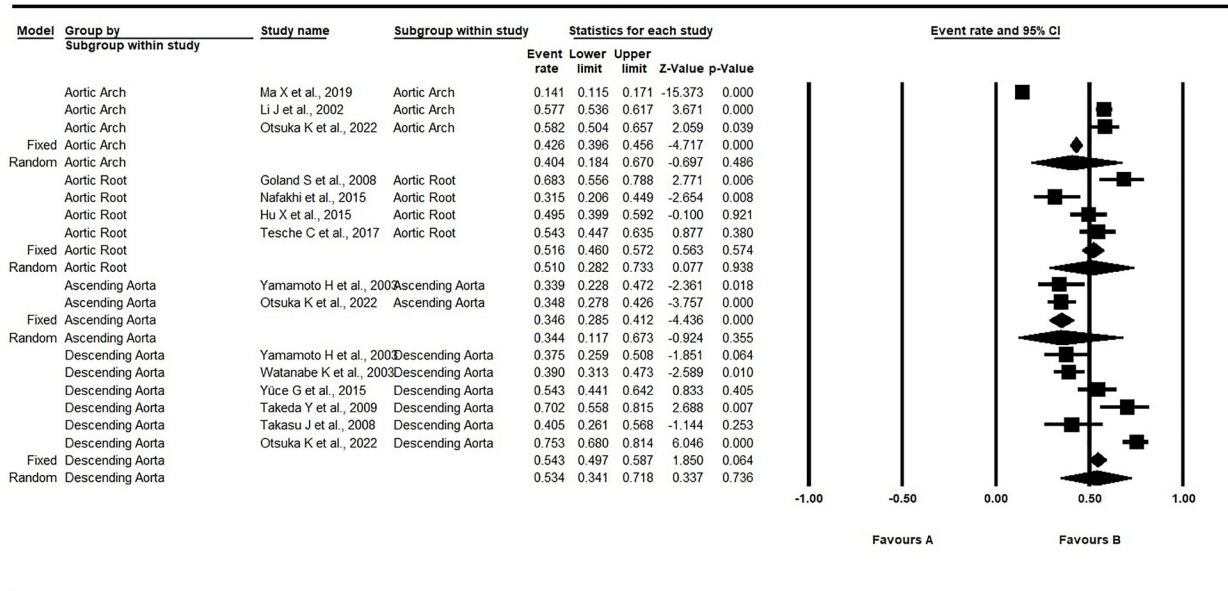
Much of the data connecting TAC and CAD are from studies on CAC. Previous research shows a strong relationship between

TAC and CAC, implying that TAC may provide valuable insights into overall coronary risk and could support the need for early screening and aggressive management of modifiable risk factors [5,6].

The findings from two large studies, MESA and HNR, align with the results of the present meta-analysis [6,11]. Kim et al. [6] reported a strong association between TAC and incident cardiovascular disease, including CAD and all-cause mortality, in unadjusted analyses of 3,415 MESA participants with baseline CAC = 0 over a median follow-up of 11 years. Similarly, Kalsch et al. [11] demonstrated that TAC progression was positively associated with incident hard coronary events after adjusting for baseline cardiovascular risk factors and CAC in 3,080 participants based on HNR study data. These findings suggest TAC as a surrogate marker for CAD risk. These population-based cohort studies support the use of TAC as a marker for CAD presence and its potential predictive role for adverse coronary events, in addition to conventional cardiovascular risk factors.

In this meta-analysis, various imaging methods were used to

Meta-analysis



Meta Analysis

Fig. 3. Subgroup analysis was performed with respect to the site complicated by thoracic aortic calcification (TAC)—whether the aortic root, aortic arch, or ascending or descending aorta. Calcification in the descending aorta and aortic root showed stronger associations with coronary artery disease (CAD) compared to that in the ascending aorta and aortic arch [12,14,16,17,22,24–26,28–30,32]. CI, confidence interval.

Table 3. Pooled odd ratios of TAC in patients with CAD

Variable	Pooled odd ratio (95% CI)	No. of studies	p-value	heterogeneity			Publication bias (Egger's regression test)		Model
				I ²	p-value	τ ²	Intercept (95% CI)	p-value	
TAC in CAD vs. TAC in non-CAD	3.874 (2.789–5.381)	17	<.001	71.749	<.001	0.323	1.590 (-1.966 to 5.147)	.177	Random effects
TAC in severe CAD vs. TAC in mild CAD	8.005 (2.611–24.542)	7	<.001	90.946	<.001	1.9996	-5.714 (-12.970 to 1.541)	.049	Random effects

TAC, thoracic aortic calcification; CAD, coronary artery disease; CI, confidence interval.

assess TAC, including CT, chest X-rays, and echocardiography. These methods can produce different results based on patient characteristics, such as symptoms or risk factors, or based on the limitations of the imaging tools. For example, severe calcification can make it difficult to measure TAC accurately using echocardiography, which also cannot assess the entire thoracic aorta. On the other hand, CT has better spatial resolution and can simultaneously evaluate coronary circulation and CAC, although it does not cover the aortic arch or proximal descending aorta [10].

Calcification in different parts of the thoracic aorta—like the ascending aorta, aortic arch, descending aorta, and aortic

root—was significantly linked to the presence of CAC and, therefore, CAD after adjusting for conventional cardiovascular risk factors [35]. However, it remains unclear whether calcification in specific aortic segments accurately reflects the systemic nature of atherosclerosis or helps predict specific disease outcomes [3]. There are also no clear guidelines on the parts of the thoracic aorta to focus on or which imaging methods to use for measuring TAC [13].

Each aortic segment has a unique embryonic origin and is exposed to different hemodynamic forces, which likely influences vulnerability to calcification. This means that the calcium levels in each segment could be related to different cardiovascular

risk factors and have varying predictive value for cardiovascular diseases [13]. The current meta-analysis found that calcification in the descending aorta and aortic root showed a stronger association with CAD risk than other segments, aligning with earlier observational studies. Previous research has shown that calcification in the descending aorta is more common (56.6%) than that in the ascending aorta (42.9%) across all age groups [11]. Some studies also suggest that descending aorta calcification has the strongest link to advanced and obstructive CAD [14,36].

The aortic root, which is part of the ascending thoracic aorta, is anatomically close to the origins of the coronary arteries. This may mean that calcification in the aortic root reflects localized atherosclerosis, rather than the more widespread patterns seen in other aortic segments. Previous studies have found strong associations between aortic root calcification, CAC, severe CAD, aging, and high blood pressure [13,28].

The present meta-analysis and systematic review was designed to examine the connections between TAC and its segments, as well as the presence and severity of CAD. This study has several strengths. First, it included a large number of studies, increasing the statistical power and accuracy of the pooled estimates. Second, it incorporated studies from different countries and populations (Europe, Asia, and the United States), making the findings more generalizable. However, there are also limitations. Many of the studies included were retrospective, which can introduce biases and limit the ability to determine cause-effect relationships between TAC and CAD. Additionally, pooling the results of different studies increases the heterogeneity, as each study may involve different populations, techniques, and methods.

Additionally, the definition of TAC varied across studies due to differences in imaging techniques (e.g., CT, echocardiography, plain chest X-ray). Even among studies using the same technique, discrepancies contributed to heterogeneity. To address this issue, subgroup and sensitivity analyses were performed using random-effects models, which confirmed the robustness of our findings. Publication bias is another challenge in meta-analyses. We attempted to mitigate this by conducting a comprehensive search for eligible studies and assessing bias both visually using funnel plots and statistically using Egger's regression test. Two independent authors selected the studies for inclusion, with disagreements resolved through discussion and oversight from a senior author. Future prospective cohort studies should aim to investigate the causal relationship be-

tween TAC and CAD risk and determine whether early detection of TAC, especially in specific aortic segments, has prognostic value for coronary and cardiovascular events. Such studies could guide the development of more targeted and appropriate interventions.

In summary, this meta-analysis significantly enhances our understanding of TAC in CAD and its severity and supports the development of personalized medicine strategies to improve patient outcomes. Future prospective cohort studies are needed to determine whether early detection of TAC, particularly in specific aortic segments, has prognostic value. These studies could also clarify the causal relationship between TAC and CAD risk, leading to more precisely targeted treatments.

In conclusion, TAC was significantly associated with CAD presence and severity. Calcification of the descending aorta and aortic root was more closely associated with CAD than was calcification of the arch or ascending part.

Supplementary Information

The Data Supplement is available with this article at <https://doi.org/10.4132/jptm.2025.03.05>.

Ethics Statement

This meta-analysis received ethical approval from the Ethical Committee for Clinical Studies at the Faculty of Medicine, University of Kufa (approval no. MEC-71, dated October 16, 2024). The authors are committed to upholding the highest ethical standards and ensuring accuracy in all reported information.

Availability of Data and Material

All data available in the published studies and the supplementary materials online.

Code Availability

Not applicable.

ORCID

Hussein Nafakhi	https://orcid.org/0000-0002-0238-0460
Alaa Salah Jumaah	https://orcid.org/0000-0001-9709-1460
Akeel Abed Yasseen	https://orcid.org/0000-0001-5050-4408

Author Contributions

Conceptualization: ASJ, AAY. Data curation: ASJ, HN. Formal analysis: ASJ, HN. Methodology: ASJ, AAY, HN. Project administration: AAY, ASJ. Resources: ASJ, HN. Software: ASJ,

HN. Supervision: ASJ, AAY. Validation: ASJ, HN. Visualization: HN, AAY. Writing—original draft: ASJ, AAY, HN. Writing—review & editing: AAY, HN. Final approval of manuscript: all authors.

Conflicts of Interest

The authors declare that they have no potential conflicts of interest.

Funding Statement

No funding to declare.

REFERENCES

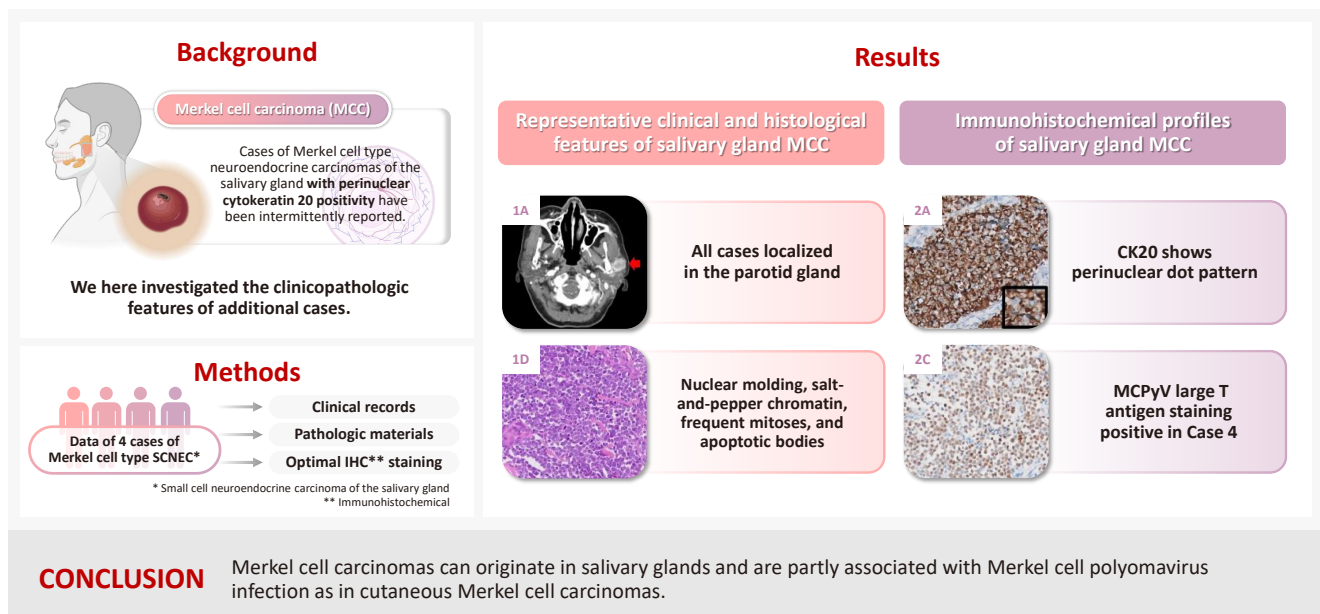
1. di Gioia CR, Ascione A, Carletti R, Giordano C. Thoracic aorta: anatomy and pathology. *Diagnostics (Basel)* 2023; 13: 2166.
2. Canan A, Ghandour AA, Saboo SS, Rajiah PS. Opportunistic screening at chest computed tomography: literature review of cardiovascular significance of incidental findings. *Cardiovasc Diagn Ther* 2023; 13: 743-61.
3. Xie JX, Shaw LJ. Arterial calcification in cardiovascular risk prediction: should we shift the target for screening beyond the coronaries? *Circ Cardiovasc Imaging* 2015; 8: e004171.
4. Garg PK, Guan W, Karger AB, Steffen BT, Budoff M, Tsai MY. Lipoprotein (a) and risk for calcification of the coronary arteries, mitral valve, and thoracic aorta: the multi-ethnic study of atherosclerosis. *J Cardiovasc Comput Tomogr* 2021; 15: 154-60.
5. Kim EJ, Yong HS, Seo HS, et al. Association between aortic calcification and stable obstructive coronary artery disease. *Int J Cardiol* 2011; 153: 192-5.
6. Kim J, Budoff MJ, Nasir K, et al. Thoracic aortic calcium, cardiovascular disease events, and all-cause mortality in asymptomatic individuals with zero coronary calcium: the Multi-Ethnic Study of Atherosclerosis (MESA). *Atherosclerosis* 2017; 257: 1-8.
7. Hartmann M, von Birgelen C. Is there a role for thoracic aortic calcium to fine-tune cardiovascular risk prediction? *Int J Cardiovasc Imaging* 2013; 29: 217-9.
8. van 't Klooster CC, Nathoe HM, Hjordnaes J, et al. Multifocal cardiovascular calcification in patients with established cardiovascular disease; prevalence, risk factors, and relation with recurrent cardiovascular disease. *Int J Cardiol Heart Vasc* 2020; 27: 100499.
9. Erbel R, Churzidse S. Calcification of the aortic wall indicates risk but not beyond current clinically used risk factors assessment. *Atherosclerosis* 2017; 257: 256-8.
10. Desai MY, Cremer PC, Schoenhagen P. Thoracic aortic calcification: diagnostic, prognostic, and management considerations. *JACC Cardiovasc Imaging* 2018; 11: 1012-26.
11. Kalsch H, Lehmann N, Mohlenkamp S, et al. Prevalence of thoracic aortic calcification and its relationship to cardiovascular risk factors and coronary calcification in an unselected population-based cohort: the Heinz Nixdorf Recall Study. *Int J Cardiovasc Imaging* 2013; 29: 207-16.
12. Takasu J, Katz R, Nasir K, et al. Relationships of thoracic aortic wall calcification to cardiovascular risk factors: the Multi-Ethnic Study of Atherosclerosis (MESA). *Am Heart J* 2008; 155: 765-71.
13. Pedrosa JF, Barreto SM, Bittencourt MS, Ribeiro AL. Anatomical references to evaluate thoracic aorta calcium by computed tomography. *Curr Atheroscler Rep* 2019; 21: 51.
14. Yamamoto H, Shavelle D, Takasu J, et al. Valvular and thoracic aortic calcium as a marker of the extent and severity of angiographic coronary artery disease. *Am Heart J* 2003; 146: 153-9.
15. Page MJ, McKenzie JE, Bossuyt PM, et al. The PRISMA 2020 statement: an updated guideline for reporting systematic reviews. *BMJ* 2021; 372: n71.
16. Li J, Galvin HK, Johnson SC, Langston CS, Sclamborg J, Preston CA. Aortic calcification on plain chest radiography increases risk for coronary artery disease. *Chest* 2002; 121: 1468-71.
17. Ma X, Hou F, Tian J, et al. Aortic arch calcification is a strong predictor of the severity of coronary artery disease in patients with acute coronary syndrome. *Biomed Res Int* 2019; 2019: 7659239.
18. Borenstein M, Hedges L, Higgins J, Rothstein HR. *Comprehensive meta-analysis, version 3.0 [Software]*. Englewood Cliffs: Biostat, 2013.
19. Higgins JP, Thompson SG, Deeks JJ, Altman DG. Measuring inconsistency in meta-analyses. *BMJ* 2003; 327: 557-60.
20. Higgins JP, Thompson SG. Quantifying heterogeneity in a meta-analysis. *Stat Med* 2002; 21: 1539-58.
21. Whiting PF, Rutjes AW, Westwood ME, et al. QUADAS-2: a revised tool for the quality assessment of diagnostic accuracy studies. *Ann Intern Med* 2011; 155: 529-36.
22. Goland S, Trento A, Czer LS, et al. Thoracic aortic arteriosclerosis in patients with degenerative aortic stenosis with and without co-existing coronary artery disease. *Ann Thorac Surg* 2008; 85: 113-9.
23. Atak R, Ileri M, Yetkin O, et al. The role of valvular and thoracic aortic calcifications in distinction between ischemic and nonischemic cardiomyopathy. *Angiology* 2004; 55: 661-7.
24. Watanabe K, Hiroki T, Koga N. Relation of thoracic aorta calcification on computed tomography and coronary risk factors to obstructive coronary artery disease on angiography. *Angiology* 2003; 54: 433-41.

25. Yuce G, Turkvatan A, Yener O. Can aortic atherosclerosis or epicardial adipose tissue volume be used as a marker for predicting coronary artery disease? *J Cardiol* 2015; 65: 143-9.
26. Takeda Y, Hoshiga M, Tatsugami F, et al. Clinical significance of calcification in ascending aorta as a marker for the requirement of coronary revascularization. *J Atheroscler Thromb* 2009; 16: 346-54.
27. Takasu J, Mao S, Budoff MJ. Aortic atherosclerosis detected with electron-beam CT as a predictor of obstructive coronary artery disease. *Acad Radiol* 2003; 10: 631-7.
28. Nafakhi H, Al-Nafakh HA, Al-Mosawi AA, Al Garaty F. Correlations between aortic root calcification and coronary artery atherosclerotic markers assessed using multidetector computed tomography. *Acad Radiol* 2015; 22: 357-62.
29. Hu X, Frellesen C, Kerl JM, et al. Association of aortic root calcification severity with the extent of coronary artery calcification assessed by calcium-scoring dual-source computed tomography. *Eur J Radiol* 2015; 84: 1910-4.
30. Tesche C, De Cecco CN, Stubenrauch A, et al. Correlation and predictive value of aortic root calcification markers with coronary artery calcification and obstructive coronary artery disease. *Radiol Med* 2017; 122: 113-20.
31. Parthenakis F, Skalidis E, Simantirakis E, Kounali D, Vardas P, Nihoyannopoulos P. Absence of atherosclerotic lesions in the thoracic aorta indicates absence of significant coronary artery disease. *Am J Cardiol* 1996; 77: 1118-21.
32. Otsuka K, Ishikawa H, Kono Y, et al. Aortic arch plaque morphology in patients with coronary artery disease undergoing coronary computed tomography angiography with wide-volume scan. *Coron Artery Dis* 2022; 33: 531-9.
33. Allam AH, Thompson RC, Eskander MA, et al. Is coronary calcium scoring too late? Total body arterial calcium burden in patients without known CAD and normal MPI. *J Nucl Cardiol* 2018; 25: 1990-8.
34. Obisesan OH, Osei AD, Berman D, et al. Thoracic aortic calcium for the prediction of stroke mortality (from the Coronary Artery Calcium Consortium). *Am J Cardiol* 2021; 148: 16-21.
35. Hata Y, Mochizuki J, Okamoto S, Matsumi H, Hashimoto K. Aortic calcification is associated with coronary artery calcification and is a potential surrogate marker for ischemic heart disease risk: a cross-sectional study. *Medicine (Baltimore)* 2022; 101: e29875.
36. Khoury Z, Schwartz R, Gottlieb S, Chenzbraun A, Stern S, Keren A. Relation of coronary artery disease to atherosclerotic disease in the aorta, carotid, and femoral arteries evaluated by ultrasound. *Am J Cardiol* 1997; 80: 1429-33.

Primary Merkel cell carcinoma of the salivary gland: a clinicopathologic study of four cases with a review of literature

Gyuheon Choi¹, Joon Seon Song¹, Hee Jin Lee¹, Gi Hwan Kim¹, Young Ho Jung², Yoon Se Lee², Kyung-Ja Cho¹

Graphical abstract



Primary Merkel cell carcinoma of the salivary gland: a clinicopathologic study of four cases with a review of literature

Gyuheon Choi¹, Joon Seon Song¹, Hee Jin Lee¹, Gi Hwan Kim¹, Young Ho Jung², Yoon Se Lee², Kyung-Ja Cho¹

¹Department of Pathology, Asan Medical Center, University of Ulsan College of Medicine, Seoul, Korea

²Department of Otorhinolaryngology – Head and Neck Surgery, Asan Medical Center, University of Ulsan College of Medicine, Seoul, Korea

Background: Primary Merkel cell carcinoma of the salivary gland is currently not listed in the World Health Organization classification. However, cases of Merkel cell type neuroendocrine carcinomas of the salivary gland with perinuclear cytokeratin 20 positivity have been intermittently reported. We here investigated the clinicopathologic features of additional cases. **Methods:** Data of four cases of Merkel cell type small cell neuroendocrine carcinoma of the salivary gland were retrieved. To confirm the tumors' primary nature, clinical records and pathologic materials were reviewed. Optimal immunohistochemical staining was performed to support the diagnosis. **Results:** All tumors were located in the parotid gland. Possibilities of metastasis were excluded in all cases through a meticulous clinicopathological review. Tumor histology was consistent with the diagnosis of small cell neuroendocrine carcinoma. Tumors' immunohistochemical phenotypes were consistent with Merkel cell carcinoma, including Merkel cell polyomavirus large T antigen positivity in two of the four cases. **Conclusions:** Merkel cell carcinomas can originate in salivary glands and are partly associated with Merkel cell polyomavirus infection as in cutaneous Merkel cell carcinomas.

Keywords: Carcinoma, neuroendocrine; Carcinoma, Merkel cell; Salivary glands; Immunohistochemistry; Merkel cell polyomavirus

INTRODUCTION

Small cell neuroendocrine carcinoma (SCNEC) is a high-grade neuroendocrine carcinoma (NEC) and can arise in several organs. It rarely originates in the salivary gland, accounting for <1% of salivary tumors [1]. SCNEC in the salivary gland deserves special attention as some of them have distinctive features compared to SCNEC of other sites, including diffuse perinuclear cytokeratin 20 (CK20) positivity [2]. A study showed that CK20-positive salivary SCNEC had significantly better prognosis than CK20-negative tumors [1]. Due to its histopathological resemblance to Merkel cell carcinoma (MCC), this group of CK20-positive SCNEC has been referred to by various

names, including Merkel cell-like, Merkel cell variant, Merkel cell type SCNEC, or MCC [1-6].

MCC is a type of NEC mostly arising in the skin with characteristic features different from typical neuroendocrine tumors. The association with the oncogenic virus, Merkel cell polyomavirus (MCPyV), is the most remarkable finding of MCC. MCPyV is a type of polyomavirus identified from MCC tissue [7]. Subsequently, MCPyV infection has been observed in the healthy population with high prevalence, usually being asymptomatic [8-10]. Its oncogenic potential proved highly specific for cutaneous MCC, being detected in approximately 80% of all MCC [11,12]. The presence of MCPyV can be detected using immunohistochemical staining targeting MCPyV large or small

Received: November 18, 2024 **Accepted:** March 25, 2025

Corresponding Author: Kyung-Ja Cho, MD, PhD

Department of Pathology, Asan Medical Center, University of Ulsan College of Medicine, 88 Olympic-ro 43-gil, Songpa-gu, Seoul 05505, Korea

Tel: +82-2-3010-1640, Fax: +82-2-472-7898, E-mail: kjc@amc.seoul.kr

This is an Open Access article distributed under the terms of the Creative Commons Attribution Non-Commercial License (<https://creativecommons.org/licenses/by-nc/4.0/>) which permits unrestricted non-commercial use, distribution, and reproduction in any medium, provided the original work is properly cited.

© 2025 The Korean Society of Pathologists/The Korean Society for Cytopathology

T antigen. In contrast, ultraviolet (UV)-related mutations are believed to be a significant pathogenetic factor in the remaining 20% of all MCC, with UV mutations and MCPyV infections being mutually exclusive [13]. Additionally, MCC are distinguished from typical neuroendocrine tumors by the expression of several proteins, including CK20, CD5, terminal deoxynucleotidyl transferase (TdT), paired box 5 (PAX5), and SRY-box transcription factor 2 (SOX2) [6,14-16].

Although most MCC originate in the skin, they could arise in extracutaneous mucosal sites in the genitourinary tract, ano-rectal area, and head and neck areas [17-19]. MCC primarily located in the lymph node is regarded as metastasis from regressed occult cutaneous MCC [20]. Some researchers regarded salivary SCNEC of Merkel cell type as being a metastasis from occult cutaneous MCC on the basis of the presence of a UV signature mutation [21]. In this study, we investigated four cases of salivary gland Merkel cell type SCNEC and discussed the controversy associated with this tumor with a review of the literature.

MATERIALS AND METHODS

Case selection and review

Six cases of NEC of the salivary gland were retrieved from the database of the Department of Pathology of Asan Medical Center, Seoul, Korea, from 2000 to 2023. Two of them were excluded because one case was a large cell NEC, and the other showed positive immunostaining for thyroid transcription factor 1

(TTF-1) and enlarged subaortic lymph nodes, not completely excluding a metastasis of a regressed pulmonary small cell carcinoma. To confirm the absence of tumors from the outside of the salivary gland, a meticulous review of the remaining four cases for available clinical and radiological resources was performed. Two pathologists (G.H.K. and K.J.C.) performed a pathologic review to analyze tumor histology and immunohistochemistry (IHC) results.

Immunohistochemistry

One representative formalin-fixed and paraffin-embedded tissue block was retrieved from each case, and 3-µm-thick sections were acquired. IHC staining was performed using Benchmark XT autostainer (Ventana Medical Systems, Tucson, AZ, USA) and OptiView DAB IHC Detection Kit (Ventana Medical Systems) following the manufacturer’s instructions. Detailed information of antibodies is provided in Table 1. All markers except p53 were assessed as positive or negative on the basis of the nuclear (TTF-1, MCPyV large T antigen, PAX5, retinoblastoma (Rb), p53, TdT, SOX2, and PTEN) or cytoplasmic (CK20, synaptophysin, chromogranin, CD56, and BRAF) staining, regardless of intensity or extent. The p53 expression was evaluated in four categories on the basis of the proportion and intensity of expression—negative, 1+ (weak), 2+ (moderate), and 3+ (strong).

Table 1. Antibody information

Antibody	Source	Clone	Dilution
CK20	DAKO, Glostrup, Denmark	Ks 20.8	1:200
Synaptophysin	Cell Marque, Rocklin, CA, USA	MRQ-40	1:100
Chromogranin	DAKO, Carpinteria, CA, USA	DAK-A3	1:1,600
CD56 (NCAM)	Cell Marque, Rocklin, CA, USA	156R-96	1:250
TTF-1	NOVO, Gatwick, UK	SPT24	1:200
MCPyV LTA	Santa Cruz Biotechnology, Santa Cruz, CA, USA	CM2B4	1:50
PAX5	Cell Marque, Rocklin, CA, USA	SP34	1:100
Rb	QED Bioscience, San Diego, CA, USA	3C8	1:10,000
p53	DAKO, Carpinteria, CA, USA	DO-7	1:1,000
TdT	Cell Marque, Rocklin, CA, USA	Polyclonal	1:100
SOX2	Abcam, Cambridge, UK	Polyclonal	1:250
PTEN	Cell Signaling, Danvers, MA, USA	138G6	1:100
BRAF	Ventana Medical Systems, Tucson, AZ, USA	VE1	Prediluent

CK, cytokeratin; TTF-1, thyroid transcription factor 1; MCPyV LTA, Merkel cell polyomavirus large T antigen; PAX5, paired box 5; Rb, retinoblastoma; TdT, terminal deoxynucleotidyl transferase; SOX2, SRY-box transcription factor 2.

RESULTS

Clinical features

The patients were three females and one male whose ages ranged from 59 to 78 years (mean, 69.7 years). All patients presented with a rapidly increasing palpable mass in the preauricular area, with accompanying pain in two of them. Computed tomography revealed enhancing mass in the parotid gland with a lobulating or partially infiltrating border (Fig. 1A). The following is the medical history of each patient: Case 1 has diabetes mellitus (DM) and rheumatoid arthritis treated with medication, case 2 has DM treated with medication, case 3 has DM treated with medication and experienced a cerebral stroke

5 months ago, and case 4 underwent a liver transplant due to hepatitis B-associated liver cirrhosis 1 year and 3 months ago. Each patient underwent total (cases 1, 2, and 4) or partial (case 3) parotidectomy. Additionally, cases 2, 3, and 4 underwent neck dissection. Notably, widespread lymph node metastases were identified in the unilateral cervical lymph nodes of case 3 (24 of 62 lymph nodes with the largest tumor dimension of 15 mm and extranodal extension) and case 4 (22 of 44 lymph nodes with the largest tumor dimension of 22 mm and extranodal extension). Adjuvant therapy was administered to two patients. Case 1 received radiotherapy as 66 Gy/25 fraction, whereas case 3 received concurrent chemoradiotherapy as 60 Gy/30 fraction with etoposide and cisplatin. In case 3, tumor

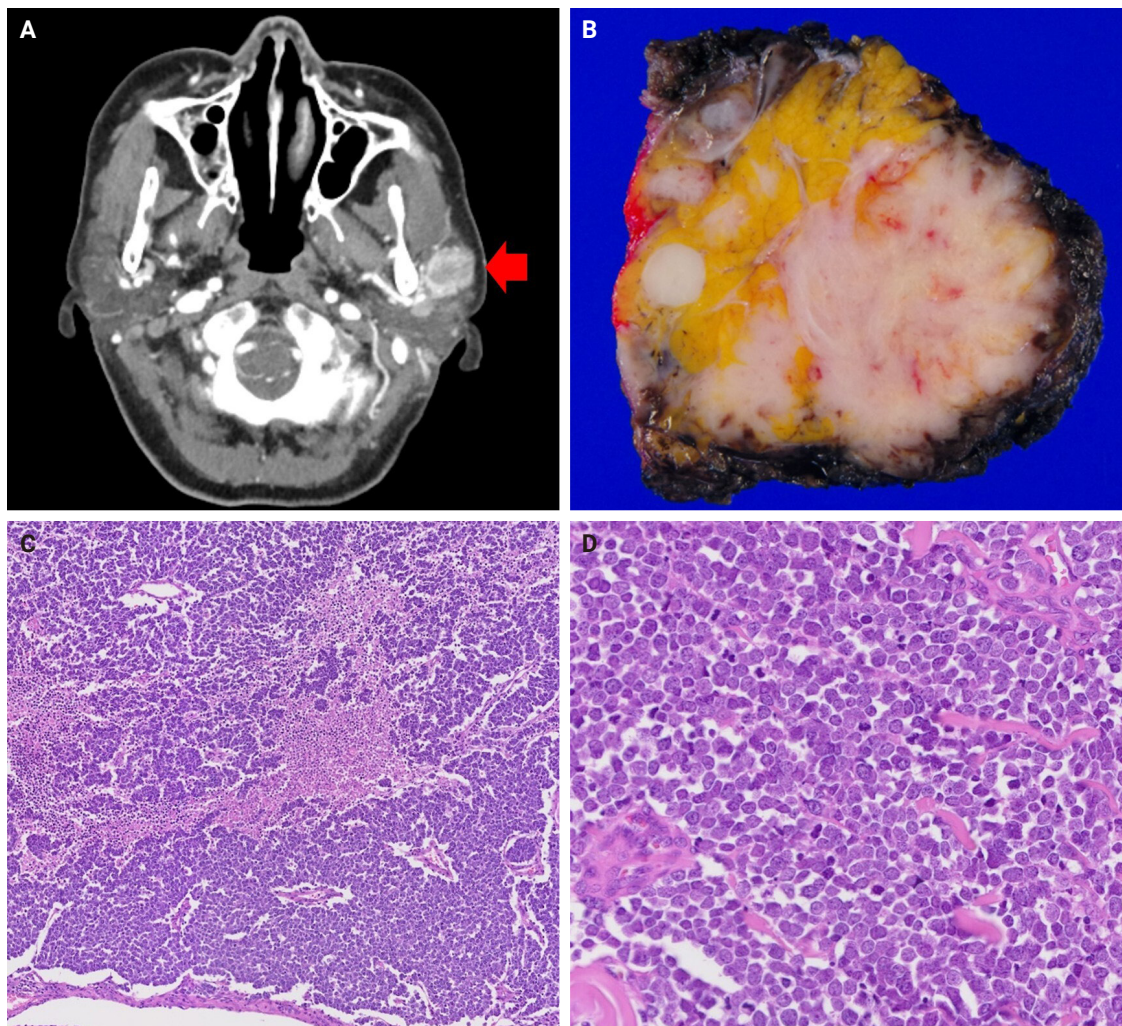


Fig. 1. Radiologic, macroscopic, and microscopic images of the representative tumor (case 4). (A) Computed tomography image revealing an ill-defined mass in the left parotid gland (arrow). (B) Gross photography exhibiting an infiltrating tumor with a fleshy section. (C) Diverse histologic pattern with spotty necrosis. (D) Nuclei with salt and pepper chromatin, numerous mitoses, and apoptotic bodies.

recurrence involving the left neck and bilateral external iliac lymph nodes was observed, leading to additional systemic chemotherapy with etoposide and cisplatin. The average follow-up period was 19.4 months. Three patients were referred to local clinics within 1 year. No cases of patient mortality were observed until the last follow-up. Clinical data are presented in Table 2.

Histology and IHC

Grossly, all tumors appeared as ill-demarcated solid masses involving the parotid gland with fleshy cut surface (Fig. 1B). The tumor size ranged from 1.3 to 4.6 cm (mean, 2.85 cm). Microscopic examination revealed infiltrating tumors composed of small monotonous tumor cells demonstrating diverse histological patterns within the tumor, including diffuse, nested, and trabecular patterns. Tumor cells exhibited hyperchromatic finely granular nuclei with nuclear molding and crush artifact. Significant mitotic activity was observed, with counts exceeding 20 per high-power field in some regions. Spotty necrosis and apoptotic debris were frequently observed (Fig. 1C, D). Results of IHC staining for MCC-associated markers are shown in Table 3. In all cases, neuroendocrine markers (synaptophysin, chromogranin, and CD56) were positive. CK20 showed diffuse expression with a perinuclear dot pattern in all cases. TTF-1 was negative in all cases (Fig. 2A, B). MCPyV large T antigen was identified in two cases (cases 3 and 4) (Fig. 2C, D). In both

cases, more than 90% of cells showed nuclear staining with variable intensity. PAX5 was focally positive in one case (case 2). PTEN loss was observed in two cases (cases 1 and 3). Rb and p53 were positive in all cases with heterogeneous expression. TdT and BRAF were negative in all cases. SOX2 showed diffuse positive staining in all cases with strong intensity.

DISCUSSION

MCC is primarily of a cutaneous origin; however, extracutaneous cases, accounting for approximately 2% of all MCC, have been steadily reported with the salivary glands being the most common site [22]. In the literature, we could identify 45 cases of Merkel cell type (CK20-positive) NEC of the salivary gland (Table 4) [1,3-6,23-34]. Including our four cases, the mean age of the total 49 cases was 70.9 years, with a male predilection (65.3%). The majority of cases (46 cases, 93.9%) originated in the parotid gland, with three originating in the submandibular gland. MCPyV was detected in six of 15 cases tested. Immunosuppression and chronic inflammatory conditions including DM and rheumatic disorders contribute as risk factors for cutaneous MCCs [35,36]. Among our cases, three patients had DM (including one with concurrent rheumatoid arthritis), and one had a liver transplantation history. The underlying mechanisms generating a correlation between MCC and immunosuppression or chronic inflammatory disorders are not well-established.

Table 2. Clinical characteristics

Case No.	Age (yr)	Sex	Site	Size (cm)	Treatment	History	LN metastasis	Recurrence (mo)	Follow-up (mo)
1	74	F	Parotid (R)	3.5	TP + RT	DM, RA	-	-	NED (9.1)
2	78	F	Parotid (R)	2	TP + SND	DM	-	-	NED (73.0)
3	66	M	Parotid (R)	1.3	RP + MRND + CCRT	DM, CVA	+	5.6	AWD (8.4)
4	59	F	Parotid (L)	4.6	TP + MRND	LT	+	-	NED (6.5)

R, right; TP, total parotidectomy; RT, radiotherapy; DM, diabetes mellitus; RA, rheumatoid arthritis; NED, no evidence of the disease; SND, selective neck dissection; RP, radical parotidectomy; MRND, modified radical neck dissection; CCRT, concurrent chemoradiotherapy; CVA, cerebrovascular accident; AWD, alive with the disease; L, left; LT, liver transplantation.

Table 3. Immunohistochemistry results

Case No.	Synaptophysin	Chromogranin	CD56	CK20	TTF-1	MCPyV LTA	PAX5	Rb	p53	TdT	SOX2	BRAF (VE1)	PTEN
1	+	+	NA	+	-	-	-	+	1+	-	+	-	-
2	+	+	+	+	-	-	+	+	1+	-	+	-	+
3	+	+	+	+	-	+	-	+	2+	-	+	-	-
4	+	-	+	+	-	+	-	+	2+	-	+	-	+

CK, cytokeratin; TTF-1, thyroid transcription factor 1; MCPyV LTA, Merkel cell polyomavirus large T antigen; PAX5, paired box 5; Rb, retinoblastoma; TdT, terminal deoxynucleotidyl transferase; SOX2, SRY-box transcription factor 2; NA, not available.

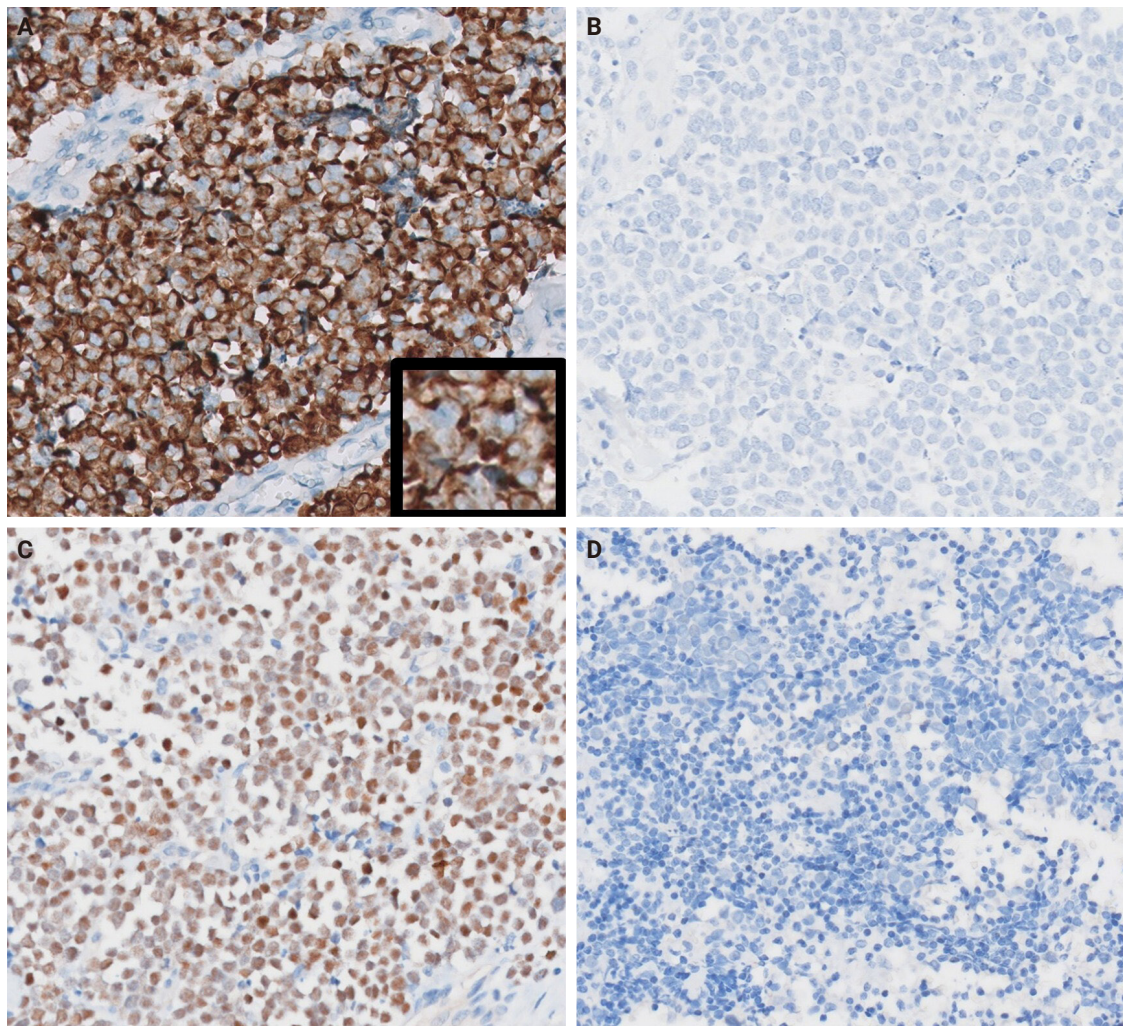


Fig. 2. Representative immunohistochemistry images. (A) Diffuse expression of cytokeratin 20 with focal dot-like staining (inset) (case 3). (B) thyroid transcription factor 1 expression is absent (case 3). (C) Merkel cell polyomavirus large T antigen (MCPyV LTA)-positive case (case 4). (D) MCPyV LTA-negative case (case 2).

lished; however, immunosuppression is linked with poor prognosis [37] and MCPyV negativity [38]. Although our patients demonstrated a relatively favorable prognosis, the small sample size and the relatively short follow-up duration were limitations. Out of a total 49 cases, 38 had documented survival status and follow-up duration. The survival duration ranged from 2 to 156 months, with a median of 36 months. This finding is better than the previously reported median survival of salivary SCNEC (25–28.5 months) [39,40], which is consistent with the previous finding that CK20-positive salivary SCNEC show better prognosis [1].

The Fifth World Health Organization classification of head and neck tumors presents that most salivary SCNEC carrying

MCPyV or UV signature mutations are best classified as metastatic MCC [41]. However, no robust tools have been developed yet, which could be used for differentiating primary or metastatic MCC, if there have been regressed or occult skin tumors. Meticulous clinical and radiological investigations for exploring primary site appear to be the most critical for proper diagnosis. Nevertheless, as the skin is the most superficial part of the body, the absence of any skin tumors in patients' histories is considered relatively reliable. MCPyV does not exclusively infect the skin cells but can be detected in systemic tissues, such as the saliva, aerodigestive tract, or liver [42]. It has been detected in extracutaneous MCC, including cases involving the maxillary sinus [18], stomach [43], and salivary glands [3-5]. UV muta-

Table 4. Reported cases of Merkel cell type neuroendocrine carcinoma of the salivary gland in the English literature

Study	No.	Age (yr)	Sex	Site	Size (cm)	MCPyV	LN metastasis	Recurrence	Follow-up
Fornelli et al. [23]	2	65	M	Parotid	4	NA	-	+	DOD (28 mo)
		70	M	Parotid	2.5	NA	-	+	AWD (2 yr)
Nagao et al. [1]	11	77	F	Parotid	1.8	NA	-	-	NED (28 mo)
		78	M	Parotid	1.5	NA	+	-	DOD (45 mo)
		81	F	Parotid	3	NA	+	-	DOD (17 mo)
		85	M	Submandibular	3.8	NA	-	-	DOD (9 mo)
		50	M	Parotid	0.7	NA	+	-	NED (155 mo)
		66	M	Parotid	5	NA	-	-	DOD (20 mo)
		76	M	Parotid	11	NA	+	-	DOD (2 mo)
		72	M	Parotid	2.9	NA	-	-	NED (4 mo)
		72	M	Parotid	2	NA	+	-	DOD (34 mo)
		67	M	Parotid	8	NA	+	-	AWD (18 mo)
		52	F	Parotid	1.5	NA	-	-	NED (4 mo)
Jorcano et al. [24]	1	91	M	Parotid	4	NA	+	-	DOC (3 yr)
Mulder et al. [25]	1	78	M	Parotid	NA	NA	+	+	DOD (3 yr)
Ghaderi et al. [26]	1	35	F	Parotid	2	NA	-	-	NA
Baca et al. [27]	1	77	M	Parotid	8.5	NA	+	NA	NA
Chernock et al. [6]	5	68	M	Parotid	NA	-	+	-	DOD (<6 mo)
		66	M	Parotid	NA	-	+	+	NED (112 mo)
		74	M	Parotid	NA	-	+	-	NED (2 yr)
		22	M	Parotid	NA	-	+	-	DOD (<6 mo)
		60	M	Parotid	NA	-	-	-	NED (13 yr)
De Biase et al. [5]	1	64	M	Parotid	4	+	+	NA	DOD (1 yr)
Kanazawa et al. [28]	1	87	F	Parotid	5.5	NA	+	-	NED (108 mo)
Fisher et al. [4]	3	64	F	Parotid	1.4	+	-	-	NED (41 mo)
		82	M	Parotid	6.5	-	-	-	DOC (8 mo)
		82	M	Parotid	2.8	+	+	-	NED (31 mo)
Lombardi et al. [3]	1	67	F	Submandibular	2.2	+	+	-	NED (12 mo)
Bizzaro et al. [29]	1	65	M	Parotid	1.7	NA	-	-	NED (24 mo)
Knopf et al. [30]	8	Mean 75	3M, 5F	Parotid	NA	NA	3 (37.5%)	5-yr RFI, 71%	5-yr OS, 29%
Alotaibi et al. [31]	1	71	M	Parotid	3.5	NA	-	-	NA
Astreidis et al. [32]	1	76	M	Parotid	2.7	NA	-	-	NED (60 mo)
Young et al. [33]	1	69	M	Parotid	4.9	-	-	+	AWD (20 mo)
De Luca et al. [34]	5	57	M	Parotid	1.5	NA	+	+	DOD (45 mo)
		79	F	Parotid	NA	NA	NA	+	DOC (24 mo)
		92	F	Submandibular	2.8	NA	-	-	DOC (16 mo)
		70	M	Parotid	3.4	NA	NA	+	DOD (14 mo)
		88	M	Parotid	2.5	NA	NA	-	DOC (46 mo)

MCPyV, Merkel cell polyomavirus; LN, lymph node; NA, not available; DOD, died of the disease; AWD, alive with the disease; NED, no evidence of the disease; DOC, died of other causes; RFI, recurrence-free interval; OS, overall survival.

tion signatures are often cited as supporting evidence for a skin origin in tumors; however, they have also been observed in a range of extracutaneous tumors [44] including salivary squamous cell carcinoma cases [45,46]. Given that whole exome sequencing is the standard method for detecting UV signature

mutations, its application was not feasible in our study due to the age of our specimens. To explore UV-related mutations, we instead employed IHC for PTEN and BRAF as surrogate markers, as mutations in these genes have been commonly associated with UV-induced damage [47,48]. Unfortunately, the IHC

results did not reveal significant findings; specifically, we found no evidence of UV mutations in the MCPyV-negative cases. While previous studies have used UV mutation signatures to argue that cases of lung melanoma [49] and salivary squamous cell carcinoma [45] may represent occult cutaneous origin metastases, relying on UV mutation signatures as definitive evidence of a cutaneous origin remains challenging due to numerous variables [50]. That is, although certain DNA damage patterns are relatively strongly associated with UV exposure, it is difficult to completely rule out other causes of similar damage, and the lack of a standardized analytical approach can lead to variation in results depending on the specific genes analyzed and the threshold values applied. Therefore, after excluding other possible primary sites through clinical evaluation, it seems reasonable to consider salivary gland MCC as a primary salivary tumor.

Interestingly, MCC tumor cells show various lymphocytic markers, including TdT, PAX5, and CD5 [14,15], and it could pose a diagnostic pitfall when distinguishing MCCs from lymphocytic neoplasms. However, our cases were nearly all negative for TdT and PAX5, except for one case with trivial positivity for PAX5. Conversely, all cases showed diffuse positivity for SOX2, which is a Merkel cell differentiation regulator and an essential oncogene of MCC [51,52]. It can be used for distinguishing MCC from other skin tumors but not from extracutaneous NEC [16]. An essential pathogenetic mechanism of MCC is Rb protein inactivation [53]. However, loss of Rb expression is frequently observed in a minor portion of MCPyV-negative cases [16,54,55]. Although our cases consistently exhibited Rb and SOX2 positivity, it is less likely that this finding is specific for salivary gland Merkel cell type NEC. Overall, salivary gland Merkel type NEC has similar clinicopathological characteristics with cutaneous MCC.

In conclusion, we propose that MCC can arise in the salivary glands, in addition to the skin. After thoroughly ruling out the possibility of metastasis, these cases should be treated in a manner appropriate for a primary salivary gland malignancy. Salivary gland MCC exhibits a phenotype identical with cutaneous MCC, including MCPyV and SOX2 positivity. We expect that MCC would be listed as a primary salivary gland malignancy in the classification.

Ethics Statement

All procedures performed in the current study were approved by the Institutional Review Board of Asan Medical Center (ap-

proval No. 2023-1328) in accordance with the 1964 Helsinki Declaration and its later amendments. Formal written informed consent was not required with a waiver by the Institutional Review Board of Asan Medical Center.

Availability of Data and Material

All data generated or analyzed during the study are included in this published article (and its supplementary information files).

Code Availability

Not applicable.

ORCID

Gyuheon Choi	https://orcid.org/0000-0002-2825-987X
Joon Seon Song	https://orcid.org/0000-0002-7429-4254
Hee Jin Lee	https://orcid.org/0000-0002-4963-6603
Gi Hwan Kim	https://orcid.org/0000-0001-6228-764X
Young Ho Jung	https://orcid.org/0000-0002-3399-8167
Yoon Se Lee	https://orcid.org/0000-0001-6534-5753
Kyung-Ja Cho	https://orcid.org/0000-0002-4911-7774

Author Contributions

Conceptualization: KJC. Data curation: GC, GHK. Formal analysis: GC, GHK. Investigation: GC, GHK. Methodology: KJC. Project administration: GC, KJC. Resources: JSS, HJL, YHJ, YSL, KJC. Supervision: KJC. Validation: JSS, HJL, KJC. Visualization: GC. Writing—original draft: GC. Writing—review & editing: JSS, HJL, KJC. Approval of final manuscript: all authors.

Conflicts of Interest

J.S.S., a contributing editor of the *Journal of Pathology and Translational Medicine*, was not involved in the editorial evaluation or decision to publish this article. All remaining authors have declared no conflicts of interest.

Funding Statement

No funding to declare.

REFERENCES

1. Nagao T, Gaffey TA, Olsen KD, Serizawa H, Lewis JE. Small cell carcinoma of the major salivary glands: clinicopathologic study with emphasis on cytokeratin 20 immunoreactivity and clinical outcome. *Am J Surg Pathol* 2004; 28: 762-70.

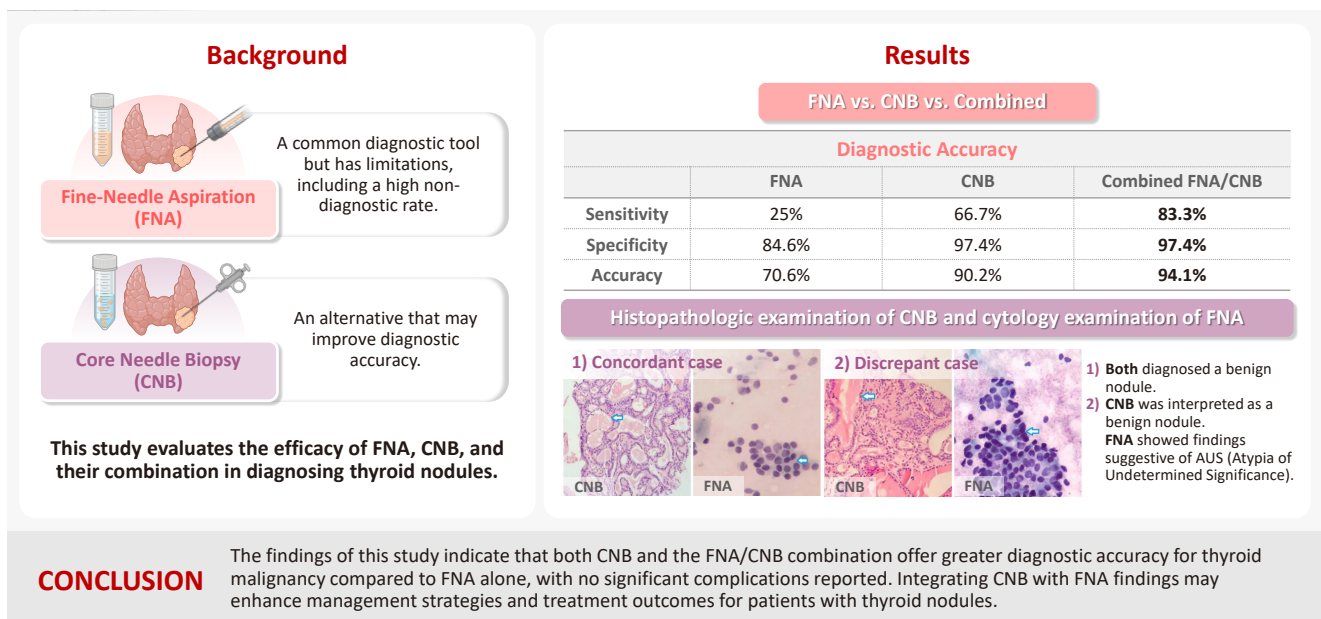
2. Chan JK, Suster S, Wenig BM, Tsang WY, Chan JB, Lau AL. Cytokeratin 20 immunoreactivity distinguishes Merkel cell (primary cutaneous neuroendocrine) carcinomas and salivary gland small cell carcinomas from small cell carcinomas of various sites. *Am J Surg Pathol* 1997; 21: 226-34.
3. Lombardi D, Accorona R, Ungari M, Melocchi L, Bell D, Nicolai P. Primary Merkel cell carcinoma of the submandibular gland: when CK20 status complicates the diagnosis. *Head Neck Pathol* 2015; 9: 309-14.
4. Fisher CA, Harms PW, McHugh JB, et al. Small cell carcinoma in the parotid harboring Merkel cell polyomavirus. *Oral Surg Oral Med Oral Pathol Oral Radiol* 2014; 118: 703-12.
5. de Biase D, Ragazzi M, Asioli S, Eusebi V. Extracutaneous Merkel cell carcinomas harbor polyomavirus DNA. *Hum Pathol* 2012; 43: 980-5.
6. Chernock RD, Duncavage EJ, Gnepp DR, El-Mofty SK, Lewis JS Jr. Absence of Merkel cell polyomavirus in primary parotid high-grade neuroendocrine carcinomas regardless of cytokeratin 20 immunophenotype. *Am J Surg Pathol* 2011; 35: 1806-11.
7. Feng H, Shuda M, Chang Y, Moore PS. Clonal integration of a polyomavirus in human Merkel cell carcinoma. *Science* 2008; 319: 1096-100.
8. Kean JM, Rao S, Wang M, Garcea RL. Seroepidemiology of human polyomaviruses. *PLoS Pathog* 2009; 5: e1000363.
9. Carter JJ, Paulson KG, Wipf GC, et al. Association of Merkel cell polyomavirus-specific antibodies with Merkel cell carcinoma. *J Natl Cancer Inst* 2009; 101: 1510-22.
10. Tolstov YL, Knauer A, Chen JG, et al. Asymptomatic primary Merkel cell polyomavirus infection among adults. *Emerg Infect Dis* 2011; 17: 1371-80.
11. Duncavage EJ, Le BM, Wang D, Pfeifer JD. Merkel cell polyomavirus: a specific marker for Merkel cell carcinoma in histologically similar tumors. *Am J Surg Pathol* 2009; 33: 1771-7.
12. Spurgeon ME, Lambert PF. Merkel cell polyomavirus: a newly discovered human virus with oncogenic potential. *Virology* 2013; 435: 118-30.
13. Harms PW, Vats P, Verhaegen ME, et al. The distinctive mutational spectra of polyomavirus-negative Merkel cell carcinoma. *Cancer Res* 2015; 75: 3720-7.
14. Kolhe R, Reid MD, Lee JR, Cohen C, Ramalingam P. Immunohistochemical expression of PAX5 and TdT by Merkel cell carcinoma and pulmonary small cell carcinoma: a potential diagnostic pitfall but useful discriminatory marker. *Int J Clin Exp Pathol* 2013; 6: 142-7.
15. Legrand M, Tallet A, Guyetant S, Samimi M, Ortonne N, Kervarrec T. CD5 expression in Merkel cell carcinoma and extracutaneous neuroendocrine carcinomas. *Pathology* 2023; 55: 141-3.
16. Thanguturi S, Tallet A, Miquelestorena-Standley E, et al. Investigation of the RB1-SOX2 axis constitutes a tool for viral status determination and diagnosis in Merkel cell carcinoma. *Virchows Arch* 2022; 480: 1239-54.
17. Aron M, Zhou M. Merkel cell carcinoma of the genitourinary tract. *Arch Pathol Lab Med* 2011; 135: 1067-71.
18. Sheldon JD, Lott Limbach AA. Merkel cell carcinoma of the maxillary sinus: an unusual presentation of a common tumor. *Head Neck Pathol* 2021; 15: 691-7.
19. van Wyk AC, Moolla Z, Motala AI, et al. Merkel cell carcinoma of the anorectum: a case report and review of the literature. *Clin J Gastroenterol* 2022; 15: 740-5.
20. Lawrence LEB, Saleem A, Sahoo MK, et al. Is Merkel cell carcinoma of lymph node actually metastatic cutaneous Merkel cell carcinoma? *Am J Clin Pathol* 2020; 154: 369-80.
21. Sun L, Cliften PF, Duncavage EJ, Lewis JS Jr, Chernock RD. UV signature mutations reclassify salivary high-grade neuroendocrine carcinomas as occult metastatic cutaneous Merkel cell carcinomas. *Am J Surg Pathol* 2019; 43: 682-7.
22. Albores-Saavedra J, Batich K, Chable-Montero F, Sagy N, Schwartz AM, Henson DE. Merkel cell carcinoma demographics, morphology, and survival based on 3870 cases: a population based study. *J Cutan Pathol* 2010; 37: 20-7.
23. Fornelli A, Eusebi V, Pasquinelli G, Quattrone P, Rosai J. Merkel cell carcinoma of the parotid gland associated with Warthin tumour: report of two cases. *Histopathology* 2001; 39: 342-6.
24. Jorcano S, Casado A, Berenguer J, Arenas M, Rovirosa A, Colombo L. Primary neuroendocrine small cell undifferentiated carcinoma of the parotid gland. *Clin Transl Oncol* 2008; 10: 303-6.
25. Mulder DC, Rosenberg AJ, Storm-Bogaard PW, Koole R. Spontaneous regression of advanced merkel-cell-like small cell carcinoma of the parotid gland. *Br J Oral Maxillofac Surg* 2010; 48: 199-200.
26. Ghaderi M, Coury J, Oxenberg J, Spector H. Primary Merkel cell carcinoma of the parotid gland. *Ear Nose Throat J* 2010; 89: E24-7.
27. Baca JM, Chiara JA, Strenge KS, Keylock JB, Jones CL, Harsha WJ. Small-cell carcinoma of the parotid gland. *J Clin Oncol* 2011; 29: e34-6.
28. Kanazawa T, Fukushima N, Tanaka H, et al. Parotid small cell carcinoma presenting with long-term survival after surgery alone: a case report. *J Med Case Rep* 2012; 6: 431.
29. Bizzarro T, Buda R, Ricci M, Bernardi L. Cytological diagnosis of a rare case of primary Merkel cell carcinoma of the parotid gland. *Cytopathology* 2017; 28: 552-4.

30. Knopf A, Bas M, Hofauer B, Mansour N, Stark T. Clinicopathological characteristics of head and neck Merkel cell carcinomas. *Head Neck* 2017; 39: 92-7.
31. Alotaibi FH, Lugo R, Patel SY, Abdulsattar J, Ghali GE. Primary Merkel cell carcinoma of the parotid gland: unusual location and clinical presentation. *Oral Maxillofac Surg Cases* 2020; 6: 100197.
32. Astreidis I, Kalaitidou I, Papaemmanouil S, Vachtsevanos K, Antoniadis K. Small cell neuroendocrine carcinoma of the parotid gland: a chronicle of publications based on the largest case series and a report of the first Greek case. *Res Rep Oral Maxillofac Surg* 2020; 4: 044.
33. Young S, Oh J, Bukhari H, Ng T, Chau N, Tran E. Primary parotid Merkel type small cell neuroendocrine carcinoma with oligometastasis to the brain and adrenal gland: case report and review of literature. *Head Neck Pathol* 2021; 15: 311-8.
34. De Luca P, Simone M, De Seta D, et al. Small cell neuroendocrine carcinoma "Merkel-like" of major salivary glands: presentation of a multicenter case series of this exceptional histological entity. *Oral Oncol* 2023; 138: 106329.
35. Cook M, Baker K, Redman M, et al. Differential outcomes among immunosuppressed patients with Merkel cell carcinoma: impact of immunosuppression type on cancer-specific and overall survival. *Am J Clin Oncol* 2019; 42: 82-8.
36. Sahi H, Sihto H, Artama M, Koljonen V, Bohling T, Pukkala E. History of chronic inflammatory disorders increases the risk of Merkel cell carcinoma, but does not correlate with Merkel cell polyomavirus infection. *Br J Cancer* 2017; 116: 260-4.
37. Paulson KG, Iyer JG, Blom A, et al. Systemic immune suppression predicts diminished Merkel cell carcinoma-specific survival independent of stage. *J Invest Dermatol* 2013; 133: 642-6.
38. Starrett GJ, Thakuria M, Chen T, et al. Clinical and molecular characterization of virus-positive and virus-negative Merkel cell carcinoma. *Genome Med* 2020; 12: 30.
39. Bai J, Zhao F, Pan S. Clinicopathological characteristics and survival of small cell carcinoma of the salivary gland: a population-based study. *Cancer Manag Res* 2019; 11: 10749-57.
40. Zhan KY, Din HA, Muus JS, Nguyen SA, Lentsch EJ. Predictors of survival in parotid small cell carcinoma: a study of 344 cases. *Laryngoscope* 2016; 126: 2036-40.
41. Lisa M, Vania N, Peter S, Byardo P, Marion C. Small cell neuroendocrine carcinoma. In: WHO Classification of Tumours Editorial Board, ed. WHO classification of tumours. 5th ed. Vol. 9. Head and neck tumours. Lyon: International Agency for Research on Cancer, 2022; 646-8.
42. Loyo M, Guerrero-Preston R, Brait M, et al. Quantitative detection of Merkel cell virus in human tissues and possible mode of transmission. *Int J Cancer* 2010; 126: 2991-6.
43. Capella C, Marando A, Longhi E, et al. Primary gastric Merkel cell carcinoma harboring DNA polyomavirus: first description of an unusual high-grade neuroendocrine carcinoma. *Hum Pathol* 2014; 45: 1310-4.
44. Mata DA, Williams EA, Sokol E, et al. Prevalence of UV mutational signatures among cutaneous primary tumors. *JAMA Netw Open* 2022; 5: e223833.
45. Fishbach S, Steinhardt G, Zhen CJ, Puranik R, Segal JP, Cipriani NA. High rates of ultraviolet-signature mutations in squamous cell carcinomas of the parotid gland and prognostic implications. *Head Neck Pathol* 2022; 16: 236-47.
46. Mai ZM, Sargen MR, Curtis RE, Pfeiffer RM, Tucker MA, Cahoon EK. Ambient ultraviolet radiation and major salivary gland cancer in the United States. *J Am Acad Dermatol* 2020; 83: 1775-7.
47. Besaratinia A, Pfeifer GP. Sunlight ultraviolet irradiation and BRAF V600 mutagenesis in human melanoma. *Hum Mutat* 2008; 29: 983-91.
48. Ming M, Han W, Maddox J, et al. UVB-induced ERK/AKT-dependent PTEN suppression promotes survival of epidermal keratinocytes. *Oncogene* 2010; 29: 492-502.
49. Yang C, Sanchez-Vega F, Chang JC, et al. Lung-only melanoma: UV mutational signature supports origin from occult cutaneous primaries and argues against the concept of primary pulmonary melanoma. *Mod Pathol* 2020; 33: 2244-55.
50. Brash DE. UV signature mutations. *Photochem Photobiol* 2015; 91: 15-26.
51. Harold A, Amako Y, Hachisuka J, et al. Conversion of Sox2-dependent Merkel cell carcinoma to a differentiated neuron-like phenotype by T antigen inhibition. *Proc Natl Acad Sci U S A* 2019; 116: 20104-14.
52. Laga AC, Lai CY, Zhan Q, et al. Expression of the embryonic stem cell transcription factor SOX2 in human skin: relevance to melanocyte and merkel cell biology. *Am J Pathol* 2010; 176: 903-13.
53. DeCaprio JA. Molecular pathogenesis of Merkel cell carcinoma. *Annu Rev Pathol* 2021; 16: 69-91.
54. Sihto H, Kukko H, Koljonen V, Sankila R, Bohling T, Joensuu H. Merkel cell polyomavirus infection, large T antigen, retinoblastoma protein and outcome in Merkel cell carcinoma. *Clin Cancer Res* 2011; 17: 4806-13.
55. Houben R, Schrama D, Alb M, et al. Comparable expression and phosphorylation of the retinoblastoma protein in Merkel cell polyoma virus-positive and negative Merkel cell carcinoma. *Int J Cancer* 2010; 126: 796-8.

Diagnostic yield of fine needle aspiration with simultaneous core needle biopsy for thyroid nodules

Mohammad Ali Hasannia^{1,2}, Ramin Pourghorban^{3,4}, Hoda Asefi⁴, Amir Aria⁵, Elham Nazar⁶,
 Hojat Ebrahiminik⁷, Alireza Mohamadian^{1,2}

Graphical abstract



Diagnostic yield of fine needle aspiration with simultaneous core needle biopsy for thyroid nodules

Mohammad Ali Hasannia^{1,2}, Ramin Pourghorban^{3,4}, Hoda Asefi⁴, Amir Aria⁵, Elham Nazar⁶, Hojat Ebrahiminik⁷, Alireza Mohamadian^{1,2}

¹Department of Radiology, School of Medicine, Tehran University of Medical Sciences, Tehran, Iran

²Advanced Diagnostic and Interventional Radiology Research Center (ADIR), Tehran University of Medical Sciences, Tehran, Iran

³Department of Medical Imaging, Nepean Hospital, Kingswood, New South Wales, Australia

⁴Department of Radiology, Sina Hospital, Tehran University of Medical Sciences, Tehran, Iran

⁵Department of Internal Medicine, Alzahra Hospital, Isfahan University of Medical Sciences, Isfahan, Iran

⁶Department of Pathology, Sina Hospital, Tehran University of Medical Sciences, Tehran, Iran

⁷Department of Interventional Radiology and Radiation Sciences Research Center, Aja University of Medical Sciences, AJA Campus, Tehran, Iran

Background: Fine needle aspiration (FNA) is a widely utilized technique for assessing thyroid nodules; however, its inherent non-diagnostic rate poses diagnostic challenges. The present study aimed to evaluate and compare the diagnostic efficacy of FNA, core needle biopsy (CNB), and their combined application in the assessment of thyroid nodules. **Methods:** A total of 56 nodules from 50 patients was analyzed using both FNA and simultaneous CNB. The ultrasound characteristics were categorized according to the American College of Radiology Thyroid Imaging Reporting and Data Systems classification system. The study compared the sensitivity, specificity, and accuracy of FNA, CNB, and the combination of the two techniques. **Results:** The concordance between FNA and CNB was notably high, with a kappa coefficient of 0.837. The sensitivity for detecting thyroid malignancy was found to be 25.0% for FNA, 66.7% for CNB, and 83.3% for the combined FNA/CNB approach, with corresponding specificities of 84.6%, 97.4%, and 97.4%. The accuracy of the FNA/CNB combination was the highest at 94.1%. **Conclusions:** The findings of this study indicate that both CNB and the FNA/CNB combination offer greater diagnostic accuracy for thyroid malignancy compared to FNA alone, with no significant complications reported. Integrating CNB with FNA findings may enhance management strategies and treatment outcomes for patients with thyroid nodules.

Keywords: Thyroid nodule; Biopsy, fine-needle; Biopsy, large-core needle; Diagnosis; ACR TI-RADS

INTRODUCTION

Thyroid nodules are a common condition, with up to 76% of the population having them, and around 7%–15% of those nodules being malignant [1]. With advancements in manufacturing high-resolution ultrasound probes, more suspicious nodules are being diagnosed, which means there is an increasing need for accurate and efficient diagnostic methods [2-4].

Fine needle aspiration (FNA) is the most cost-effective, safest, and quickest diagnostic method used in the initial evaluation of

thyroid nodules. However, the Bethesda System classification used to diagnose thyroid nodules using FNA results can be unreliable, with unclear results reported in 10%–47% of cases, either non-diagnostic (Bethesda I) or atypia of undetermined significance (Bethesda III) [1,5,6]. This leads to the need for repeat FNA or core needle biopsy (CNB) procedures to obtain more conclusive results [7-9].

CNB is a complementary diagnostic method that can overcome the limitations of FNA, including non-diagnostic or uncertain outcomes and the need for repeat procedures or unne-

Received: December 6, 2024 **Revised:** February 1, 2025 **Accepted:** March 4, 2025

Corresponding Author: Alireza Mohamadian, MD, MPH

Department of Radiology, School of Medicine, Tehran University of Medical Sciences, Sina Hospital, Imam Khomeini St., Tehran 11367-46911, Iran

Tel: +98-937-323-3713, Fax: +98-21-8889-8532, E-mail: alirezamohamadian.md@gmail.com

This is an Open Access article distributed under the terms of the Creative Commons Attribution Non-Commercial License (<https://creativecommons.org/licenses/by-nc/4.0/>) which permits unrestricted non-commercial use, distribution, and reproduction in any medium, provided the original work is properly cited.

© 2025 The Korean Society of Pathologists/The Korean Society for Cytopathology

essary surgeries [8-13]. CNB is more sensitive and reliable than FNA due to the availability of tissue samples, which can be used for immunohistochemistry and molecular studies [2,7]. As a result, CNB is becoming increasingly competitive with surgical gold standards in terms of diagnostic value [3].

Given the high prevalence of thyroid nodular diseases, it is crucial to select the most appropriate diagnostic method that provides optimal accuracy for assessing the nature of thyroid nodules. In particular, CNB may be a fruitful choice for diagnosing thyroid nodules, especially in cases with cytologic Bethesda I and III results. While many studies have reported that the FNA/CNB combination provides superior diagnostic accuracy [12-19], some suggest there is no significant difference between the two methods [20,21]. Therefore, this study aims to evaluate the diagnostic yield of FNA and CNB separately and in combination for the diagnosis of thyroid nodules.

MATERIALS AND METHODS

Participants

This study was conducted on 50 patients with a total of 56 nodules. The inclusion criteria were based on the American College of Radiology (ACR) Thyroid Imaging Reporting and Data System (TI-RADS) criteria [22,23], where patients had at least one TI-RADS 3 (TR3) thyroid nodule with a diameter of 25 mm or more, a TI-RADS 4 (TR4) thyroid nodule with a diameter of 15 mm or more, and a TI-RADS 5 (TR5) thyroid nodule with a diameter of 10 mm. Exclusion criteria included a history of thyroid cancer, coagulative disorders, recent antiplatelet or anticoagulant consumption, opioid use over the past 6 months, allergies to local anesthetics, and chronic pain syndrome.

Procedures

An experienced radiologist performed all procedures using an ultrasound machine (model WS80A, Samsung, Seoul, Korea). Prior to the aspiration and biopsy, an ultrasonographic evaluation was conducted to assess the nodule size, distance from the skin surface, type of nodule calcification, and ACR TI-RADS score. Local anesthesia was administered, and FNA was performed twice with a G23 needle and a 10 mL syringe from different sites of the nodule. If sampling was improper or insufficient, it was repeated with a larger diameter needle. Two samples were collected from the solid and suspicious parts of the nodules using a CNB sampling needle with a length of 10 cm and Gauge-18. FNA was always performed before CNB due

to the destruction and disintegration of the nodule parenchyma after CNB. Patients were monitored for acute complications such as hematoma around the thyroid and voice changes or hoarseness. Follow-up was conducted for 18 months, and pathology reports of patients who underwent surgery were recorded as the gold standard.

Pathologic analysis

Samples obtained from FNA and CNB were classified into six categories based on the Bethesda 2023 system and the CNB sample reporting guideline [6,24]. The findings were considered equivalent one by one, and discrepancy between FNA and CNB results led to use of that with the higher probability of malignancy. The management approach for such cases involved either recommending surgery or a follow-up to assess any changes in their ultrasonographic features during 18 months.

Statistical analysis

The agreement between FNA and CNB methods in classifying nodules was assessed using the kappa coefficient, with values ranging from 0 to 1. Kappa values of 0–0.20, 0.21–0.40, 0.41–0.60, 0.61–0.80, and 0.81–1.0 represent no agreement, slight agreement, fair agreement, moderate agreement, and substantial agreement, respectively [25]. Sensitivity, specificity, positive predictive value, negative predictive value, and accuracy were calculated and reported for FNA, CNB, and FNA/CNB diagnostic parameters. Data were analyzed using SPSS software ver. 22 (IBM Corp., Armonk, NY, USA), and statistical significance was set at $p < .05$.

RESULTS

Between October 2020 and April 2021, 56 thyroid nodule samples were obtained at Sina Hospital, Tehran, which is affiliated with Tehran University of Medical Sciences. A convenient sampling method was employed and 50 patients were included in the study, comprising 11 males and 39 females. All nodules were sampled for the first time, and the participants were followed for 18 months to determine the outcome. The mean nodule diameter was 27 ± 12.3 mm, ranging from 12 to 67 mm. The nodules were classified according to the TI-RADS system, with 33.9% ($n = 19$) classified as TR3, 51.8% ($n = 29$) as TR4, and 14.3% ($n = 8$) as TR5. Calcification was observed in 46.4% ($n = 26$) of the nodules, with 21.4% ($n = 12$) showing punctate echogenic foci, 17.9% ($n = 10$) showing macrocalcification,

5.4% (n = 3) showing large comet-tail artifact, and 1.8% (n = 1) showing peripheral/rim calcification. In three-fourths of the malignant findings mentioned in the preoperative FNA cytologic reports, there was a suspicion of papillary thyroid carcinoma (PTC) (Tables 1 and 2).

Of the 56 thyroid nodules studied, 39 (76.5%) were benign and 12 (23.5%) were malignant. During the follow-up period, five patients with follicular neoplasm (FN) as the primary cytologic and CNB-based pathologic results were not operated on and were excluded from the final analysis due to the unavailability of postoperative pathologic tissue reports. Overall, the results indicate strong agreement between the FNA and CNB methods in the diagnosis of thyroid nodules, with a kappa coefficient of 0.837 (Fig. 1)

Among the nodules diagnosed using the FNA method,

Table 1. Characteristics of thyroid nodules

Variable	Value
Age (y/o)	54.23 ± 8.63
Size of nodule (mm)	27.0 ± 12.3
Distance from skin (mm)	12.2 ± 4.7
TI-RADS	
3	19 (33.9)
4	29 (51.8)
5	8 (14.3)
Calcification type	
None	30 (53.6)
Large comet-tail artifact	3 (5.4)
Macrocalcification	10 (17.9)
Peripheral/rim calcification	1 (1.8)
Punctate echogenic foci	12 (21.4)

Values are presented as mean ± SD or number (%). SD, standard deviation; TI-RADS, Thyroid Imaging Reporting and Data System.

Table 2. Stratification regarding cytologic and CNB-based pathologic evaluation

Category	FNA	CNB	FNA/CNB
I	6 (11.8)	0	0
II	34 (66.7)	39 (76.5)	38 (74.5)
III	4 (7.8)	2 (3.9)	3 (5.9)
IV	1 (1.9)	2 (3.9)	0
V	3 (5.9)	0	0
VI	3 (5.9)	8 (15.7)	10 (19.6)

Values are presented as number (%). CNB, core needle biopsy; FNA, fine needle aspiration.

66.7% (n = 34) were benign (Bethesda II), 5.4% (n = 3) were suspicious for malignancy (Bethesda V), and 5.4% (n = 3) were malignant (Bethesda VI). The CNB method revealed 76.5% (n = 39) benign and 15.7% (n = 8) malignant nodules (category VI), with all FNA Bethesda V nodules being confirmed by the CNB method. One of the two indeterminate nodules marked by the CNB method was found to be benign, while the other was diagnosed as PTC in the postoperative pathology reports. Additionally, two FN nodules (Bethesda IV) were identified as Follicular Thyroid Carcinoma and Oncocytic carcinoma of the thyroid. Furthermore, all six non-diagnostic nodules identified by FNA were diagnosed as benign by CNB (Fig. 2).

The combination of FNA and CNB methods resulted in 74.5% (n = 38) benign and 19.6% (n = 10) malignant (Bethesda VI) nodules. Following the FNA/CNB application, the number of non-diagnostic reports decreased, leaving only three nodules (5.8%) in the indeterminate category (category III).

After an 18-month imaging follow-up, 38 nodules that were initially diagnosed as benign using the combined method remained unchanged. On the contrary, 13 individuals underwent thyroidectomy, with 12 of these cases classified as malignant. The post-surgery pathological evaluation revealed the follow-

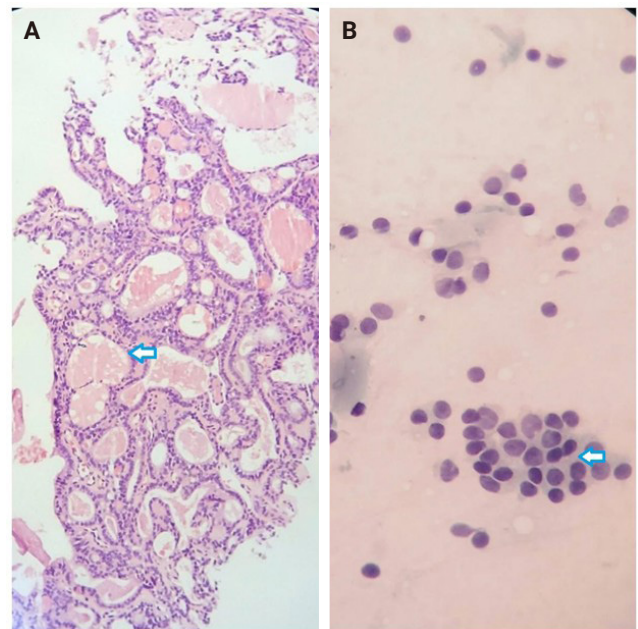


Fig. 1. In the histopathologic examination (A) of core needle biopsy and cytology examination (B) of fine needle aspiration, the arrows indicate similar bland-looking thyroid follicular cells suggestive of benign follicular nodules.

Table 3. Thyroid nodules based on postoperative pathology, delineated by the diagnostic methods employed

Category	FNA		CNB		FNA/CNB	
	Benign (n = 39)	Malignant (n = 12)	Benign (n = 39)	Malignant (n = 12)	Benign (n = 39)	Malignant (n = 12)
I	6 (15.4)	0	0	0	0	0
II	33 (84.6)	1 (8.3)	38 (97.4)	1 (8.3)	38 (97.4)	0
III	0	4 (33.3)	1 (2.6)	1 (8.3)	1 (2.6)	2 (16.7)
IV	0	1 (8.3)	0	2 (16.7)	0	0
V	0	3 (25)	0	0	0	0
VI	0	3 (25)	0	8 (66.7)	0	10 (83.3)

Values are presented as number (%).

FNA, fine needle aspiration; CNB, core needle biopsy.

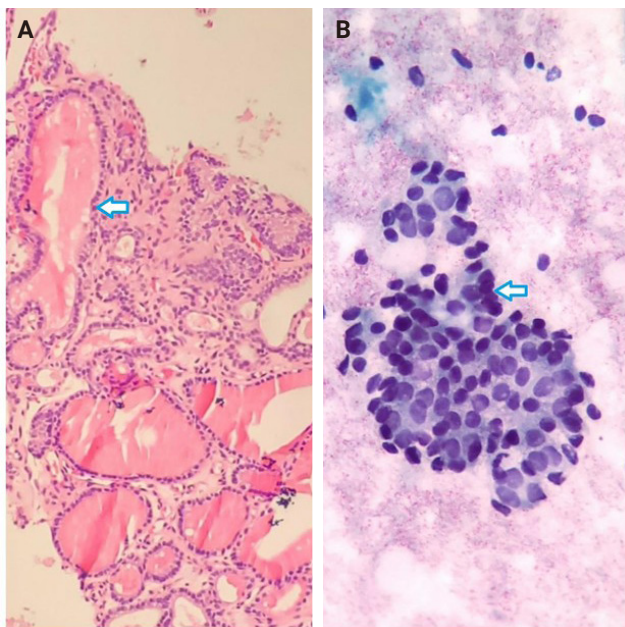


Fig. 2. There was a discrepancy between core needle biopsy (CNB) and fine needle aspiration (FNA). While in histopathologic examination (A), the arrow points to bland-looking thyroid follicular cells suggestive of benign follicular nodule on CNB, in cytologic examination (B), the arrow indicates a cluster of thyroid follicular cells with anisonucleosis and overlapping nuclei suggestive of atypia of undetermined significance on FNA.

ing diagnoses: one case of oncocytic carcinoma of the thyroid, one case of follicular thyroid carcinoma, one case of metastatic lesion, and nine cases of PTC (Table 3).

The results of Table 4 suggest that the CNB and FNA/CNB methods improve sensitivity and specificity in the diagnosis of malignancy compared to the FNA or CNB method alone. The FNA/CNB method showed a sensitivity of 83.3%, specificity of 97.4%, positive predictive value of 100%, negative predic-

Table 4. Diagnostic values of FNA, CNB, and FNA/CNB for malignant thyroid nodules

Diagnostic values	FNA	CNB	FNA/CNB
Sensitivity (%)	25	66.7	83.3
Specificity (%)	84.6	97.4	97.4
Positive predictive value (%)	100	100	100
Negative predictive value (%)	97.1	97.4	100
Accuracy	70.6	90.2	94.1

FNA, fine needle aspiration; CNB, core needle biopsy.

tive value of 100%, and a diagnostic accuracy of 94.1% for the malignancies. The CNB method had a sensitivity of 66.7%, specificity of 97.4%, positive predictive value of 100%, negative predictive value of 97.4%, and accuracy of 90.2% in diagnosis of malignant nodules. Overall, the combination of FNA and CNB methods resulted in a higher diagnostic accuracy in diagnosis of malignant thyroid lesions than either method alone. There were no cases of gross hematoma with compressive effect on the upper airways or changes in voice observed during the diagnostic procedures including FNA/CNB method (Table 4).

DISCUSSION

The study demonstrated a strong agreement between the FNA and CNB methods for diagnosing benign and malignant thyroid nodules. The frequency of non-diagnostic results in FNA was dependent on the radiologist's skill and experience, as well as nodule characteristics. In this study, an experienced radiologist performed the FNA procedure and made an effort to obtain sufficient tissue samples with each needle application. Nonetheless, a considerable portion of FNA reports (10.7%) were non-diagnostic, whereas all non-diagnostic nodules were reported as benign with CNB.

As expected, CNB had an advantage over FNA in eliminating non-diagnostic nodules. With precise penetration of the CNB needle, the results are less dependent on the operator's skill, and the obtained tissues have more cells, which reduces the frequency of non-diagnostic results. Consistent with our findings, previous studies have reported that CNB is more valuable than FNA for reducing the frequency of non-diagnostic results and providing more reliable diagnostic accuracy [7,26-28].

The CNB method had a higher frequency of atypia of undetermined significance (AUS) and FN nodules compared to FNA, possibly due to larger tissue samples and additional pathologic findings. Sometimes, nodules with suspicious ultrasound features might have normal records in FNA, indicating the possibility of FN [29,30]. In Na et al. [7], the diagnostic rate of FN was higher with CNB than FNA.

It is well-known that the rate of suspicious nodules for malignancy in FNA is higher than in CNB. Hahn et al. [26] reported that the definite diagnostic rate in CNB was significantly higher than in FNA, especially for nodules larger than 2 cm. Our results similarly showed that FNA had a lower diagnostic sensitivity than CNB.

The diagnostic accuracy of FNA/CNB and CNB was significantly higher than that of FNA alone, as expected. The combination of CNB and FNA can reduce the need for repeated FNA and diagnostic surgeries in thyroid nodules, particularly by reducing non-diagnostic cases. Although some studies have reported a diagnostic advantage of CNB over FNA alone, other studies, including our own, have shown that the combination of CNB and FNA is more beneficial than CNB alone [12-15].

While low-risk neoplasms such as non-invasive follicular thyroid neoplasm with papillary-like nuclear features (NIFTP) are classified as a surgical disease and cannot be definitively diagnosed through FNA, the cytological characteristics of this indolent tumor frequently result in its categorization as either AUS (Bethesda III), FN (Bethesda IV), or suspicious for malignancy (Bethesda V) on FNA [6]. In the cohort of 13 patients who underwent thyroidectomy in the present study, post-surgical histopathological examination revealed nine nodules diagnosed as PTC, one as follicular thyroid carcinoma, one as oncocytic carcinoma of the thyroid, and one as a metastatic lesion. Given our emphasis on diagnosing malignant lesions, we aimed to exclude any low-grade lesions (like NIFTP) from the malignant category; however, no low-grade lesions were identified in our study.

In this study, the high rate of non-diagnostic cases in nodules

examined with FNA reduced its diagnostic value compared to CNB. Among the 80% of malignant nodules not reported by FNA, most were PTC. Previous studies have reported that papillary cancer may be mistakenly classified as benign due to macrofollicular manifestations in the absence of cytological changes and atypia. Most of the false negatives in FNA were attributed to the follicular adenoma with papillary architecture [31,32].

One nodule was reported as benign in FNA but as FN/suspicious for follicular neoplasm with CNB. Subsequently, it was diagnosed as oncocytic carcinoma of the thyroid during follow-up and after surgery. Yeh et al. [33] also encountered several patients with thyroid cancer in postoperative tissue diagnosis despite having FNA reports without malignant or suspected cells. False-negative rates in FNA could be due to poor cell aspiration or sampling error.

Thyroid nodules containing calcified foci can reduce the diagnostic sensitivity of FNA. While peripheral calcification is rare among suspicious nodules and more common in benign lesions, in some cases, it may be necessary to sample from a calcified nodule. Macrocalcifications are not significantly associated with an increased risk of malignancy, while punctate echogenic foci are often linked to psammomatous calcification in papillary thyroid cancer and carry a high risk of malignancy. Peripheral calcification presents challenges for nodule sampling, including difficulties in penetrating the shell, visualizing the needle tip within the lesion, and unexpected complications [34-36].

The results of the current study indicate that all AUS nodules, except for one malignant case, had calcified foci in their postoperative reports (five nodules with punctate echogenic foci and one nodule with macrocalcifications). In cases where there is clinical suspicion of malignancy in a lesion with macrocalcification, it may be reasonable to use CNB as a complementary diagnostic method to FNA.

The current study encountered several limitations, particularly a reduction in sample size. Due to the infrequent use of CNB for thyroid nodules in Iran, as well as many other regions, this study was designed as a pilot project to establish a foundation for future research with larger cohorts. The coronavirus disease 2019 pandemic further exacerbated the situation, as many patients were hesitant to seek medical care, leading to the loss of numerous potentially eligible participants.

While the study's setting and regional relevance are significant strengths, the limited follow-up period of 18 months and

the potential impact of operator expertise on FNA results are other important limitations. The literature establishes that the TI-RADS criteria recommend a five-year follow-up for nodules scoring 3 or higher, with TR3 and TR4 lesions monitored at 1, 3, and 5 years, and TR5 lesions requiring annual assessments. This protocol is contingent upon the nodule size evaluated via FNA [23].

In contrast, there is a lack of consensus regarding follow-up protocols for nodules subjected to CNB. The combination of CNB with FNA offers a significant advantage by potentially reducing follow-up intervals and enhancing decision-making in thyroid nodule management. Given that all nodules were subjected to the CNB, it is logical to propose a reduction in the follow-up period for patients compared to the conventional post-FNA follow-up duration outlined in TI-RADS. Therefore, the researchers established a maximum follow-up duration of 18 months for the patients involved in the study. However, extending follow-up for CNB-subjected nodules to 3 to 5 years could markedly improve diagnostic accuracy.

Additionally, the diagnostic accuracy of FNA for thyroid nodules varies widely across studies, reported between 28% and 72% [8,16-18]. This variability arises from several factors, including lesion characteristics (solid and cystic components, calcifications), FNA technique, use of ultrasound guidance, quality of ultrasound equipment, experience of the technician, the pathologist expertise in cytological evaluation. Despite FNA's affordability and accessibility, these limitations diminish its diagnostic accuracy [37-40]. Determining the specific contribution of each factor to FNA outcomes is challenging and may not be particularly beneficial. Therefore, employing CNB, which provides tissue samples, appears to be a reasonable strategy to overcome these limitations. Even with experienced technicians, optimal control over other influencing factors remains problematic [8,16,18,19,41].

In conclusion, our study findings suggest that FNA/CNB is more effective than either FNA or CNB alone in nodules with a TI-RADS score ≥ 3 , particularly when the initial FNA report is non-diagnostic. Therefore, we recommend using CNB in conjunction with FNA for nodules with a TI-RADS score ≥ 3 to decrease the need for further evaluations. This combined approach could also minimize unnecessary surgeries and enhance diagnostic accuracy.

Ethics Statement

All procedures were in compliance with the guidelines of the

1964 Helsinki Declaration and its later amendments and also were approved and monitored by the Medical Ethics Committee of Tehran University of Medical Sciences (reference number: IR.TUMS.SINAHOSPITAL.REC.1400.029). Patients who met the inclusion criteria were also provided a full explanation of the study procedure and were enrolled after signing a written informed consent.

Availability of Data and Material

All data generated or analyzed during the study are included in this published article (and its supplementary information files).

Code Availability

Not applicable.

ORCID

Mohammad Ali Hasannia	https://orcid.org/0009-0001-5964-8456
Ramin Pourghorban	https://orcid.org/0000-0001-8543-7540
Hoda Asefi	https://orcid.org/0000-0002-2277-9436
Amir Aria	https://orcid.org/0000-0002-5553-5884
Elham Nazar	https://orcid.org/0000-0001-6182-3893
Hojat Ebrahimini	https://orcid.org/0000-0002-6583-4386
Alireza Mohamadian	https://orcid.org/0000-0002-3476-8400

Author Contributions

Conceptualization: RP, HA, HE. Data curation: MAH, AM. Formal analysis: EN. Funding acquisition: MAH. Investigation: MAH, AA. Methodology: RP, EN. Project administration: MAH. Resources: MAH, AM. Software: AA. Supervision: RP, HA, HE. Validation: RP. Visualization: EN, AM. Writing – original draft: MAH, AM. Writing – review & editing: RP, AA. Approval of final manuscript: all authors.

Conflicts of Interest

The authors declare that they have no potential conflicts of interest.

Funding Statement

The present study was supported by Tehran University of Medical Sciences.

Acknowledgments

This study formed a part of MAH's radiology specialty graduation thesis.

REFERENCES

1. Chen H, Song A, Wang Y, et al. *BRAF*(V600E) mutation test on fine-needle aspiration specimens of thyroid nodules: Clinical correlations for 4600 patients. *Cancer Med* 2022; 11: 40-9.
2. Choi SH, Baek JH, Lee JH, et al. Thyroid nodules with initially non-diagnostic, fine-needle aspiration results: comparison of core-needle biopsy and repeated fine-needle aspiration. *Eur Radiol* 2014; 24: 2819-26.
3. Strauss EB, Iovino A, Upender S. Simultaneous fine-needle aspiration and core biopsy of thyroid nodules and other superficial head and neck masses using sonographic guidance. *AJR Am J Roentgenol* 2008; 190: 1697-9.
4. Yoon JH, Kim EK, Kwak JY, Moon HJ. Effectiveness and limitations of core needle biopsy in the diagnosis of thyroid nodules: review of current literature. *J Pathol Transl Med* 2015; 49: 230-5.
5. Na DG, Kim JH, Sung JY, et al. Core-needle biopsy is more useful than repeat fine-needle aspiration in thyroid nodules read as non-diagnostic or atypia of undetermined significance by the Bethesda system for reporting thyroid cytopathology. *Thyroid* 2012; 22: 468-75.
6. Ali SZ, Baloch ZW, Cochand-Priollet B, Schmitt FC, Vielh P, VanderLaan PA. The 2023 Bethesda System for Reporting Thyroid Cytopathology. *Thyroid* 2023; 33: 1039-44.
7. Na DG, Baek JH, Jung SL, et al. Core needle biopsy of the thyroid: 2016 consensus statement and recommendations from Korean Society of Thyroid Radiology. *Korean J Radiol* 2017; 18: 217-37.
8. Su X, Yue C, Yang W, Ma B. A comparative analysis of core needle biopsy and repeat fine needle aspiration in patients with inconclusive initial cytology of thyroid nodules. *Front Endocrinol (Lausanne)* 2024; 15: 1309005.
9. Pyo JS, Sohn JH, Kang G. Core needle biopsy is a more conclusive follow-up method than repeat fine needle aspiration for thyroid nodules with initially inconclusive results: a systematic review and meta-analysis. *J Pathol Transl Med* 2016; 50: 217-24.
10. Baloch ZW, Cibas ES, Clark DP, et al. The National Cancer Institute Thyroid fine needle aspiration state of the science conference: a summation. *Cytojournal* 2008; 5: 6.
11. Park KT, Ahn SH, Mo JH, et al. Role of core needle biopsy and ultrasonographic finding in management of indeterminate thyroid nodules. *Head Neck* 2011; 33: 160-5.
12. Samir AE, Vij A, Seale MK, et al. Ultrasound-guided percutaneous thyroid nodule core biopsy: clinical utility in patients with prior nondiagnostic fine-needle aspirate. *Thyroid* 2012; 22: 461-7.
13. Yi KS, Kim JH, Na DG, et al. Usefulness of core needle biopsy for thyroid nodules with macrocalcifications: comparison with fine-needle aspiration. *Thyroid* 2015; 25: 657-64.
14. Renshaw AA, Pinnar N. Comparison of thyroid fine-needle aspiration and core needle biopsy. *Am J Clin Pathol* 2007; 128: 370-4.
15. Sung JY, Na DG, Kim KS, et al. Diagnostic accuracy of fine-needle aspiration versus core-needle biopsy for the diagnosis of thyroid malignancy in a clinical cohort. *Eur Radiol* 2012; 22: 1564-72.
16. Cortazar-Garcia R, Martin-Escalante MD, Robles-Cabeza L, Martinez-Santos C. Usefulness of ultrasound-guided core biopsy in thyroid nodules with inconclusive fine-needle aspiration biopsy findings. *Radiologia (Engl Ed)* 2022; 64: 195-205.
17. Ahn SH. Usage and diagnostic yield of fine-needle aspiration cytology and core needle biopsy in thyroid nodules: a systematic review and meta-analysis of literature published by Korean authors. *Clin Exp Otorhinolaryngol* 2021; 14: 116-30.
18. Kwon H, Lee J, Hong SW, Kwon HJ, Kwak JY, Yoon JH. Fine needle aspiration cytology vs. core needle biopsy for thyroid nodules: a prospective, experimental study using surgical specimen. *Tae-han Yongsang Uihakhoe Chi* 2022; 83: 645-57.
19. Aysan E, Guler B, Kiran T, Idiz UO. Core needle biopsy in the diagnosis of thyroid nodules. *Am Surg* 2023; 89: 5170-4.
20. Silverman JF, West RL, Finley JL, et al. Fine-needle aspiration versus large-needle biopsy or cutting biopsy in evaluation of thyroid nodules. *Diagn Cytopathol* 1986; 2: 25-30.
21. Stangierski A, Wolinski K, Martin K, Leitgeber O, Ruchala M. Core needle biopsy of thyroid nodules: evaluation of diagnostic utility and pain experience. *Neuro Endocrinol Lett* 2013; 34: 798-801.
22. Tessler FN, Middleton WD, Grant EG. Thyroid Imaging Reporting and Data System (TI-RADS): a user's guide. *Radiology* 2018; 287: 29-36.
23. Tessler FN, Middleton WD, Grant EG, et al. ACR Thyroid Imaging, Reporting and Data System (TI-RADS): white paper of the ACR TI-RADS Committee. *J Am Coll Radiol* 2017; 14: 587-95.
24. Jung CK, Baek JH, Na DG, Oh YL, Yi KH, Kang HC. 2019 Practice guidelines for thyroid core needle biopsy: a report of the Clinical Practice Guidelines Development Committee of the Korean Thyroid Association. *J Pathol Transl Med* 2020; 54: 64-86.
25. Landis JR, Koch GG. The measurement of observer agreement for categorical data. *Biometrics* 1977; 33: 159-74.
26. Hahn SY, Shin JH, Oh YL, Park KW, Lim Y. Comparison between fine needle aspiration and core needle biopsy for the diagnosis of thyroid nodules: effective indications according to US findings.

- Sci Rep 2020; 10: 4969.
27. Trimboli P, Nasrollah N, Guidobaldi L, et al. The use of core needle biopsy as first-line in diagnosis of thyroid nodules reduces false negative and inconclusive data reported by fine-needle aspiration. *World J Surg Oncol* 2014; 12: 61.
 28. Yeon JS, Baek JH, Lim HK, et al. Thyroid nodules with initially nondiagnostic cytologic results: the role of core-needle biopsy. *Radiology* 2013; 268: 274-80.
 29. Moon WJ, Baek JH, Jung SL, et al. Ultrasonography and the ultrasound-based management of thyroid nodules: consensus statement and recommendations. *Korean J Radiol* 2011; 12: 1-14.
 30. Seo HS, Lee DH, Park SH, Min HS, Na DG. Thyroid follicular neoplasms: can sonography distinguish between adenomas and carcinomas? *J Clin Ultrasound* 2009; 37: 493-500.
 31. Mehanna R, Murphy M, McCarthy J, et al. False negatives in thyroid cytology: impact of large nodule size and follicular variant of papillary carcinoma. *Laryngoscope* 2013; 123: 1305-9.
 32. Jung CK, Bychkov A, Kakudo K. Update from the 2022 World Health Organization classification of thyroid tumors: a standardized diagnostic approach. *Endocrinol Metab (Seoul)* 2022; 37: 703-18.
 33. Yeh MW, Demircan O, Ituarte P, Clark OH. False-negative fine-needle aspiration cytology results delay treatment and adversely affect outcome in patients with thyroid carcinoma. *Thyroid* 2004; 14: 207-15.
 34. Erdem Toslak I, Martin B, Barkan GA, Kilic AI, Lim-Dunham JE. Patterns of sonographically detectable echogenic foci in pediatric thyroid carcinoma with corresponding histopathology: an observational study. *AJNR Am J Neuroradiol* 2018; 39: 156-61.
 35. Gwon HY, Na DG, Noh BJ, et al. Thyroid nodules with isolated macrocalcifications: malignancy risk of isolated macrocalcifications and postoperative risk stratification of malignant tumors manifesting as isolated macrocalcifications. *Korean J Radiol* 2020; 21: 605-13.
 36. Nabahati M, Ghaemian N, Moazezi Z, Mehraeen R. Different sonographic features of peripheral thyroid nodule calcification and risk of malignancy: a prospective observational study. *Pol J Radiol* 2021; 86: e366-71.
 37. Choi SH, Han KH, Yoon JH, et al. Factors affecting inadequate sampling of ultrasound-guided fine-needle aspiration biopsy of thyroid nodules. *Clin Endocrinol (Oxf)* 2011; 74: 776-82.
 38. Garcia Pascual L, Surralles ML, Morlius X, Gonzalez Minguez C, Viscasillas G, Lao X. Ultrasound-guided fine needle aspiration of thyroid nodules with on-site cytological examination: Diagnostic efficacy, prevalence, and factors predicting for Bethesda category I results. *Endocrinol Diabetes Nutr (Engl Ed)* 2019; 66: 495-501.
 39. Wang CY, Zhou Y, Ren YY, Luan YS, Jiang ZC, Wang ZX. Analysis of the influencing factors on fine-needle aspiration biopsy results of the thyroid. *Front Surg* 2022; 9: 907086.
 40. Fu Y, Sun Y, Pei Q, et al. Factors influencing the sample adequacy of ultrasound-guided fine-needle aspiration from solid thyroid nodules for liquid-based cytology: a demographic, sonographic, and technical perspective. *Medicina (Kaunas)* 2022; 58: 1639.
 41. Pantanowitz L, Thompson LDR, Jing X, Rossi ED. Is thyroid core needle biopsy a valid compliment to fine-needle aspiration? *J Am Soc Cytopathol* 2020; 9: 383-8.

Histopathological characteristics of Epstein-Barr virus (EBV)-associated encephalitis and colitis in chronic active EBV infection

Betty A Kasimo¹, James J Yahaya², Sun Och Yoon³, Se Hoon Kim³, Minsun Jung³

¹Department of Pathology, Faculty of Health Sciences, Busitema University, Mbale, Uganda

²Department of Pathology, School of Health Sciences, Soroti University, Soroti, Uganda

³Department of Pathology, Yonsei University College of Medicine, Seoul, Korea

Chronic active Epstein-Barr virus (CAEBV) can induce complications in various organs, including the brain and gastrointestinal tract. A 3-year-old boy was referred to the hospital with a history of fever and seizures for 15 days. A diagnosis of encephalitis based on computed tomography (CT) and magnetic resonance imaging findings and clinical correlation was made. Laboratory tests showed positive serology for Epstein-Barr virus (EBV) and negative for Rotavirus antigen and IgG and IgM antibodies for cytomegalovirus, herpes simplex virus, and varicella zoster virus, respectively. Abdominal CT showed diffuse wall thickening with fluid distension of small bowel loops, lower abdomen wall thickening, and a small amount of ascites. The biopsy demonstrated positive Epstein-Barr encoding region in situ hybridization in cells within the crypts and lamina propria. The patient was managed with steroids and hematopoietic stem cell transplantation (HSCT). This case showed histopathological characteristics of concurrent EBV-associated encephalitis and colitis in CAEBV infection. The three-step strategy of immunosuppressive therapy, chemotherapy, and allogeneic HSCT should be always be considered for prevention of disease progression.

Keywords: Epstein-Barr virus infections; Lymphoproliferative disorders; Colitis; Encephalitis, viral

INTRODUCTION

Epstein-Barr virus (EBV), a double-stranded DNA virus categorized within the Herpesviridae family, causes a ubiquitous infection in more than 90% of the world's population [1,2]. EBV is usually acquired during childhood or adolescence and then establishes a permanent latent infection in B lymphocytes in immunocompetent patients [3-5]. Chronic active EBV (CAEBV) infection is a rare lymphoproliferative disorder characterized by persistent infectious mononucleosis-like symptoms for more than 3 months, increased EBV DNA ($>10^{2.5}$ copies/mg) in peripheral blood, and organ involvement in an immunocompetent patient [6-8]. Various organs can

be affected in CAEBV infection and they show a spectrum of manifestations. The ill-defined, diverse clinicopathological characteristics of CAEBV infection often delay the diagnosis and treatment [1,9,10]. In this study, we report a 3-year-old patient with CAEBV infection, who was confirmed to have both EBV encephalitis and EBV colitis through pathological examination. The diagnosis of EBV encephalitis and EBV colitis can be a challenge in pathological practice because of the deceptive morphologies. Using microscopic examination and in situ hybridization technique, we diagnosed EBV infection in both the brain and colon tissue, resulting in successful diagnosis and treatment.

Received: June 21, 2024 **Revised:** January 11, 2025 **Accepted:** February 21, 2025

Corresponding Author: Minsun Jung, MD, PhD

Department of Pathology, Yonsei University College of Medicine, 50-1 Yonsei-ro, Seodaemun-gu, Seoul 03722, Korea

Tel: +82-2-2228-1771, Fax: +82-2-362-0860, E-mail: jjunglammy@gmail.com

This is an Open Access article distributed under the terms of the Creative Commons Attribution Non-Commercial License (<https://creativecommons.org/licenses/by-nc/4.0/>) which permits unrestricted non-commercial use, distribution, and reproduction in any medium, provided the original work is properly cited.

© 2025 The Korean Society of Pathologists/The Korean Society for Cytopathology

CASE REPORT

A 3-year-old boy was admitted to the Severance Hospital (Seoul, Korea) with a history of fever and seizures for 15 days. The boy did not have any history of recurrent infections or family history of immune disease. Computed tomography (CT) and magnetic resonance imaging (MRI) showed swelling in the basal ganglia, thalamus, midbrain, pons, cerebellum, and left hypothalamus (Fig. 1A). The initial EBV level was elevated to 1,685,506 U/mL in the serum and 103,285 U/mL in the cerebrospinal fluid. In serology, anti-viral capsid antigen (VCA) IgM was undetected while anti-VCA IgG was positive which indicated chronic response to EBV. Although the patient was managed empirically with steroids, his mental status remained unstable. To confirm the diagnosis, brain biopsy was performed. The brain tissue sections showed focal perivascular and subarachnoid lymphocyte infiltration and focal microglial cell proliferation (Fig. 1B). However, CD3-positive T lymphocytes infiltrated the perivascular area (Fig. 1C) and these cells were positive to EBV in situ hybridization (Fig. 1D). Further testing revealed that CD3-positive cells expressed CD8 (Fig. 1E), but not CD4. Moreover, molecular analysis showed no evidence of T-cell receptor (TCR) beta or TCR gamma gene rearrangement. A week later, the patient developed perianal ulceration, diarrhea, and abdominal pain. Abdominal CT showed diffuse wall thickening and distension in the small bowel loops indicating high risk of perforation. The patient un-

derwent ileocecectomy (Fig. 2A). The resected colon showed dense infiltration of lymphocytes, neutrophils, and plasma cells in the lamina propria and widespread neutrophilic cryptitis, crypt abscess, and distortion. The lymphocytes showed minimal atypia. Multifocal submucosal edema with serositis was prominent (Fig. 2B). Diagnosis of EBV-associated colitis was made based on Epstein-Barr encoding region (EBER) in situ hybridization of positive CD3 T lymphocytes that infiltrated the mucosa, submucosa, and intestinal walls (Fig. 2C, D). Immunohistochemical staining for CD56 showed a few scattered natural killer (NK) cells. The diagnosis of CAEBV also befits the patient. Germline testing using next-generation sequencing analysis revealed no pathogenic gene mutations associated with immune dysregulation. The human leukocyte antigen (HLA) typing results were as follows: HLA-A*02:06/02:06, -B*15:18/51:01, -C*08:01/14:02, -DRB1*04:05/14:05, -DQA1*01:04/03:03, -DQB1*04:01/05:03, -DPA1*01:03/02:02, and -DPB1*02:01/05:01. Full matched allogeneic hematopoietic stem cell transplantation (HSCT) was performed 6 months after the initial diagnosis. EBV level decreased to 34,262 copies/mL in serum 12 months after treatment (Fig. 3).

DISCUSSION

We herein report a patient with CAEBV infection showing both EBV encephalitis and colitis. It is an infection induced by infiltration of EBV-infected lymphocytes into the affected tissues

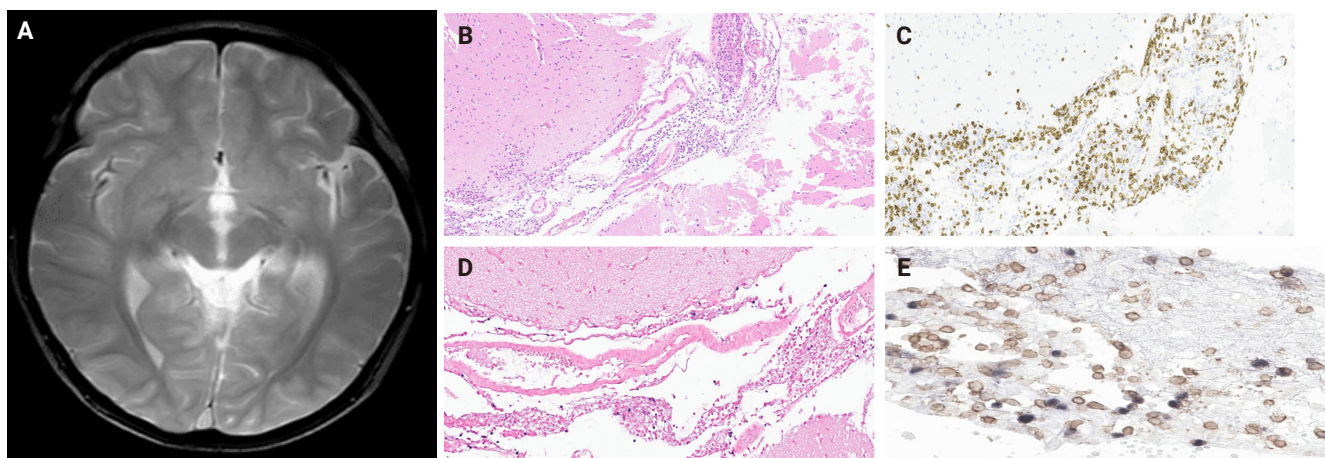


Fig. 1. (A) Magnetic resonance imaging showing swollen and multifocal T2 high signal intensity with swelling of the basal ganglia, thalamus, midbrain, pons, cerebellum, and left hypothalamus. (B) Brain tissue sections showing focal perivascular and subarachnoid lymphocyte infiltration and focal microglial cell proliferation. (C) CD3-positive T-lymphocytes infiltrating the perivascular area. (D, E) In situ hybridization of Epstein-Barr encoding region and CD8-positive Epstein-Barr virus double-staining cells from the brain tissue.

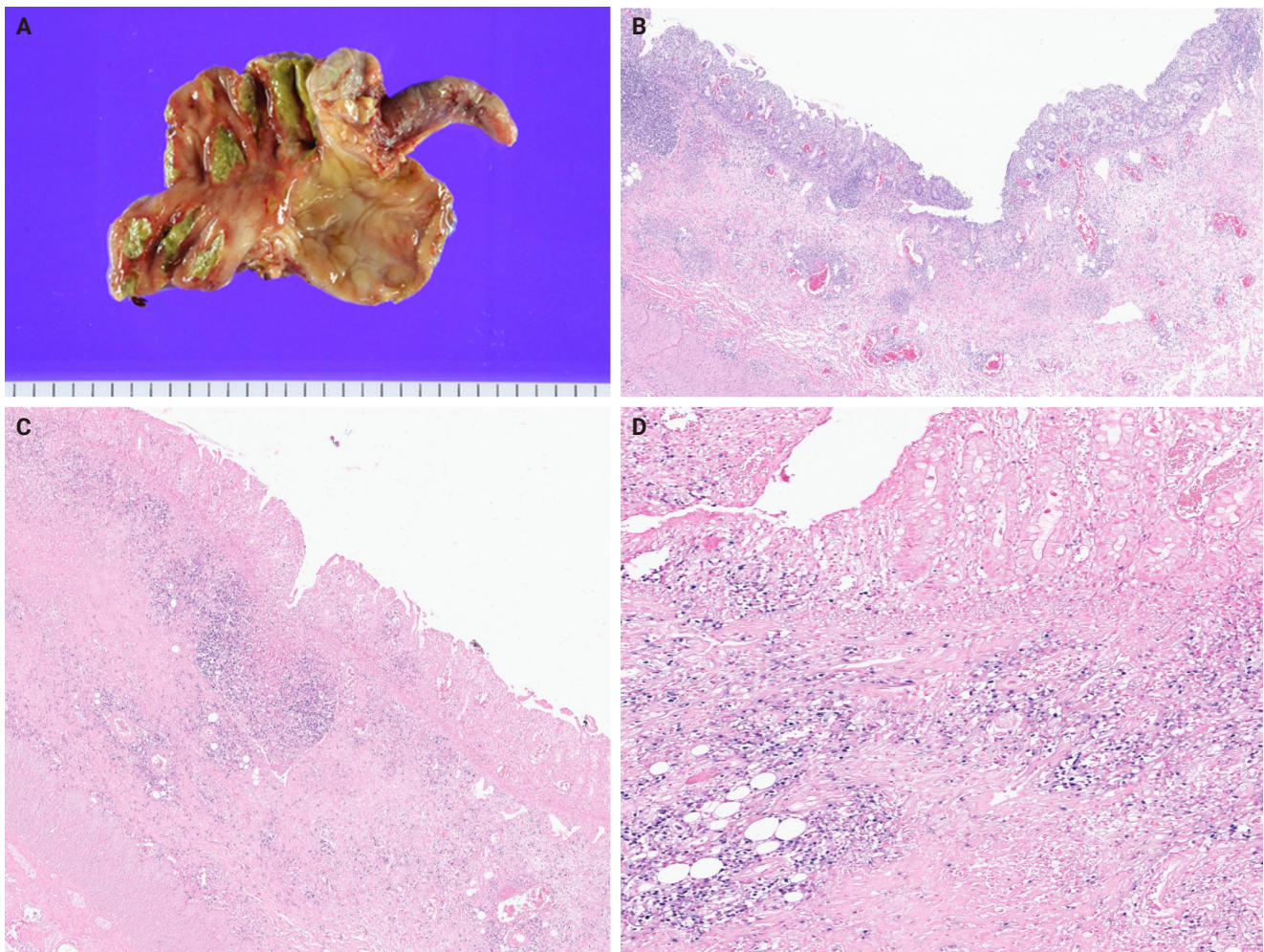


Fig. 2. (A) Gross appearance of the ileocecectomy specimen with appendix attached, the mucosa surface showing multiple ulcerative lesions in the cecum. (B) The ileocecectomy specimen demonstrating infiltration of the lymphocytes, neutrophils, and plasma cells in the lamina and widespread neutrophilic cryptitis, crypt abscess, and distortion. (C, D) CD3-positive Epstein-Barr encoding region (EBER) in situ hybridization cells from the colon tissue (EBER antibody staining).

[11,12]. EBV infects NK and T cells in CAEBV; T-cell CAEBV is further classified into CD4- and CD8-positive types [12,13].

Comprehensive assessment of multiple organs with high suspicion and correct recognition of EBV-associated histopathological features are important for the diagnosis of CAEBV infection [14]. It was difficult to diagnose EBV encephalitis and colitis in our patient owing to the subtle and deceptive morphologies. A brain biopsy performed after steroid treatment demonstrated mild lymphocytic infiltration and subtle microglial proliferation. The colon showed inflammatory bowel disease (IBD)-like microscopic changes, including marked glandular distortion and transmural chronic inflammation with cryptitis and crypt abscess. The detection of EBV in tissue sam-

ples using in situ hybridization demonstrated an EBV-induced pathological process, highlighting the critical role of EBV assay in the diagnosis of CAEBV infection [4].

EBV can lead to various central nervous system complications [15]. Some authors have suggested that there has been an increase in the occurrence of neurological complications of EBV infection [16,17]. A study examining pediatric EBV-associated encephalitis found that EBV infection was present in 9.7% of the children hospitalized with neurological complications [18]. EBV encephalitis is rare in children but can have severe neurological complications; usually, the positive MRI findings occur in the brain stem, basal ganglia, cerebellum, and thalamus [19-21]. This was somewhat similar to MRI findings of the

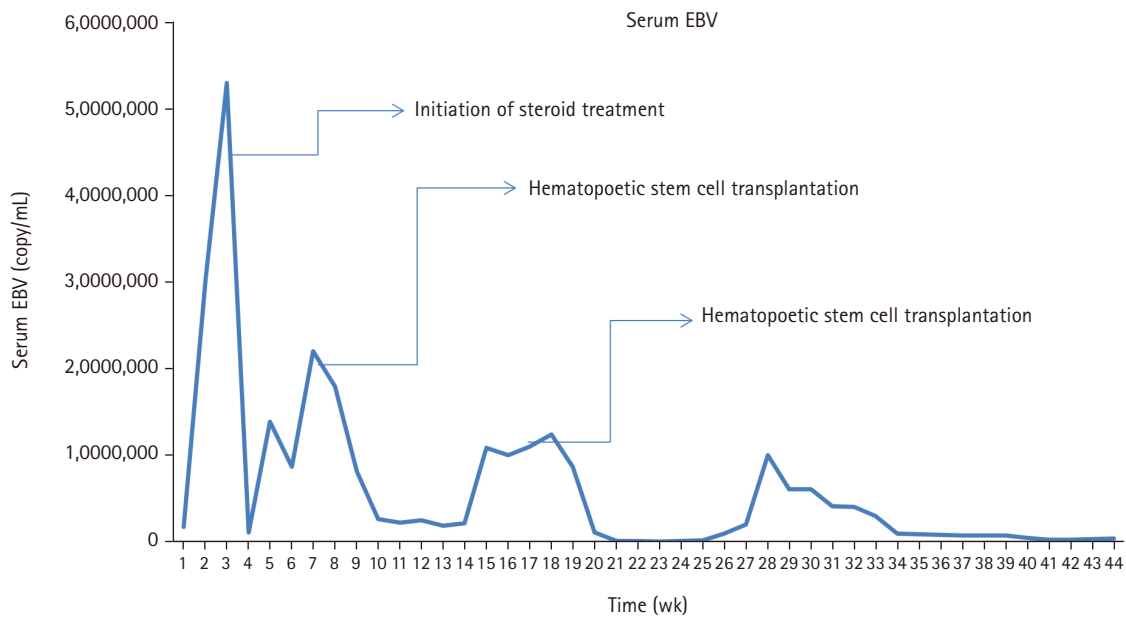


Fig. 3. The serum Epstein-Barr virus (EBV) titers before and after hematopoietic stem cell transplantation.

present case that showed hyperintense T2 lesion in the thalamus, basal ganglia, and brain stem.

EBV encephalitis can show various clinical and histological characteristics [16,22]. Establishing a diagnosis of EBV encephalitis is difficult; consequently, molecular, serological, and imaging techniques should be used when investigating children with encephalitis [15]. Biopsy is important to confirm general pediatric encephalitis because it may reveal the underlying infective process, chronic inflammatory change, or neoplastic disease [23]. Diagnosing EBV encephalitis requires demonstration of EBV-infected cells. Our case showed EBV-infected T lymphocytes infiltrating the perivascular area; this is consistent with the previous reports [16,22,24]. The EBV-infected T lymphocytes in our case were CD8-positive, thereby confirming EBV encephalitis involving CD8-positive T lymphocytes. Another study conducted on EBV encephalitis reported features of cortical infiltration of T lymphocytes with perivascular and perineuronal clusters, while the B lymphocytes were frequently seen in the perivascular cuffs [25]. The prognosis associated with EBV encephalitis is controversial. Some reports have suggested it to be a relatively benign, self-limited disease with an almost full recovery; however, others have documented the occurrence of various neurologic sequelae in a substantial number of cases [15,18,26].

Gastrointestinal involvement is very rare and few cases of

immunocompetent hosts have been reported [27-29]. Among these, the lymphoid cells that were involved were of the B-cell lineage. However, our case had involvement of the T-cell lineage. EBV colitis is rare in children, and few cases have been reported [30]. EBV colitis is difficult to differentiate from IBD owing to overlapping symptoms and endoscopic findings, and discerning whether the severity of symptoms is attributable to CAEBV or the exacerbation of IBD is challenging, thereby making diagnosis of EBV colitis and IBD difficult [9,31,32]. Our case demonstrated findings that were consistent with the pathological findings observed by other authors in their studies [9,33,34]. Despite the similarity between IBD and EBV colitis, it was noted that atypical infiltrates were more frequently observed in patients with EBV positivity. Consequently, every patient with IBD should undergo the EBV test [35]. Although further studies are warranted to clarify the role of EBV in inflammatory gut disorders, it was proposed that EBV may induce immune alterations in the colon, thereby aiding the pathogenesis of EBV colitis [36]. The molecular detection of EBV-encoded RNA transcripts by in situ hybridization remains the gold standard in the identification of EBV in biopsies [35].

Our patient's viral load was initially high on admission, after the initiation of steroids and immunosuppressive agents; it reduced gradually with significant improvement after HSCT. The effective treatment strategy for eradicating EBV-infected Tor

NK-positive cells is HSCT, if initiated before deterioration of the patient's condition. HSCT is, by far, considered the most effective treatment for CAEBV by revitalizing the hematopoietic system. However, because not all patients with CAEBV may undergo HSCT, immunosuppression and chemotherapy can also be considered with or without HSCT [37]. Although the outcome of patients with active disease accompanied by fever, liver dysfunction among others may be worse [1,38]. Studies have proved that manifestation of signs and symptoms is subject to the host immune responses [9,39]. Usually, patients with EBV infection have serious clinical abnormalities that may persist for 6 months or more with high antibody titers against EBV but not against EBV nuclear antigen [9,39]. Thus, multiple organ involvement in CAEBV infection often results in poor prognosis [14,40]. The present case may be slightly different owing to early recognition; awareness of CAEBV, especially regarding the histological changes, EBER, and EBV DNA, are crucial for patients with EBV, similar to what was observed in another study [34]. CAEBV disease and post-HSCT lymphoproliferative disorders share similarities. However, although both post-HSCT posttransplant lymphoproliferative disorders (PTLD) and CAEBV disease involve EBV reactivation and immune dysfunction, distinct differences exist between conditions [3,6]. PTLD is predominantly of B-cell origin, compared to CAEBV being of T-cell origin. Although monomorphic PTLD of T-cell origin exist, it is typically EBV-negative [41].

Several genetic factors of CAEBV have been found to increase genetic susceptibility of the hosts. For example, candidate gene studies of transplant HLA have reported that transplant recipients have haplotypes, such as HLA-A26 and B36, that are associated with a higher risk of developing EBV-positive B-cell origin PTLD [42]. The HLA result of our patient indicated no increased risk to CAEBV disease.

This case showed histopathological characteristics of concurrent EBV-associated encephalitis and colitis in CAEBV infection. CAEBV is an extremely rare and severe complication that can arise from EBV infection. It is a life-threatening medical condition that is more likely to occur as a result of primary infection, reactivation, and immunosuppression. Histopathological features will help the discrimination, serum EBV DNA and in situ hybridization for EBV-encoded RNA are recommended to exclude. This condition is more likely to pose treatment challenges, especially when the treatment is initiated at a late stage. HSCT should be considered a crucial therapeutic option for preventing the progression of disease.

Ethics Statement

All procedures performed in the current study were approved by the institutional review board (IRB) of Severance Hospital (reference # 4-2024-0533 dated 19th June 2024) in accordance with the 1964 Helsinki Declaration and its later amendments. Patient consent waiver was obtained for this study.

Availability of Data and Material

All relevant data and information pertaining to the patient presented in this case report are included in the manuscript.

Code Availability

Not applicable.

ORCID

Betty A Kasimo	https://orcid.org/0009-0007-3150-3830
James J Yahaya	https://orcid.org/0000-0003-3647-5262
Sun Och Yoon	https://orcid.org/0000-0002-5115-1402
Se Hoon Kim	https://orcid.org/0000-0001-7516-7372
Minsun Jung	https://orcid.org/0000-0002-8701-4282

Author Contributions

Conceptualization: MJ. Data curation: BKA, MJ. Formal analysis: SOY, SHK, MJ. Funding acquisition: MJ. Investigation: BKA, MJ. Methodology: MJ. Project administration: MJ. Resources: SOY, SHK, MJ. Software: BKA. Supervision: JJY, MJ. Validation: MJ. Visualization: BKA. Writing—original draft: BKA, MJ. Writing—review & editing: all authors. Approval of final manuscript: all authors.

Conflicts of Interest

S.H.K., a contributing editor of the *Journal of Pathology and Translational Medicine*, was not involved in the editorial evaluation or decision to publish this article. All remaining authors have declared no conflicts of interest.

Funding Statement

This work was supported by the National Research Foundation of Korea (NRF) grant funded by the Korean government (MSIT) (RS-2024-00341570).

REFERENCES

1. Arai A. Advances in the study of chronic active Epstein-Barr virus infection: clinical features under the 2016 WHO classification

- and mechanisms of development. *Front Pediatr* 2019; 7: 14.
2. Zhang T, Fu Q, Gao D, Ge L, Sun L, Zhai Q. EBV associated lymphomas in 2008 WHO classification. *Pathol Res Pract* 2014; 210: 69-73.
 3. Kimura H. Pathogenesis of chronic active Epstein-Barr virus infection: is this an infectious disease, lymphoproliferative disorder, or immunodeficiency? *Rev Med Virol* 2006; 16: 251-61.
 4. Cohen JI, Jaffe ES, Dale JK, et al. Characterization and treatment of chronic active Epstein-Barr virus disease: a 28-year experience in the United States. *Blood* 2011; 117: 5835-49.
 5. Kimura H, Hoshino Y, Hara S, et al. Differences between T cell-type and natural killer cell-type chronic active Epstein-Barr virus infection. *J Infect Dis* 2005; 191: 531-9.
 6. Kimura H, Cohen JI. Chronic active Epstein-Barr virus disease. *Front Immunol* 2017; 8: 1867.
 7. Ambinder RF. Epstein-Barr virus-associated lymphoproliferative disorders. *Rev Clin Exp Hematol* 2003; 7: 362-74.
 8. Hong M, Ko YH, Yoo KH, et al. EBV-positive T/NK-Cell lymphoproliferative disease of childhood. *Korean J Pathol* 2013; 47: 137-47.
 9. Xu W, Jiang X, Chen J, et al. Chronic active Epstein-Barr virus infection involving gastrointestinal tract mimicking inflammatory bowel disease. *BMC Gastroenterol* 2020; 20: 257.
 10. Quintanilla-Martinez L, Ko YH, Kimura H, Jaffe ES. EBV-positive T-cell and NK-cell lymphoproliferative diseases of childhood. In: Swerdlow SH, Campo E, Harris N, eds. *WHO classification of tumours of haematopoietic and lymphoid tissues*. Lyon: IARC Press, 2017; 355-60.
 11. Kimura H, Morishima T, Kanegane H, et al. Prognostic factors for chronic active Epstein-Barr virus infection. *J Infect Dis* 2003; 187: 527-33.
 12. Kimura H, Hoshino Y, Kanegane H, et al. Clinical and virologic characteristics of chronic active Epstein-Barr virus infection. *Blood* 2001; 98: 280-6.
 13. Kimura H, Ito Y, Kawabe S, et al. EBV-associated T/NK-cell lymphoproliferative diseases in nonimmunocompromised hosts: prospective analysis of 108 cases. *Blood* 2012; 119: 673-86.
 14. Liu R, Wang M, Zhang L, et al. The clinicopathologic features of chronic active Epstein-Barr virus infective enteritis. *Mod Pathol* 2019; 32: 387-95.
 15. Hashemian S, Ashrafzadeh F, Akhondian J, Beiraghi Toosi M. Epstein-barr virus encephalitis: a case report. *Iran J Child Neurol* 2015; 9: 107-10.
 16. Hausler M, Ramaekers VT, Doenges M, Schweizer K, Ritter K, Schaade L. Neurological complications of acute and persistent Epstein-Barr virus infection in paediatric patients. *J Med Virol* 2002; 68: 253-63.
 17. Jang YY, Lee KH. Transient asymptomatic white matter lesions following Epstein-Barr virus encephalitis. *Korean J Pediatr* 2011; 54: 389-93.
 18. Doja A, Bitnun A, Ford Jones EL, et al. Pediatric Epstein-Barr virus-associated encephalitis: 10-year review. *J Child Neurol* 2006; 21: 384-91.
 19. Phowthongkum P, Phantumchinda K, Jutivorakool K, Suankratay C. Basal ganglia and brainstem encephalitis, optic neuritis, and radiculomyelitis in Epstein-Barr virus infection. *J Infect* 2007; 54: e141-4.
 20. Shian WJ, Chi CS. Fatal brainstem encephalitis caused by Epstein-Barr virus. *Pediatr Radiol* 1994; 24: 596-7.
 21. Johkura K, Momoo T, Kuroiwa Y. Thalamic involvement of Epstein-Barr virus encephalitis demonstrated by MRI. *J Neurol* 2003; 250: 357-8.
 22. Francisci D, Sensini A, Fratini D, et al. Acute fatal necrotizing hemorrhagic encephalitis caused by Epstein-Barr virus in a young adult immunocompetent man. *J Neurovirol* 2004; 10: 414-7.
 23. Layard Horsfall H, Toescu SM, Grover PJ, et al. The utility of brain biopsy in pediatric cryptogenic neurological disease. *J Neurosurg Pediatr* 2020; 26: 431-8.
 24. Kano K, Katayama T, Takeguchi S, et al. Biopsy-proven case of Epstein-Barr virus (EBV)-associated vasculitis of the central nervous system. *Neuropathology* 2017; 37: 259-64.
 25. Hart M. Greenfield's neuropathology. *J Neuropathol Exp Neurol* 2008; 67: 828.
 26. Domachowske JB, Cunningham CK, Cummings DL, Crosley CJ, Hannan WP, Weiner LB. Acute manifestations and neurologic sequelae of Epstein-Barr virus encephalitis in children. *Pediatr Infect Dis J* 1996; 15: 871-5.
 27. Clayton RA, Malcomson RD, Gilmour HM, Crawford DH, Parks RW. Profuse gastrointestinal haemorrhage due to delayed primary Epstein-Barr virus infection in an immunocompetent adult. *Histopathology* 2005; 47: 439-41.
 28. Na HK, Ye BD, Yang SK, et al. EBV-associated lymphoproliferative disorders misdiagnosed as Crohn's disease. *J Crohns Colitis* 2013; 7: 649-52.
 29. Karlitz JJ, Li ST, Holman RP, Rice MC. EBV-associated colitis mimicking IBD in an immunocompetent individual. *Nat Rev Gastroenterol Hepatol* 2011; 8: 50-4.
 30. Tseng YJ, Ding WQ, Zhong L, Chen J, Luo ZG. Chronic active Epstein-Barr virus (CAEBV) enteritis. *Int J Infect Dis* 2019; 82: 15-7.

31. Wakefield AJ, Fox JD, Sawyerr AM, et al. Detection of herpesvirus DNA in the large intestine of patients with ulcerative colitis and Crohn's disease using the nested polymerase chain reaction. *J Med Virol* 1992; 38: 183-90.
32. Zhang B, Wang X, Tian X, Cai Y, Wu X. Chronic active Epstein-Barr virus-associated enteritis: CT findings and clinical manifestation. *Biomed Res Int* 2020; 2020: 2978410.
33. Wang Y, Li Y, Meng X, et al. Epstein-Barr virus-associated T-cell lymphoproliferative disorder presenting as chronic diarrhea and intestinal bleeding: a case report. *Front Immunol* 2018; 9: 2583.
34. Tian S, Westbrook LM, Xiao SY, Zhang Y, Huang Y, Wang HL. The morphologic features of primary Epstein-Barr virus infection in the gastrointestinal tract: an approach to correct diagnosis. *Am J Surg Pathol* 2019; 43: 1253-63.
35. Nissen LH, Nagtegaal ID, de Jong DJ, et al. Epstein-Barr virus in inflammatory bowel disease: the spectrum of intestinal lymphoproliferative disorders. *J Crohns Colitis* 2015; 9: 398-403.
36. Ryan JL, Shen YJ, Morgan DR, et al. Epstein-Barr virus infection is common in inflamed gastrointestinal mucosa. *Dig Dis Sci* 2012; 57: 1887-98.
37. Sawada A, Inoue M, Kawa K. How we treat chronic active Epstein-Barr virus infection. *Int J Hematol* 2017; 105: 406-18.
38. Okamura T, Hatsukawa Y, Arai H, Inoue M, Kawa K. Blood stem-cell transplantation for chronic active Epstein-Barr virus with lymphoproliferation. *Lancet* 2000; 356: 223-4.
39. Yamashita S, Murakami C, Izumi Y, et al. Severe chronic active Epstein-Barr virus infection accompanied by virus-associated hemophagocytic syndrome, cerebellar ataxia and encephalitis. *Psychiatry Clin Neurosci* 1998; 52: 449-52.
40. Huang L, Zhang X, Fang X. Case report: Epstein-Barr virus encephalitis complicated with brain stem hemorrhage in an immune-competent adult. *Front Immunol* 2021; 12: 618830.
41. Ok CY, Li L, Young KH. EBV-driven B-cell lymphoproliferative disorders: from biology, classification and differential diagnosis to clinical management. *Exp Mol Med* 2015; 47: e132.
42. Reshef R, Luskin MR, Kamoun M, et al. Association of HLA polymorphisms with post-transplant lymphoproliferative disorder in solid-organ transplant recipients. *Am J Transplant* 2011; 11: 817-25.

Cytological features of atypical adenomatous hyperplasia and adenocarcinoma in situ of the lung: a case report

Misa Takahashi¹, Seiya Homma¹, Chisato Setoguchi¹, Yoko Umezawa², Atsuhiko Sakamoto¹

¹Department of Pathology and Laboratory Medicine, Omori Red Cross Hospital, Tokyo, Japan

²Department of Pathology, Fukushima Medical University Hospital, Fukushima, Japan

Atypical adenomatous hyperplasia (AAH) and adenocarcinoma in situ (AIS) are generally treated as different lesions, depending on the differences in lesion size and histological findings. However, these differences are not absolute; thus, AAH and AIS are often difficult to distinguish. Moreover, whether AAH and AIS can be regarded as different lesions remains unknown because cytological specimens, especially those of AAH, are rare. In this study, we examined these uncommon cytological specimens and compared the cytological findings between AAH and AIS. We observed many common cytological features with no obvious differences between AAH and AIS. These findings suggest that these two distinct lesions can be grouped into a single category. Therefore, we propose creating a new cytological category.

Keywords: Atypical adenomatous hyperplasia; Adenocarcinoma in situ; Cytology; Case report

INTRODUCTION

Atypical adenomatous hyperplasia (AAH) is generally defined as lesions ≤ 0.5 cm in diameter [1,2]. These lesions are difficult to detect with preoperative computed tomography (CT) scans owing to the 0.5 cm detection limit of thin-slice CT [3,4]. Therefore, most AAHs are incidentally discovered during visual examination of the cut surfaces of resected lung cancer specimens or through the investigation of pathological specimens using microscopy. Thus, cytological specimens of AAH are rare and their details remain unclear [4]. The present study aimed to address this gap by preparing cytological specimens of lesions diagnosed as AAH or adenocarcinoma in situ (AIS), respectively. We examined the cytological features of AAH and compared them with those of AIS. We then investigated the differences between AAH and AIS, and whether they could be distinguished based on cytological findings. We also compared the definitional, histological, and genetic differences and sim-

ilarities between AAH and AIS to investigate the need to consider them as different lesions.

CASE REPORT

Case 1 involved a 53-year-old Japanese non-smoking female. The patient's comorbidities included chronic cough due to gastroesophageal reflux disease, cough variant asthma, hyperlipidemia, hypertension, and leiomyoma. The patient's uncle had tongue cancer. Chest CT was performed to investigate the chronic cough and revealed ground-glass opacity (GGO) 0.7 cm in diameter in the left upper lobe of the lung. Subsequently, as the GGO could have been lung cancer, the patient underwent thoracoscopic partial resection of the left upper lobe.

Case 2 involved a 78-year-old Japanese female exposed to secondhand smoke. The patient's comorbidities included severe mitral stenosis and atrial fibrillation. The patient's father and brother had pancreatic cancer. Chest CT was performed for

Received: February 18, 2025 **Revised:** April 4, 2025 **Accepted:** April 9, 2025

Corresponding Author: Misa Takahashi, CT

Department of Pathology and Laboratory Medicine, Omori Red Cross Hospital, 4-30-1, Chuo, Ota-ku, Tokyo 143-8527, Japan

Tel: +81-3-3775-3111, Fax: +81-3-3776-0004, E-mail: mishaaa000.t@gmail.com

*This article was presented at the 20th Korea-Japan Joint Meeting for Diagnostic Cytopathology, September 2, 2023, in Gunsan, Korea.

This is an Open Access article distributed under the terms of the Creative Commons Attribution Non-Commercial License (<https://creativecommons.org/licenses/by-nc/4.0/>) which permits unrestricted non-commercial use, distribution, and reproduction in any medium, provided the original work is properly cited.

© 2025 The Korean Society of Pathologists/The Korean Society for Cytopathology

preoperative evaluation of severe mitral stenosis and revealed multiple GGOs in both lungs. These GGOs were followed up with CT. During follow-up, one of the multiple GGOs at the apex of the right upper lobe increased from 0.6 cm to 0.8 cm in diameter and its density also increased. These CT findings suggested that the precancerous lesion may have transformed into invasive cancer. Therefore, thoracoscopic partial resection of the right upper lobe was performed.

Cytological findings

In both cases, we rubbed the respective lesions on isolated lung specimens with Orcellex Brush RT (Rovers Medical Devices BV, Oss, Netherlands) and collected the lesions in BD Cytorich

red preservation solution (Becton Dickinson and Company, Sparks, MD, USA). Then, we performed liquid-based cytological examination of the Papanicolaou-stained specimens using the BD Cytorich method.

Case 1

The low-power view showed sheet-like, mildly overlapping cell aggregates (Fig. 1A). The high-power view revealed that the atypical cells comprising these aggregates had pale cytoplasm, nuclei with finely granular chromatin, and tiny, prominent nucleoli (Fig. 1B). Nuclear irregularities, including nuclear wrinkles, were often observed (Fig. 1C), while intranuclear cytoplasmic inclusion bodies (Fig. 1B) and nuclear grooves ap-

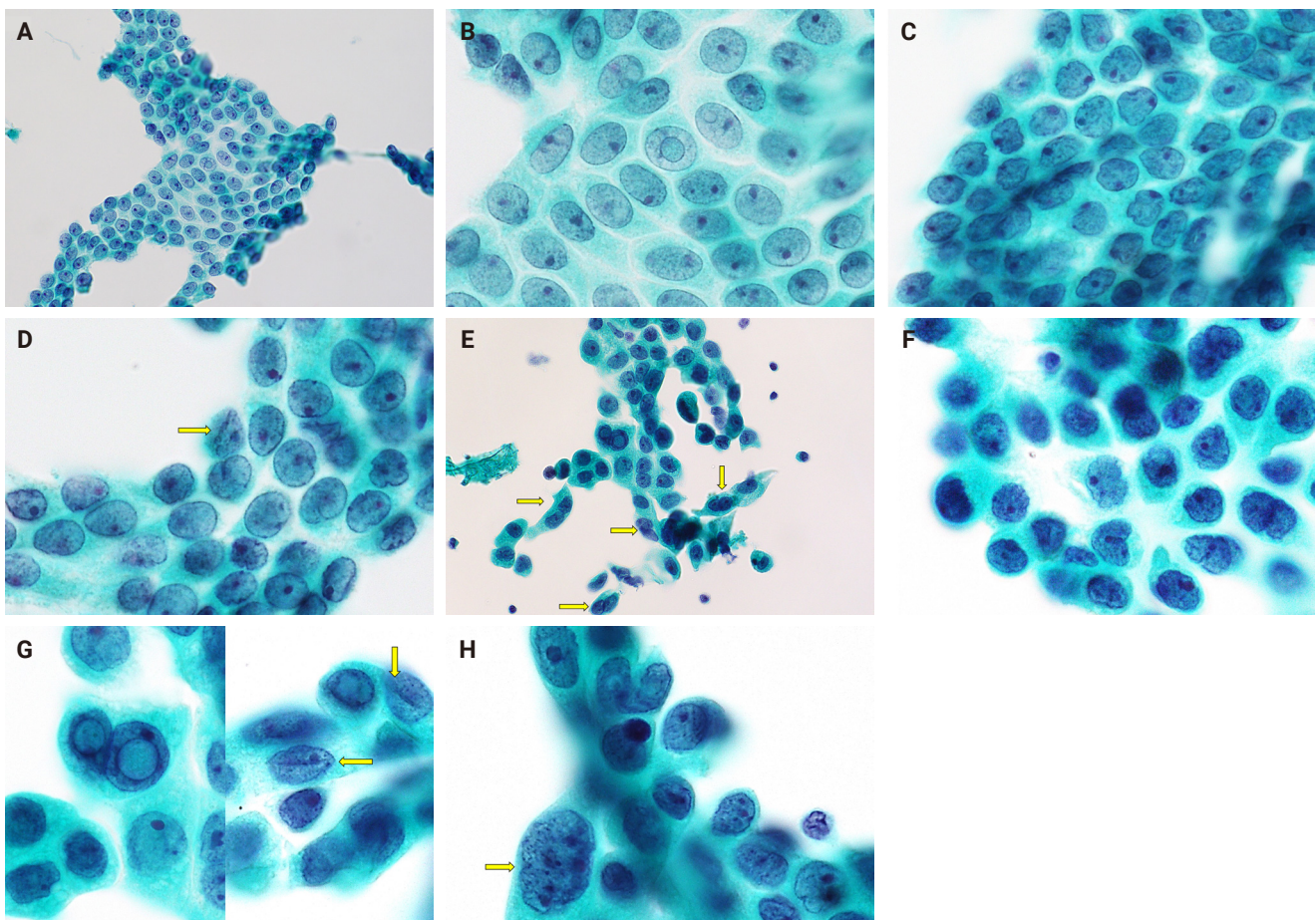


Fig. 1. Cytological features of atypical adenomatous hyperplasia (AAH) and adenocarcinoma in situ (AIS). (A) Low-power view of AAH cells showing sheet-like aggregates. (B) High-power view of AAH cells showing intranuclear cytoplasmic inclusion bodies in the center. (C) Conspicuous nuclear wrinkles in AAH cells. (D) Nuclear groove in AAH cells (yellow arrow). (E) Sheet-like appearance of AIS cell clusters at low-magnification, as well as several binuclear cells (yellow arrows). (F) High-magnification of AIS cells showing clear nuclear wrinkles. (G) Intranuclear cytoplasmic inclusion bodies and nuclear grooves (yellow arrows) in AIS cells. (H) Mild cell size variation observes in AIS cells. The cell in the lower left (yellow arrow) is twice as large as the other cells (A–H, Pap).

pearing similar to coffee beans, were sometimes observed (Fig. 1D). Binuclear cells were rarely identified.

Case 2

At low-magnification, atypical cell clusters appeared sheet-like and showed mild overlap, with several binuclear cells observed in a single cell cluster (Fig. 1E). Binuclear cells were often observed on the cytological slides. At high-magnification, the atypical cells were small and had high nucleus-to-cytoplasm (N/C) ratios, pale cytoplasm, nuclei with finely granular chromatin, small prominent nucleoli, and often clear nuclear wrinkles (Fig. 1F). Intranuclear cytoplasmic inclusion bodies and nuclear grooves were occasionally observed (Fig. 1G). The atypical cells were usually uniform but showed mild size variation (Fig. 1H).

Histological findings

Case 1

The alveolar septal walls were thickened (Fig. 2A). Atypical cells resembling type II alveolar epithelial cells and Clara cells had proliferated and replaced the existing alveolar epithelium (Fig. 2B). These atypical cells were small, uniform, and hyperchromatic. Moreover, they also had high N/C ratios and sometimes showed intranuclear cytoplasmic inclusion bodies (Fig. 2B). Based on these histological findings and the lesion size (0.5 cm in diameter), we diagnosed the lesion as AAH.

Case 2

The alveolar septal walls were thickened with inflammatory cell infiltration and papillary architecture (Fig. 2C). Atypical cells that resembled type II alveolar epithelial cells and Clara cells

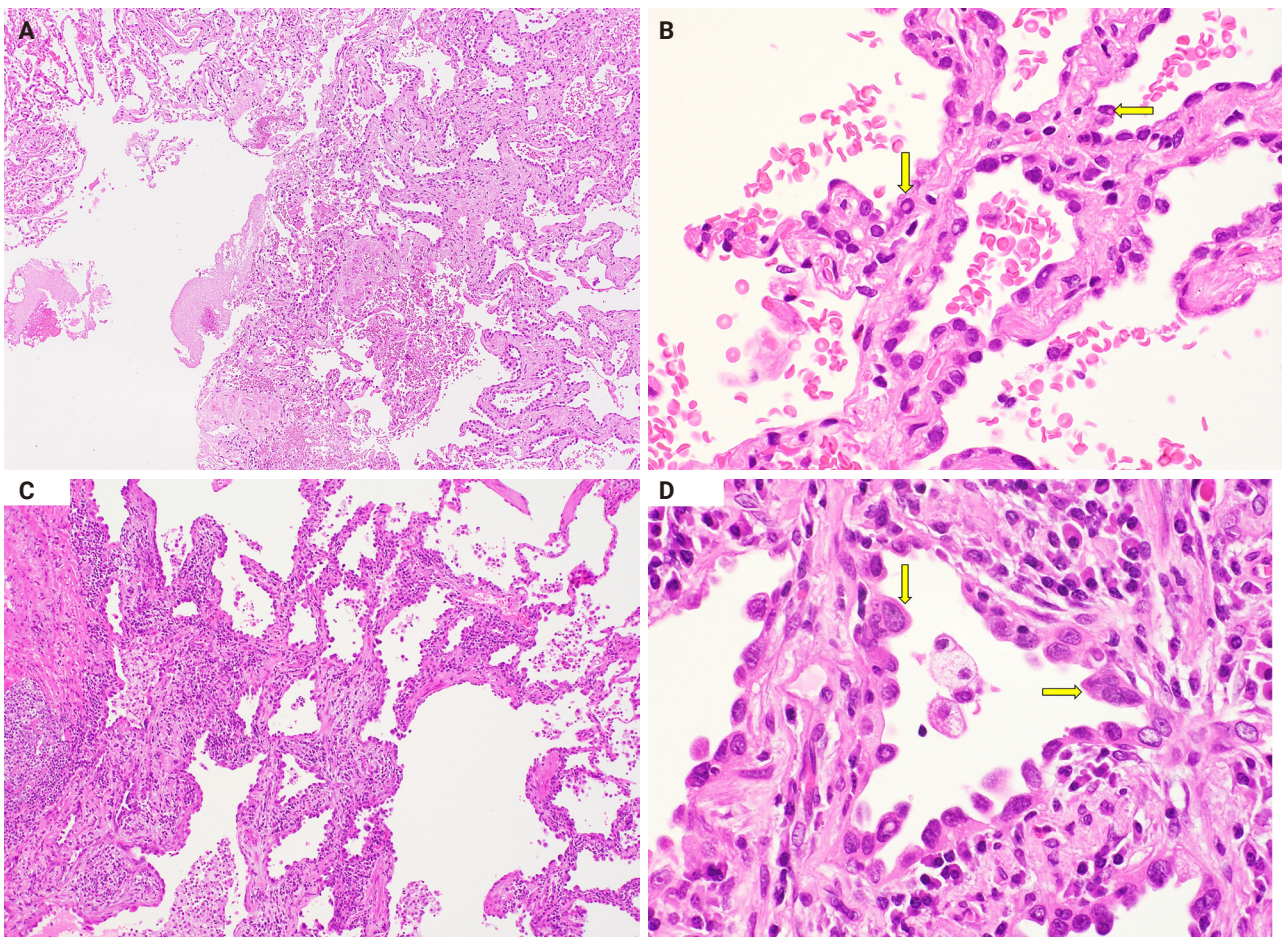


Fig. 2. Histological features of atypical adenomatous hyperplasia (AAH) and adenocarcinoma in situ (AIS). (A) Low-power view of an AAH lesion showing alveolar septal wall thickening. (B) Similarity of AAH cells with type II alveolar epithelial and Clara cells. Intranuclear cytoplasmic inclusion bodies are shown (yellow arrows). (C) Low-magnification showing thickened alveolar septal walls with permeated inflammatory cells, along with papillary structures. (D) Mild size variation and overlap in AIS cells (yellow arrows).

had proliferated, replacing the existing alveolar epithelium (Fig. 2D). These atypical cells were small, hyperchromatic, and had high N/C ratios (Fig. 2D). Mild size variations were observed, with partial nuclei overlap (Fig. 2D). Intranuclear cytoplasmic inclusion bodies and binuclear cells were also observed. Based on these histological findings and the lesion size (0.8 cm in diameter), we diagnosed the lesion as AIS.

DISCUSSION

We initially compared the histological findings of AAH and AIS. Both AAH and AIS cells resemble type II alveolar epithelial cells and Clara cells, and proliferate and replace existing alveolar epithelium. However, AAH and AIS differ in lesion size, overall lesion structure, and the presence of mild variations in cell size. In addition to lesion size, the cell density and chromatin condition [5,6] can be used to differentiate AAH from AIS, as in the present study. However, distinguishing these conditions remains challenging [4]. Thus, differentiating AAH from AIS should consider both histological findings and lesion size.

Second, we compared the cytological findings between AAH and AIS. Many cytological features were shared between AAH and AIS, including sheet-like and mildly overlapping cell aggregates; small cells; high N/C ratio; pale cytoplasm; fine granular chromatin; small prominent nucleoli; and cell irregularities such as intranuclear cytoplasmic inclusion bodies, nuclear wrinkles, and some nuclear grooves. Slight differences were observed between the two conditions. The first was the size variation in atypical cells. While the AAH cells were generally uniform in size, some AIS cells exhibited mild size variation. The second was the frequency of binuclear cells, as more binuclear cells were observed on AIS slides than on AAH slides, and more than one binuclear cell was identified in each AIS cell cluster. In contrast, binuclear cells were barely observed on the AAH slides. Despite these two slight differences, they did not differentiate AAH from AIS as the mild size variations were not seen on the entire AIS specimen, and binuclear cells are also observed in AAH [6]. In addition, the overall lesion structures and lesion sizes could not be determined in the cytological specimens. Therefore, our cases suggest that cytological specimens alone cannot be used to differentiate AAH from AIS.

These slight cytological differences between AAH and AIS are also observed in severe dysplasia and carcinoma in situ in the gynecological region. These types show slight cytological differences, including the N/C ratio and nuclear findings [7].

Severe dysplasia shows an N/C ratio $\leq 80\%$ and nuclear irregularities [7]. In contrast, carcinoma in situ has an N/C ratio $> 80\%$ and smooth and taut nuclear edges [7]. Both severe dysplasia and carcinoma in situ are atypical parabasal cells of approximately the same size, with fine granular chromatin. Despite these differences, they are often difficult to distinguish; therefore, they are treated as a single category (CIN3) in the World Health Organization (WHO) classification [7]. Thus, the same categorization might be considered for cytological findings in AAH and AIS.

Finally, we summarize the histological, genetic, and definitional differences and similarities between AAH and AIS. One difference was lesion size. The “General Rule for Clinical and Pathological Record of Lung Cancer” defines AAH as a localized precancerous lesion of peripheral adenocarcinoma of the lung with a diameter ≤ 0.5 cm [1]. It defines AIS as a localized adenocarcinoma ≤ 3.0 cm in diameter, with tumor cells resembling type II alveolar epithelial and Clara cells and dense proliferation [1]. AIS is further defined as replacement growth without stromal, vascular, or pleural invasion [1]. However, AAH measuring > 0.5 cm has been reported [3,8,9]; in such cases, lesion sizes cannot inform their differentiation. Other differences between AAH and AIS include the histological type and findings. AIS rarely has a mucinous type, whereas AAH only has a nonmucinous type [1,6]. While some histological findings may also help to differentiate AAH and AIS [5,6], the potential for strong cell atypia in AAH [9] can make this challenging. The histological similarities between AAH and AIS include type II alveolar epithelial cells and Clara cells and proliferation displacing the alveolar epithelium [1,4,6]. Additionally, both have thick alveolar septal walls [6] and show immunohistochemical positivity for thyroid transcription factor-1 [1,6]. In addition, if surgically removed, the survival rate is almost 100% [4,10]. Peripheral-type lung adenocarcinoma is thought to occur through a multistage process involving AAH, AIS, and invasive adenocarcinoma with gradual accumulation of genetic mutations [6,9,11,12]. *KRAS* mutations have been detected as early as the AAH stage [11], with comparable detection rates between AAH and AIS [11,13].

Although AAH and AIS differ in lesion size and histological findings, the criteria for their differentiation are not always clear. However, as they share cytological, histological, genetic, and definition similarities, AAH and AIS may not need to be treated as different lesions. The WHO Reporting System for Lung Cytopathology does not differentiate AAH from AIS in

the diagnosis of cytopathology specimens [14]. The monograph does not use AIS as cytodiagnostic terminology, and AAH is not mentioned [14]. Additionally, new criteria for assessing tumor invasion from the International Association for the Study of Lung Cancer Pathology Committee suggests the precise classification of AIS as low-risk lesions [10], supporting the findings of the present case report. Therefore, at least in the cytological field, where lesion sizes are not relevant, we suggest that AAH and AIS be regarded as a single category.

The conclusions of this study require validation in future studies including additional cytology specimens from patients with AAH. However, as discussed above, such cases are rare [4], which complicates the collection of such specimens. In our experience, cytology specimens of AIS are easier to collect than those of AAH. Therefore, we intend to substantiate our conclusions by comparing the cytological images of AAH presented in this report with those of AIS we will collect in the future.

Ethics Statement

This report was approved by the Institutional Review Board (IRB) of Omori Red Cross Hospital (No 24-61, 2025.1.10) and complied with the principles of the 1964 Declaration of Helsinki and its later amendments. Informed consent was obtained from all individual participants included in this study.

Availability of Data and Material

The datasets generated or analyzed during the study are available from the corresponding author upon reasonable request.

Code Availability

Not applicable.

ORCID

Misa Takahashi <https://orcid.org/0009-0009-4261-6616>
 Seiya Homma <https://orcid.org/0009-0001-8606-4456>
 Chisato Setoguchi <https://orcid.org/0009-0002-1731-2855>
 Yoko Umezawa <https://orcid.org/0009-0001-7757-7153>
 Atsuhiko Sakamoto <https://orcid.org/0009-0004-7610-0689>

Author Contributions

Conceptualization: MT, SH, CS, AS. Investigation: MT. Methodology: MT, YU, AS. Project administration: MT. Resources: MT, SH, CS. Supervision: MT, AS. Visualization: MT. Writing—original draft preparation: MT, YU, AS. Writing—review & editing: MT, YU, AS. Approval of final manuscript: all authors.

Conflicts of Interest

The authors declare that they have no potential conflicts of interest.

Funding Statement

No funding to declare.

REFERENCES

1. Japan Lung Cancer Society. General rule for clinical and pathological record of lung cancer. 8th ed. Tokyo: Kanehara, 2021; 89-90.
2. Thoracic tumor histology based on WHO 5th ed vol 1.3 ed [Internet]. Tokyo: Japan Lung Cancer Society, 2022 [cited 2024 Dec 15]. Available from: <https://www.haigan.gr.jp/publication/guidance/who-histopathology/>.
3. Sakaguchi M. A case of atypical adenomatous hyperplasia incidentally detected in resected specimen of spontaneous pneumothorax in a young adult. *J Jpn Assoc Chest Surg* 2022; 36: 75-9.
4. Kitamura A, Yatabe Y. Atypical adenomatous hyperplasia. *Pathol Clin* 2019; 37: 113-5.
5. Kunugi S, Kawamoto M. Pathology of lung cancer WHO classification and future revisions. *Clin Images* 2010; 26: 124-33.
6. Minami Y. Differentiation of preinvasive lesions of the glandular types (atypical adenomatous hyperplasia, adenocarcinoma in situ, minimally invasive adenocarcinoma). *Pathol Clin* 2016; 34: 256-9.
7. Aozasa K, Kinjo M, Kamei T, Higuchi K. Color atlas of differential diagnosis in cytology. Tokyo: Ishiyaku, 2021; 70-3.
8. Koizumi N, Sonoyama Y, Oi H, Asatani M, Ozaki T, Seki H. Ground-glass opacity nodule/subsolid nodules on thin-section CT of the lung. *J Niigata Cancer Center Hosp* 2019; 57: 48-52.
9. Kitaguchi S, Iwamoto Y, Inata J, Oyakawa T, Fujiwara T. Recent overview of atypical adenomatous hyperplasia of the lung. *Med J Hiroshima City Hosp* 2010; 26: 10-4.
10. Hong TH, Hwang S, Cho J, et al. Clinical significance of the proposed pathologic criteria for invasion by the International Association for the Study of Lung Cancer in resected nonmucinous lung adenocarcinoma. *J Thorac Oncol* 2024; 19: 425-33.
11. Minami Y, Noguchi M. Atypical adenomatous hyperplasia and lung cancer. *Nippon Rinsho* 2013; 71: 140-5.
12. Kitamura H, Hayashi H, Nozawa A, Ito T, Kanisawa M. Developmental mechanism of lung adenocarcinoma. *Sougo Rinsho* 2001; 50: 2229-35.
13. Yoshida Y, Shibata T, Kokubu A, et al. Mutations of the epidermal

growth factor receptor gene in atypical adenomatous hyperplasia and bronchioalveolar carcinoma of the lung. *Lung Cancer* 2005; 50: 1-8.

14. IAC-IARC-WHO Joint Editorial Board. WHO Reporting System for Lung Cytopathology. Lyon: International Agency for Research on Cancer, 2022; 2-4, 111.

Erratum: Diagnostic challenges in the assessment of thyroid neoplasms using nuclear features and vascular and capsular invasion: a multi-center interobserver agreement study

Agnes Stephanie Harahap^{1,2}, Mutiah Mutmainnah³, Maria Francisca Ham^{1,2}, Dina Khoirunnisa⁴, Abdillah Hasbi Assadyk⁵, Husni Cangara⁶, Aswiyanti Asri⁷, Diah Prabawati Retnani⁸, Fairuz Quzwain⁹, Hasrayati Agustina¹⁰, Hermawan Istiadi¹¹, Indri Windarti¹², Krisna Murti¹³, Muhammad Takbir¹⁴, Ni Made Mahastuti¹⁵, Nila Kurniasari¹⁶, Nungki Anggorowati¹⁷, Pamela Abineno¹⁸, Yulita Pundewi Setyorini¹⁹, Kennichi Kakudo²⁰

¹Department of Anatomical Pathology, Faculty of Medicine, Universitas Indonesia/Dr. Cipto Mangunkusumo Hospital, Jakarta, Indonesia

²Human Cancer Research Center-Indonesian Medical Education and Research Institute, Faculty of Medicine, Universitas Indonesia, Jakarta, Indonesia

³Faculty of Medicine, Universitas Muhammadiyah Palembang, Palembang, Indonesia

⁴Faculty of Medicine, Universitas Padjadjaran/Hasan Sadikin General Hospital, Bandung, Indonesia

⁵Department of Otorhinolaryngology, Head and Neck Surgery, Harapan Kita National Women and Children Health Center, Jakarta, Indonesia

⁶Department of Anatomical Pathology, Faculty of Medicine, Hasanuddin University, Makassar, Indonesia

⁷Department of Anatomical Pathology, Faculty of Medicine, Andalas University, Padang, Indonesia

⁸Department of Anatomical Pathology, Faculty of Medicine, Universitas Brawijaya/RSUD dr. Saiful Anwar, Malang, Indonesia

⁹Department of Anatomical Pathology, Faculty of Medicine and Health Science, Universitas Jambi, Jambi, Indonesia

¹⁰Department of Anatomical Pathology, Faculty of Medicine, Universitas Padjadjaran/Hasan Sadikin General Hospital, Bandung, Indonesia

¹¹Department of Anatomical Pathology, Faculty of Medicine, Universitas Diponegoro, Semarang, Indonesia

¹²Department of Anatomical Pathology, Faculty of Medicine, Universitas Lampung, Lampung, Indonesia

¹³Department of Anatomical Pathology, Faculty of Medicine, Universitas Sriwijaya, Palembang, Indonesia

¹⁴Department of Anatomical Pathology, Labuha Hospital, South Halmahera, Indonesia

¹⁵Department of Anatomical Pathology, Faculty of Medicine, Universitas Udayana, Prof. Dr. I.G.N.G. Ngoerah Hospital, Denpasar, Indonesia

¹⁶Department of Anatomical Pathology, Faculty of Medicine, Universitas Airlangga/Dr. Soetomo Academic Hospital, Surabaya, Indonesia

¹⁷Department of Anatomical Pathology, Faculty of Medicine, Public Health, and Nursing, Universitas Gadjah Mada/UGM Academic Hospital, Yogyakarta, Indonesia

¹⁸Department of Anatomical Pathology, Dr. Ben Mboi Hospital, Kupang, Indonesia

¹⁹Kanujoso Djatwibowo Hospital, Balikpapan, Indonesia

²⁰Department of Pathology and Thyroid Disease Center, Izumi City General Hospital, Izumi, Japan

To the Editor:

We found an error in our published article.

Harahap AS, Mutmainnah M, Ham MF, et al. Diagnostic challenges in the assessment of thyroid neoplasms using nuclear features and vascular and capsular invasion: a multi-center interobserver agreement study. *J Pathol Transl Med.* 2024; 58(6): 299-309. <https://doi.org/10.4132/jptm.2024.07.25>.

Page 308, right column.

The sentence “This study was approved by the Ethics Committee of the Faculty of Medicine Universitas Indonesia – Dr. Cipto Mangunkusumo Hospital, under protocol number KET-620/UN2.F1/ETIK/PPM.00.02.2023.” on Ethics Statement should read “This study was approved by the Ethics Committee of the Faculty of Medicine Universitas Indonesia – Dr. Cipto Mangunkusumo Hospital, under protocol number KET-610/UN2.F1/ETIK/PPM.00.02.2023.”

We apologize for the inconvenience caused by this error.

Corresponding Author: Agnes Stephanie Harahap

Department of Anatomical Pathology, Faculty of Medicine, Universitas Indonesia/Dr. Cipto Mangunkusumo Hospital, Jl. Salemba Raya No. 6, Jakarta, 14320, Indonesia

Tel: +62-8-18765563, Fax: +62-21-3912477, E-mail: agnes.stephanie01@ui.ac.id

This is an Open Access article distributed under the terms of the Creative Commons Attribution Non-Commercial License (<https://creativecommons.org/licenses/by-nc/4.0/>) which permits unrestricted non-commercial use, distribution, and reproduction in any medium, provided the original work is properly cited.

© 2025 The Korean Society of Pathologists/The Korean Society for Cytopathology